

نموذج رقم (1)

إقرار

أنا الموقع أدناه مقدم الرسالة التي تحمل العنوان:

## Reflection and Transmission from a Multilayer Structure with Conducting Interfaces

أقر بأن ما اشتملت عليه هذه الرسالة إنما هو نتاج جهدي الخاص، باستثناء ما تمت الإشارة إليه حيثما ورد، وإن هذه الرسالة ككل أو أي جزء منها لم يقدم من قبل لنيل درجة أو لقب علمي أو بحثي لدى أي مؤسسة تعليمية أو بحثية أخرى.

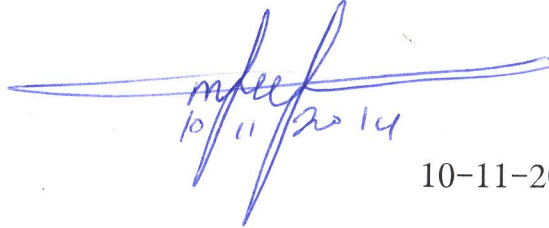
### DECLARATION

The work provided in this thesis, unless otherwise referenced, is the researcher's own work, and has not been submitted elsewhere for any other degree or qualification

Student's name:

اسم الطالب: محمد خالد محمود الهباش

Signature:



10/11/2014

التوقيع:

Date:

10-11-2014

التاريخ:

**Islamic University of Gaza  
Deanery of Higher Studies  
Faculty of Science  
Department of Physics**



# **Reflection and Transmission from a Multilayer Structure with Conducting Interfaces**

**By**

**Mohammed K. El-Habbash**

**B.Sc. Electrical Engineering/communication and  
control**

**Supervisors**

**Dr. Sofyan Taya  
Associate Professor**

**Dr. Taher El-Agez  
Associate Professor**

**Submitted to the Faculty of Science as a Partial  
Fulfillment of the Master of Science ( M. Sc. ) in Physics**

**1435 – 2013**



## نتيجة الحكم على أطروحة ماجستير

بناءً على موافقة شئون البحث العلمي والدراسات العليا بالجامعة الإسلامية بغزة على تشكيل لجنة الحكم على أطروحة الباحث/ محمد خالد محمود الهباش لنيل درجة الماجستير في كلية العلوم /قسم الفيزياء وموضوعها:

### Reflection and Transmission from a Multilayer Structure with Conducing Interfaces

وبعد المناقشة التي تمت اليوم الأربعاء 19 ربيع الآخر 1435 هـ، الموافق 2014/02/19م الساعة

التاسعة والنصف صباحاً بمبنى الحديدان، اجتمعت لجنة الحكم على الأطروحة والمكونة من:

.....

مشرفاً ورئيساً

د. سفيان عبد الرحمن تايه

.....  
Tahar M. E. Agor

مشرفاً

د. ظاهر محمد العاجز

.....  
M.S.

مناقشاً داخلياً

أ.د. محمد موسى شبات

.....  
.....

مناقشاً خارجياً

أ.د. علي حامد الأسطل

وبعد المداولة أوصت اللجنة بمنح الباحث درجة الماجستير في كلية العلوم / قسم الفيزياء.

واللجنة إذ تمنحه هذه الدرجة فإنها توصيه بتقوى الله ولزوم طاعته وأن يسخر علمه في خدمة دينه ووطنه.

والله ولي التوفيق ،،،

مساعد نائب الرئيس للبحث العلمي و للدراسات العليا

أ.د. فؤاد علي العاجز



بِسْمِ اللَّهِ الرَّحْمَنِ الرَّحِيمِ

وَلَقَدْ أَنْزَلْنَا إِلَيْكُمْ آيَاتٍ مُبَيِّنَاتٍ وَمَثَلًا مِّنَ الَّذِينَ خَلَوْا مِن قَبْلِكُمْ وَمَوْعِظَةً لِّلْمُتَّقِينَ

(34) اللَّهُ نُورُ السَّمَاوَاتِ وَالْأَرْضِ مَثَلُ نُورِهِ كَمِشْكَاةٍ فِيهَا مِصْبَاحٌ الْمِصْبَاحُ فِي

زُجَاجَةٍ الزُّجَاجَةُ كَأَنَّهَا كَوْكَبٌ دُرِّيٌّ يُوقَدُ مِن شَجَرَةٍ مُّبَارَكَةٍ زَيْتُونَةٍ لَّا شَرْقِيَّةٍ وَلَا غَرْبِيَّةٍ

يَكَادُ زَيْتُهَا يُضِيءُ وَلَوْ لَمْ تَمْسَسْهُ نَارٌ نُورٌ عَلَى نُورٍ يَهْدِي اللَّهُ لِنُورِهِ مَن يَشَاءُ

وَيَضْرِبُ اللَّهُ الْأَمْثَالَ لِلنَّاسِ وَاللَّهُ بِكُلِّ شَيْءٍ عَلِيمٌ (35)

سورة النور

*To my father and mother.*

*To my wife and son.*

*Mohammed K. ElHabbash*

## **ACKNOWLEDGMENTS**

In the name of Allah, the Merciful, the most Merciful. All praises and thanks be to Allah, who (Alone) created the heavens and the earth, and originated the darkness and the light. My thanks and respect to my Professor Dr.TaherElAjez, and Professor Dr.Sofyan Taya

This thesis would not have been possible unless the continuous support of Professor TaherElAjez, and Professor SofyanTayeh.

I am indebted to Prof. Dr. SinaKhorasani, my professors, my parents, and my classmates.

I cannot find words to express my gratitude to my father, mother, sisters, brothers, and my lovely family.

## ABSTRACT

A lot of previous researches and studies discussed during the past two decades reflectance and transmittance and ellipsometric characteristics of waves in multi-layered thin films.

The angle of incidence and the number of layers and the quality of material consisting of layers attract the most attention of researchers, as well as the type of polarization of the wave .

The polarization types are two: electric transverse field  $r$  (TE- mode) and the magnetic transverse field (TM-mode).

While this thesis discusses the reflectivity and permeability and ellipsometric characteristics of visible incident light on a multi-layered thin film for both types of polarization (TE- mode) and (TM-mode) in the presence of a surface with a conductivity.

The conducting surface can be controlled by a transverse voltage . The ability of controlling the conductivity of the surfaces comes from the existence of accumulated charges between the layers of different insulating material when neighboring.

The incident voltage influences the accumulated charges and thus the conductivity of the surfaces, which affects the optical properties of thin films.

This thesis based on mathematical formulas to calculate the reflection coefficient and permeability coefficient takes into account the conductivity at surfaces.

A mathematical conductivity-formula to calculate the reflectivity and ellipsometric characteristics is used in the third chapter in this thesis.

The conductivity values have been manually changed and simulated using the MATLAB program. The simulation results have been extracted as Excel file. The Excel file has been imported to be plotted using the Origin program.

The plots were compared at different values of conductivity.

Reflectance and transmittance from a conventional Bragg reflector with alternating layers of high and low refractive indices will be studied and analyzed in details.

The effect of all structure parameters such as the refractive index ratio, number of layers, and the angle of incidence will be presented. Reflection and transmission from simple dielectric layers in the presence of interface free charge layers will be explored. The influence of the interface charge layer will be studied for TM or TE polarized light. The effect of a transverse dc voltage on the density of free charges and hence on the reflectance and transmittance will be presented. A Bragg reflector with conducting interfaces will be considered in terms of reflectance, transmittance, phase, band-gap, and tune ability.

Based on the positive results of the simulation in third chapter, researcher derived in the fourth chapter of his dissertation a mathematical formula to calculate the effect of a transverse voltage on the conductivity of multi-layered thin film.

Simulation in the fourth chapter was made for structure of two famous materials silicon and copper.

The ability of controlling the value of conductivity led to the ability to influence the value of the reflectivity and ellipsometric properties.

The simulation has been done with several variables, including the wavelength and transverse voltage and angle of incidence.

The research summary comes in Chapter five as a new device can modulates the optical wave by two types of modulation, one of them based on the reflectivity and the other based on ellipsometric properties.



## ملخص البحث

ناقشت كثير من الأبحاث و الدراسات السابقة خلال العفدين الماضيين الانعكاس و النفاذية و خصائص (ellipsometric) للموجات في الرقائق متعددة الطبقات, و استولت زاوية السقوط و عدد الطبقات و نوعية المادة المكونة للطبقات على جل اهتمام الباحثين و كذلك نوع استقطاب الموجة و هما نوعان المجال الكهربى المستعرض (TE- mode) و المجال المغناطيسى المستعرض (TM-mode).

في حين أن هذه الأطروحة تناقش الانعكاسية و النفاذية و خصائص (ellipsometric) للضوء المرئى الساقط على الرقائق متعددة الطبقات لكلى نوعى الاستقطاب (TE- mode) و (TM- mode) في وجود سطح ذو موصلية يمكن التحكم بها عن طريق جهد مستعرض, وتكمن القدرة على التحكم في موصلية الأسطح على وجود شحنات متراكمة بين طبقات المواد العازلة المختلفة عند تجاوزها , يقوم الجهد المستعرض بالتأثير على الشحنات المتراكمة و بالتالى على موصلية الأسطح مما ينعكس على الخصائص الضوئية للرقائق, و تستند هذه الأطروحة على صيغة رياضية لحساب معامل الانعكاس و معامل النفاذية تأخذ بعين الاعتبار الموصلية عند الأسطح.

طبقت في الفصل الثالث خلال الأطروحة الصيغة الرياضية ذات الموصلية لحساب الانعكاسية و خصائص (ellipsometric), تم تغيير قيمة الموصلية بشكل تجريبي و محاكاة الحسابات (simulation) على برنامج MATLAB و رسم النتائج لمقارنتها عند قيم مختلفة للموصلية.

بناءً على النتائج الإيجابية للمحاكاة (simulation) اشتق الباحث في الفصل الرابع من أطروحته صيغة رياضية لحساب تأثير الجهد المستعرض على موصلية الرقائق متعددة الطبقات للتحكم في قيمتها, و قد تمت المحاكاة في الفصل الرابع على رقائق متعددة الطبقات مصنوعة من مادتي السيليكون و النحاس و هما مادتان شائعتان و رخيستان نسبياً, و قد أدى التحكم في قيمة الموصلية إلى القدرة على التأثير في قيمة الانعكاسية و خصائص (ellipsometric), و قد تم محاكاة النظام مع عدة متغيرات تشمل الطول الموجي و فرق الجهد المستعرض و زاوية السقوط.

جاءت خلاصة البحث في الفصل الخامس على هيئة جهاز جديد يقوم بعملية توليف للموجة الضوئية بنوعين من التوليف أحدهما يعتمد على الانعكاسية و الآخر على خصائص (ellipsometric).

# List of Figures

## CHAPTER ONE

Figure 1.1	Two media of permittivities $\epsilon_1$ and $\epsilon_2$ are separated by an interface	4
Figure 1.2	Illustration of the field components	4
Figure 1.3	Illustrating of the refraction of a plane wave.	10
Figure 1.4	Propagation of a plane wave.	11
Figure 1.5	Scattering of electromagnetic waves at an interface: TE case.	13
Figure 1.6	Scattering of an electromagnetic wave at an interface: TM case.	14
Figure 1.7	Wave vectors for an electromagnetic wave incident on a boundary separating two different media.	15

## CHAPTER Two

Figure 2.1	Schematic description of the transmission of an electromagnetic wave through a slab with width $\ell$ .	26
Figure 2.2	Schematic of a multilayer system. $A_i$ represent the amplitude of the right traveling wave and $B_i$ that of the left-traveling one. Note that $A_i$ and $B_i$ are not continuous at the interfaces.	30

## CHAPTER Three

Figure 3.1	Configuration of reflected and refracted waves at an interface for TM mode.	39
Figure 3.2	Configuration of reflected and refracted waves at an interface between two media for the TE mode.	45
Figure 3.3	Schematic diagram of three-layer Bragg reflector.	48
Figure 3.4	Calculated reflectivity of three-layer-quarter-wavelength Bragg reflector, at $\theta_o = 18^\circ$ in the spectral range of 350-850 nm for different values of $\sigma$ .	51

Figure 3.5	The ellipsometric parameter $\psi$ of three-layer-quarter-wavelength Bragg reflector, at $\theta_o = 18^\circ$ in the spectral range of 350-850 nm for different values of $\sigma$ .	<b>51</b>
Figure 3.6	The ellipsometric parameter $\Delta$ of three-layer-quarter-wavelength Bragg reflector, at $\theta_o = 18^\circ$ in the spectral range of 350-850 nm for different values of $\sigma$ .	<b>52</b>
Figure 3.7	Structure of brag reflector of five layers	<b>52</b>
Figure 3.8	Calculated reflectivity of five-layer-quarter-wavelength Bragg reflector, at $\theta_o = 18^\circ$ in the spectral range of 350-850 nm for different values of $\sigma$ .	<b>53</b>
Figure 3.9	The ellipsometric parameter $\psi$ of five-layer-quarter-wavelength Bragg reflector, at $\theta_o = 18^\circ$ in the spectral range of 350-850 nm for different values of $\sigma$	<b>54</b>
Figure 3.10	The ellipsometric parameter $\Delta$ of five-layer-quarter-wavelength Bragg reflector, at $\theta_o = 18^\circ$ in the spectral range of 350-850 nm for different values of $\sigma$	<b>54</b>

#### **CHAPTER Four**

Figure 4.1	Three-layer Bragg reflector with an applied voltage V.	<b>56</b>
Figure 4.2	Five-layer Bragg reflector with an applied voltage V.	<b>58</b>
Figure 4.3	Reflectivity from three-layer Bragg reflector for Si-Cu structure for different values of voltage and for $\theta_i=20^\circ$ .	<b>61</b>
Figure 4.4	Reflectivity difference from three-layer Bragg reflector for Si-Cu structure for different values of voltage and for $\theta_i=20^\circ$ .	<b>61</b>
Figure 4.5	$\psi$ of three-layer Bragg reflector for Si-Cu structure for different values of voltage and for $\theta_i=20^\circ$	<b>62</b>

Figure 4.6	$\psi$ difference of three-layer Bragg reflector for Si-Cu structure for different values of voltage and for $\theta_i=20^\circ$ .	<b>63</b>
Figure 4.7	$\Delta$ of three-layer Bragg reflector for Si-Cu structure for different values of voltage and for $\theta_i=20^\circ$	<b>63</b>
Figure 4.8	$\Delta$ difference of three-layer Bragg reflector for Si-Cu structure for different values of voltage and for $\theta_i=20^\circ$	<b>64</b>
Figure 4.9	Reflectivity of five-layer Bragg reflector for Si-Cu structure for different values of the voltage and $\theta_i=20^\circ$ .	<b>65</b>
Figure 4.10	$\psi$ of five-layer Bragg reflector for Si-Cu structure for different values of voltage and $\theta_i=20^\circ$ .	<b>65</b>
Figure 4.11	$\Delta$ of five-layer Bragg reflector for Si-Cu structure for different values of voltage and $\theta_i=20^\circ$ .	<b>66</b>
Figure 4.12	Reflectivity of nine-layer Bragg reflector for Si-Cu structure for different values of voltage and for $\theta_i=20^\circ$ .	<b>67</b>
Figure 4.13	$\psi$ of nine-layer Bragg reflector for Si-Cu structure for different values of voltage and for $\theta_i=20^\circ$ .	<b>67</b>
Figure 4.14	$\Delta$ of nine-layer Bragg reflector for Si-Cu structure for different values of voltage and for $\theta_i=20^\circ$ .	<b>68</b>
Figure 4.15	Reflectivity of fifteen-layer Bragg reflector for Si-Cu structure for $\theta_i=20^\circ$ , and with 0, and 1000 volt.	<b>69</b>
Figure 4.16	$\psi$ of fifteen-layer Bragg reflector for Si-Cu structure for different values of voltage and for $\theta_i=20^\circ$ .	<b>69</b>
Figure 4.17	$\Delta$ of fifteen-layer Bragg reflector for Si-Cu structure for different values of voltage and for $\theta_i=20^\circ$ .	<b>70</b>
Figure 4.18	Reflectivity of three-layer Bragg reflector for Si-Cu structure versus the incidence angle with transverse voltage of 0 volt	<b>71</b>

Figure 4.19	$\psi$ of three-layer Bragg reflector for Si-Cu structure versus the incidence angle with transverse voltage of 0 volt	<b>72</b>
Figure 4.20	$\Delta$ of three-layer Bragg reflector for Si-Cu structure versus the incidence angle with transverse voltage of 0 volt for different values of $\lambda$	<b>72</b>
Figure 4.21	Reflectivity of three-layer Bragg reflector for Si-Cu structure versus the incidence angle with transverse voltage of 1000 volt	<b>74</b>
Figure 4.22	$\psi$ of three-layer Bragg reflector for Si-Cu structure versus the incidence angle with transverse voltage of 1000 volt	<b>74</b>
Figure 4.23	$\Delta$ of three-layer Bragg reflector for Si-Cu structure versus the incidence angle with transverse voltage of 1000 volt	<b>75</b>
Figure 4.24	Reflectivity of three-layer Bragg reflector for Si-Cu structure versus the incidence angle with transverse voltage of 5000 volt	<b>76</b>
Figure 4.25	$\psi$ of three-layer Bragg reflector for Si-Cu structure versus the incidence angle with transverse voltage of 5000 volt	<b>76</b>
Figure 4.26	$\Delta$ of three-layer Bragg reflector for Si-Cu structure versus the incidence angle with transverse voltage of 5000 volt	<b>77</b>
Figure 4.27	Reflectivity of five-layer Bragg reflector for Si-Cu structure versus the incidence angle with transverse voltage of 0 volt	<b>78</b>
Figure 4.28	$\psi$ of five-layer Bragg reflector for Si-Cu structure versus the incidence angle with transverse voltage of 0 volt	<b>79</b>
Figure 4.29	$\Delta$ of five-layer Bragg reflector for Si-Cu structure versus the incidence angle with transverse voltage of 0 volt	<b>79</b>
Figure 4.30	Reflectivity of five-layer Bragg reflector for Si-Cu structure versus the incidence angle with transverse voltage of 1000 volt	<b>80</b>
Figure 4.31	$\psi$ of five-layer Bragg reflector for Si-Cu structure versus the incidence angle with transverse voltage of 1000 volt	<b>80</b>

Figure 4.32	$\Delta$ of five-layer Bragg reflector for Si-Cu structure versus the incidence angle with transverse voltage of 1000 volt	<b>81</b>
Figure 4.33	Reflectivity of five-layer Bragg reflector for Si-Cu structure versus the incidence angle with transverse voltage of 5000 volt	<b>81</b>
Figure 4.34	$\psi$ of five-layer Bragg reflector for Si-Cu structure versus the incidence angle with transverse voltage of 5000 volt	<b>82</b>
Figure 4.35	$\Delta$ of five-layer Bragg reflector for Si-Cu structure versus the incidence angle with transverse voltage of 5000 volt	<b>82</b>
Figure 4.36	Reflectivity of nine-layer Bragg reflector for Si-Cu structure versus the incidence angle with transverse voltage of 0 volt	<b>83</b>
Figure 4.37	$\psi$ of nine-layer Bragg reflector for Si-Cu structure versus the incidence angle with transverse voltage of 0 volt	<b>84</b>
Figure 4.38	$\Delta$ of nine-layer Bragg reflector for Si-Cu structure versus the incidence angle with transverse voltage of 0 volt	<b>84</b>
Figure 4.39	Reflectivity of nine-layer Bragg reflector for Si-Cu structure versus the incidence angle with transverse voltage of 1000 volt	<b>85</b>
Figure 4.40	$\psi$ of nine-layer Bragg reflector for Si-Cu structure versus the incidence angle with transverse voltage of 1000 volt	<b>85</b>
Figure 4.41	$\Delta$ of nine-layer Bragg reflector for Si-Cu structure versus the incidence angle with transverse voltage of 1000 volt	<b>86</b>
Figure 4.42	Reflectivity of nine-layer Bragg reflector for Si-Cu structure versus the incidence angle with transverse voltage of 5000 volt	<b>86</b>
Figure 4.43	$\psi$ of nine-layer Bragg reflector for Si-Cu structure versus the incidence angle with transverse voltage of 5000 volt	<b>87</b>
Figure 4.44	$\Delta$ of nine-layer Bragg reflector for Si-Cu structure versus the incidence angle with transverse voltage of 5000 volt	<b>87</b>

Figure 4.45	Reflectivity of fifteen-layer Bragg reflector for Si-Cu structure versus the incidence angle with transverse voltage of 0 volt	<b>88</b>
Figure 4.46	$\psi$ of fifteen-layer Bragg reflector for Si-Cu structure versus the incidence angle with transverse voltage of 0 volt	<b>89</b>
Figure 4.47	$\Delta$ of fifteen-layer Bragg reflector for Si-Cu structure versus the incidence angle with transverse voltage of 0 volt	<b>89</b>
Figure 4.48	Reflectivity of fifteen-layer Bragg reflector for Si-Cu structure versus the incidence angle with transverse voltage of 1000 volt	<b>90</b>
Figure 4.49	$\psi$ of fifteen-layer Bragg reflector for Si-Cu structure versus the incidence angle with transverse voltage of 1000 volt	<b>91</b>
Figure 4.50	$\Delta$ of fifteen-layer Bragg reflector for Si-Cu structure versus the incidence angle with transverse voltage of 1000 volt	<b>91</b>
Figure 4.51	Reflectivity of fifteen-layer Bragg reflector for Si-Cu structure versus the incidence angle with transverse voltage of 5000 volt	<b>92</b>
Figure 4.52	$\psi$ of fifteen-layer Bragg reflector for Si-Cu structure versus the incidence angle with transverse voltage of 5000 volt	<b>92</b>
Figure 4.53	$\Delta$ of fifteen-layer Bragg reflector for Si-Cu structure versus the incidence angle with transverse voltage of 5000 volt	<b>93</b>
Figure 4.54	Reflectivity of three-layer Bragg reflector for Si-Cu structure versus the incidence angle with transverse voltage of 0, 1000, and 5000 volt	<b>94</b>
Figure 4.55	$\psi$ of three-layer Bragg reflector for Si-Cu structure versus the incidence angle with transverse voltage of 0, 1000, and 5000 volt	<b>94</b>
Figure 4.56	$\Delta$ of three-layer Bragg reflector for Si-Cu structure versus the incidence angle with transverse voltage of 0, 1000, and 5000 volt	<b>95</b>

Figure 4.57	Reflectivity of five-layer Bragg reflector for Si-Cu structure versus the incidence angle with transverse voltage of 0, 1000, and 5000 volt	96
Figure 4.58	$\psi$ of five-layer Bragg reflector for Si-Cu structure versus the incidence angle with transverse voltage of 0, 1000, and 5000 volt	96
Figure 4.59	$\Delta$ of five-layer Bragg reflector for Si-Cu structure versus the incidence angle with transverse voltage of 0, 1000, and 5000 volt	97
Figure 4.60	Reflectivity of nine-layer Bragg reflector for Si-Cu structure versus the incidence angle with transverse voltage of 0, 1000, and 5000 volt	98
Figure 4.61	$\psi$ of nine-layer Bragg reflector for Si-Cu structure versus the incidence angle with transverse voltage of 0, 1000, and 5000 volt	98
Figure 4.62	$\Delta$ of nine-layer Bragg reflector for Si-Cu structure versus the incidence angle with transverse voltage of 0, 1000, and 5000 volt	99
Figure 4.63	Reflectivity of fifteen-layer Bragg reflector for Si-Cu structure versus the incidence angle with transverse voltage of 0, 1000, and 5000 volt	100
Figure 4.64	$\psi$ of fifteen-layer Bragg reflector for Si-Cu structure versus the incidence angle with transverse voltage of 0, 1000, and 5000 volt	100
Figure 4.65	$\Delta$ of fifteen-layer Bragg reflector for Si-Cu structure versus the incidence angle with transverse voltage of 0, 1000, and 5000 volt	101

## CHAPTER Five

Figure 5.1	Amplitude modulation of a light depending on a transverse voltage pulse train.	106
------------	--	-----



# CONTENTS

## Chapter One: Introduction to electromagnetic theory

1.1. Maxwell's equations and electromagnetic field.....	1
1.2. Boundary conditions.....	3
1.3. Index of Refraction.....	5
1.4. Plane wave.....	8
1.5. Polarization of light (TE and TM) .....	11
1.6. Transmission and reflection of a plane wave at an interface...	15
1.6.1. Plane wave at an interface.....	15
1.6.2. Transmission and Reflection Coefficients.....	17
1.6.2.1. The TE Polarization.....	17
1.6.2.2. The TM Polarization.....	19
1.6.3. Total transmission and total reflection.....	20
1.6.3.1. Total Transmission.....	20
1.6.3.2. Brewster Angles.....	21
1.6.3.3. Total Reflection.....	22
1.6.3.4. State of the Art .....	24

## Chapter Two: Analysis of multilayer structure

2. Transmission and Reflection Coefficients for a Slab.....	25
2.1.1. Transmission and Reflection Amplitudes: TE polarization	26
2.1.2. Transmission and Reflection Amplitudes: TM polarization.....	28
2.2. Multilayer media.....	28
2.3. Mathematical methods for the analysis and simulation of multilayers.....	29
2.3.1. Transfer Matrix Method (TMM) .....	29
2.3.2. Polynomial approach.....	32
2.3.3. BCITL Model.....	33
2.4. Application of Multilayer structures.....	34

**Chapter Three: Transmission and reflection in multilayer structure  
with conducting interfaces**

3.1. Basic Relations.....	<b>36</b>
3.2. Reflection and transmission of a polarized electromagnetic wave at a conducting interface.....	<b>37</b>
3.2.1. Reflection and transmission of plane TM polarized light at a conducting interface.....	<b>37</b>
3.2.2. Reflection and transmission of plane TE polarized light at a conducting interface.....	<b>44</b>
3.3. Simulation of multilayer structures. ....	<b>47</b>
3.3.1. Simulation of Bragg reflector with three layers .....	<b>47</b>
3.3.1.1. Results of simulation of three-layer Bragg reflector .....	<b>49</b>
3.3.2. Simulation of a Bragg reflector with five layers .....	<b>52</b>
3.3.3. Result of simulation of Bragg reflector with five layers....	<b>53</b>

**Chapter Four: Manipulation of the conducting interface in multilayer  
structure**

4.1. Three-layer Bragg reflector with conducting interfaces and transverse voltage .....	<b>55</b>
4.2. Five-layer Bragg reflector with conducting interfaces and transverse voltage .....	<b>58</b>
4.3. Simulation results for Bragg reflector .....	<b>59</b>
4.3.1. Investigation of the effect of wavelength and voltage.....	<b>60</b>
4.3.1.1. Results of a three-layer structure .....	<b>60</b>
4.3.1.2. Results of a five-layer structure .....	<b>64</b>
4.3.1.3. Results of a nine-layer structure.....	<b>66</b>
4.3.1.4. Results for a fifteen-layer structure.....	<b>68</b>
4.3.2. Investigation of Bragg reflector with the incidence angle,	

applied potential, and wavelength.. .....	70
4.3.2.1. Results of a three-layer Bragg structure. ....	70
4.3.2.2. Results of a five-layer structure. ....	77
4.3.2.3. Results for a nine-layer structure.. .....	83
4.3.2.4. Results of a fifteen-layer structure.....	88
4.3.3. Investigation of Bragg reflector performance with the incidence angle and transverse voltage.....	93
4.3.3.1. Results of a three-layer structure.....	93
4.3.3.2. Results of a five-layer structure.....	95
4.3.3.3. Results of a nine-layer structure.....	97
4.3.3.4. Results of a fifteen-layer structure.....	99
 <b>Chapter Five: General conclusion</b>	 <b>104</b>
 <b>References</b> .....	 <b>106</b>

# Chapter One

## Introduction to electromagnetic theory

In this chapter, a review of electromagnetic theory is presented. Maxwell's equations, boundary conditions, plane wave, and polarization of light are studied. Moreover, reflection and transmission at one interface between two different media are presented.

### 2.5. Maxwell's equations and electromagnetic field

Maxwell's equations are the cornerstone of electromagnetic theory. They fully describe the electromagnetic field. Optics, as a branch of physics, describes the phenomena associated with the propagation of light and its interaction with matter. The field of optics usually deals with the behavior of visible light, infrared, and ultraviolet waves. The time dependent Maxwell equations are given by [1]

$$\vec{\nabla} \times \vec{E} = -\frac{\partial \vec{B}}{\partial t}, \quad (1.1)$$

$$\vec{\nabla} \times \vec{H} = \vec{J}_f + \frac{\partial \vec{D}}{\partial t}, \quad (1.2)$$

$$\nabla \cdot \vec{D} = \rho_f, \quad (1.3)$$

$$\nabla \cdot \vec{B} = 0. \quad (1.4)$$

The first is Faraday's law of induction; the second is Ampere's law as amended by Maxwell to include the displacement current  $\partial \vec{D} / \partial t$ , the third is Gauss' law for the electric field, and the fourth is the nonexistence of magnetic monopole.

The displacement current term  $\partial \vec{D} / \partial t$  in Ampere's law is essential in predicting the

existence of propagating electromagnetic waves.

The quantities  $\vec{E}$  and  $\vec{H}$  are the electric and magnetic field intensities and are measured in units of [volt/m] and [ampere/m], respectively. The quantities  $\vec{D}$  and  $\vec{B}$  are the electric and magnetic flux densities in units of [coulomb/m<sup>2</sup>] and [weber/m<sup>2</sup>], or [tesla] respectively. The quantities  $\rho$  and  $\vec{J}$  are the volume charge density and electric current density of any external charges (that is, not including any induced polarization charges and currents.) They are measured in units of [coulomb/m<sup>3</sup>] and [ampere/m<sup>2</sup>].

These equations describe all macroscopic electromagnetic phenomena where the primary sources of the electromagnetic fields are free charges and currents.

For wave propagation phenomena considered in optics, media without free charges and conduction currents are most relevant. With  $\rho = 0$  and  $\vec{J} = 0$ , Maxwell equations become

$$\vec{\nabla} \times \vec{E} = -\frac{\partial \vec{B}}{\partial t}, \quad (1.5)$$

$$\vec{\nabla} \times \vec{H} = \vec{J}_f + \frac{\partial \vec{D}}{\partial t}, \quad (1.6)$$

$$\nabla \cdot \vec{D} = \rho_f, \quad (1.7)$$

$$\nabla \cdot \vec{B} = 0. \quad (1.8)$$

The behavior of substances under the influence of electric and magnetic fields is described by relation known as material equations (or constitutive relations). In general they are rather complicated; but if the field is time-harmonic, and the material is isotropic (i.e. when its physical properties at each point are independent of direction), they take the form

$$\vec{j} = \sigma \vec{E}, \quad (1.9)$$

$$\vec{D} = \epsilon \vec{E}, \quad (1.10)$$

$$\vec{B} = \mu \vec{H}, \quad (1.11)$$

where  $\sigma$  is called the specific conductivity,  $\epsilon$  is the dielectric constant (or permittivity) and  $\mu$  is the magnetic permeability.

Equation (1.9) is the differential form of Ohm's law. Substances for which  $\sigma \neq 0$  are called conductors. Metals are very good conductors, but there are other classes of good conducting materials such as ionic solutions in liquids and also in solids. In metals the conductivity decreases with increasing temperature. However, in other classes of materials, known as semiconductors, conductivity increases with temperature over a wide range. Substances for which  $\sigma$  is negligibly small are called insulators or dielectrics. Their electric and magnetic properties are then completely determined by  $\epsilon$  and  $\mu$ . For most substances the relative nonmagnetic permeability  $\mu_r$  is practically unity. If this is not the case, i.e. if  $\mu_r$  differs appreciably from unity, the substance is said to be magnetic. In particular, if  $\mu_r > 1$ , the substance is said to be paramagnetic (e.g. platinum, oxygen, nitrogen dioxide), while if  $\mu_r < 1$  it is said to be diamagnetic (e.g. bismuth, copper, hydrogen, water).

## 2.6. Boundary conditions

Figure 1.1 shows two media of permittivities  $\epsilon_1$  and  $\epsilon_2$  separated by an interface. The boundary conditions for the electromagnetic fields across material boundaries are given by [2]

$$E_{1t} - E_{2t} = 0, \quad (1.12)$$

$$H_{1t} - H_{2t} = \vec{J}_s \times \hat{n}, \quad (1.13)$$

$$D_{1n} - D_{2n} = \rho_s, \quad (1.14)$$

$$B_{1n} - B_{2n} = 0, \quad (1.15)$$

where  $\hat{n}$  is a unit vector normal to the boundary pointing from medium-2 into medium-1. The subscript t and n denote tangential and normal components,

respectively. The quantities  $\rho_s, \vec{J}_s$  are any external surface charge and surface current densities on the boundary .

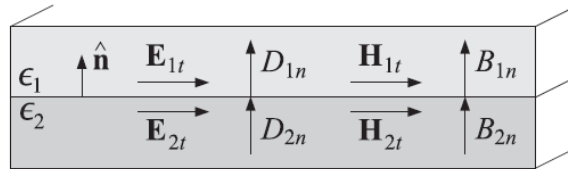


Figure 1.1. Two media of permittivities  $\epsilon_1$  and  $\epsilon_2$  are separated by an interface.

In words, the tangential components of the  $\vec{E}$ -field are continuous across the interface; the difference of the tangential components of the  $\vec{H}$ -field are equal to the surface current density ( $J_s$ ); the difference of the normal components of the flux density  $\vec{D}$  are equal to the surface charge density ( $\rho_s$ ); and the normal components of the magnetic flux density  $\vec{B}$  are continuous. The relative directions of the field vectors are shown in Fig.1.2. Each vector may be decomposed as the sum of a part tangential to the surface and a part perpendicular to it, that is

$$\vec{E}_t = \hat{n} \times (\vec{E} \times \hat{n}) \quad , \quad \vec{E}_n = \hat{n}(\hat{n} \cdot \vec{E}), \quad (1.16)$$

and

$$\vec{H}_t = \hat{n} \times (\vec{H} \times \hat{n}), \quad \vec{H}_n = \hat{n}(\hat{n} \cdot \vec{H}). \quad (1.17)$$

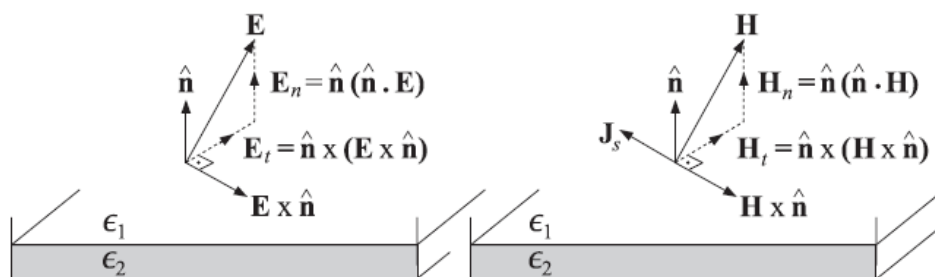


Figure 1.2. Illustration of the field components.

+The first two boundary conditions that appear in equations (1.12) and (1.13) can be written in the following vectorial forms.

$$\hat{n}_{21} \times (\vec{E}_1 \times \hat{n}_{21}) - \hat{n}_{21} \times (\vec{E}_2 \times \hat{n}_{21}) = 0, \quad (1.18)$$

$$\hat{n}_{21} \times (\vec{H}_1 \times \hat{n}_{21}) - \hat{n}_{21} \times (\vec{H}_2 \times \hat{n}_{21}) = \vec{J}_s \times \hat{n}_{21}. \quad (1.19)$$

The above two equations can be simplified as

$$\hat{n}_{21} \times (\vec{E}_1 - \vec{E}_2) = 0, \quad (1.20)$$

$$\hat{n}_{21} \times (\vec{H}_1 - \vec{H}_2) = \vec{J}_s. \quad (1.21)$$

## 2.7. Index of Refraction

We assume an isotropic, homogeneous, and non-conducting medium (i.e.  $J_{free} = 0$ ). In this case, we expect  $\vec{E}$  and  $\vec{P}$  to be parallel to each other so  $\nabla \cdot \vec{P} = 0$ , where  $\vec{P}$  is the polarization. The general wave equation for the electric field reduces in this case to [3]

$$\nabla^2 \vec{E} - \epsilon_0 \mu_0 \frac{\partial^2 \vec{E}}{\partial t^2} = \mu_0 \frac{\partial^2 \vec{P}}{\partial t^2}. \quad (1.22)$$

For sinusoidal waves, the solutions are considered to have the forms

$$E = E_0 e^{i(k \cdot r - \omega t)}, \quad (1.23)$$

$$P = P_0 e^{i(k \cdot r - \omega t)}. \quad (1.24)$$



An electric field stimulates a medium at frequency  $\omega$ , then the polarization in the medium also oscillates at frequency  $\omega$ . This assumption is typically rather good except for extreme electric fields, which can generate frequency harmonics through nonlinear effects. Substitution of the trial solutions (1.23) and (1.24) into (1.22) yields

$$-K^2 E_o e^{i(k \cdot r - \omega t)} + \epsilon_o \mu_o \omega^2 E_o e^{i(k \cdot r - \omega t)} = -\mu_o \omega^2 P_o e^{i(k \cdot r - \omega t)}. \quad (1.25)$$

In a linear medium, the polarization amplitude is proportional to the strength of the applied electric field

$$P_o(\omega) = \epsilon_o \chi(\omega) E_o(\omega), \quad (1.26)$$

where  $\chi(\omega)$  is the susceptibility which depends on the frequency of the field. By inserting Eq.(1.26) into Eq.(1.25) and canceling the field terms, we obtain the dispersion relation in dielectrics

$$K^2 = \epsilon_o \mu_o [1 + \chi(\omega)] \omega^2 \quad \text{or} \quad K = \frac{\omega}{c} \sqrt{1 + \chi(\omega)}, \quad (1.27)$$

where  $c = 1/\sqrt{\epsilon_o \mu_o}$ . In general,  $\omega$  is a complex number, which leads to a complex

index of refraction, defined by

$$N(\omega) = n(\omega) + i\kappa(\omega) = \sqrt{1 + \chi(\omega)}, \quad (1.28)$$

where  $n$  and  $\kappa$  are respectively the real and imaginary parts of the index. According to Eq.(1.27), the magnitude of the wave vector is also complex according to

$$K = \frac{N\omega}{c} = \frac{(n + i\kappa)\omega}{c}. \quad (1.29)$$

The use of complex index of refraction only makes sense in the context of complex

representation of plane waves. The complex index  $N$  takes into account absorption as well as the usual oscillatory behavior of the wave. This can be seen by explicitly placing Eq.(1.29) into Eq.(1.23)

$$E(\mathbf{r}, t) = E_o e^{-Im\{K\} \cdot \mathbf{r}} e^{i(Re\{K\} \cdot \mathbf{r} - \omega t)} = E_o e^{-\frac{k\omega}{c} \hat{\mathbf{u}} \cdot \mathbf{r}} e^{i\left(\frac{n\omega}{c} \hat{\mathbf{u}} \cdot \mathbf{r} - \omega t\right)}. \quad (1.30)$$

where  $\hat{\mathbf{u}}$  is a real unit vector specifying the direction of  $\mathbf{K}$ . When looking at Eq.(1.30), the real part should be considered

$$E(\mathbf{r}, t) = E_o e^{-\frac{k\omega}{c} \hat{\mathbf{u}} \cdot \mathbf{r}} \cos\left(\frac{n\omega}{c} \hat{\mathbf{u}} \cdot \mathbf{r} - \omega t + \phi\right) \quad (1.31)$$

Figure 1.3 shows a graph of Eq.(1.31). The imaginary part of the index causes the wave to decay as it travels. The real part of the index  $n$  is associated with the oscillations of the wave. From Eq.(1.28)

$$(n + i\kappa)^2 = n^2 - \kappa^2 + i2n\kappa = 1 + Re\{\chi\} + iIm\{\chi\} = 1 + \chi. \quad (1.32)$$

The real and imaginary parts in the above equation are separately equal

$$n^2 - \kappa^2 = 1 + Re\{\chi\} \quad \text{and} \quad 2n = Im\{\chi\}. \quad (1.33)$$

From the latter equation

$$\kappa = Im\{\chi\} / 2n. \quad (1.34)$$

When this is substituted into the first equation of (1.33) we get a quadratic in  $n^2$

$$n^4 - (1 + Re\{\chi\})n^2 - \frac{(Im\{\chi\})^2}{4} = 0. \quad (1.35)$$

The positive real root to this equation is given by

$$n = \sqrt{\frac{(1 + \text{Re}\{\chi\}) + \sqrt{(1 + \text{Re}\{\chi\})^2 + (\text{Im}\{\chi\})^2}}{2}}. \quad (1.36)$$

The imaginary part of the index is then obtained from Eq.(1.34). When absorption is small one can neglect the imaginary part of  $(\omega)$ , and Eq.(1.36) reduces to [3]

$$n(\omega) = \sqrt{1 + \chi(\omega)}. \quad (1.37)$$

## 2.8. Plane wave

Maxwell's equations relate the field vectors by means of simultaneous differentialequations. Confining our attention to that part of the field which contains no charges or currents, i.e. where  $J = 0$ , and  $\rho = 0$ , then substituting for  $\vec{B}$  from Eq.(1.11) into the first Maxwell Eq.(1.1), dividing both sides by  $\mu$ , and applying the operator curl ( $\nabla \times$ ); this gives

$$\vec{\nabla} \times \left( \frac{1}{\mu} \vec{\nabla} \times \vec{E} \right) + \frac{1}{c} \vec{\nabla} \times \left( \frac{\partial \vec{H}}{\partial t} \right) = 0. \quad (1.38)$$

Differentiating Eq.(1.1) with respect to time, using Eq.(1.10) for  $\vec{D}$ , and eliminating  $\vec{\nabla} \times \left( \frac{\partial \vec{H}}{\partial t} \right)$  between the resulting equation and Eq.(1.2); this gives

$$\vec{\nabla} \times \left( \frac{1}{\mu} \vec{\nabla} \times \vec{E} \right) + \frac{\epsilon_r}{c^2} \frac{\partial^2 \vec{E}}{\partial t^2} = 0. \quad (1.39)$$

Using the identities  $\vec{\nabla} \times (uv) = u\vec{\nabla} \times \vec{v} + (\vec{\nabla}u) \times \vec{v}$  and  $\vec{\nabla} \times \vec{\nabla} \times = \vec{\nabla}(\vec{\nabla} \cdot) - \nabla^2$ , Equation (1.39) becomes

$$\nabla^2 \vec{E} - \frac{\epsilon_r \mu_r}{c^2} \frac{\partial^2 \vec{E}}{\partial t^2} + (\vec{\nabla} \ln \mu_r) \times \vec{\nabla} \times \vec{E} - \vec{\nabla}(\vec{\nabla} \cdot \vec{E}) = 0. \quad (1.40)$$

Also from Eq.(1.7), using again the material equation for  $\vec{D}$  and applying the identity  $\vec{\nabla} \cdot (\vec{u}\vec{v}) = u \vec{\nabla} \cdot \vec{v} + \vec{v} \cdot \vec{\nabla}u$ ,

$$\varepsilon \vec{\nabla} \cdot \vec{E} + \vec{E} \cdot \vec{\nabla}\varepsilon = 0. \quad (1.41)$$

Hence Equation (1.40) may be written as

$$\nabla^2 \vec{E} - \frac{\varepsilon\mu}{c^2} \frac{\partial^2 \vec{E}}{\partial t^2} + (\vec{\nabla} \ln \mu) \times \vec{\nabla} \times \vec{E} + \vec{\nabla}(\vec{E} \cdot \vec{\nabla} \ln \varepsilon) = 0. \quad (1.42)$$

In a similar way we obtain an equation for  $\vec{H}$  field as

$$\nabla^2 \vec{H} - \frac{\varepsilon\mu}{c^2} \frac{\partial^2 \vec{H}}{\partial t^2} + (\vec{\nabla} \ln \varepsilon) \times \vec{\nabla} \times \vec{H} + \vec{\nabla}(\vec{H} \cdot \vec{\nabla} \ln \mu) = 0. \quad (1.43)$$

In particular, if the medium is homogeneous,  $\vec{\nabla}(\ln \varepsilon) = \vec{\nabla}(\ln \mu) = 0$ , and Equations.(1.42) and (1.43) reduce to [4]

$$\nabla^2 \vec{E} - \frac{\varepsilon_r \mu_r}{c^2} \frac{\partial^2 \vec{E}}{\partial t^2} = 0, \quad (1.44)$$

$$\nabla^2 \vec{H} - \frac{\varepsilon_r \mu_r}{c^2} \frac{\partial^2 \vec{H}}{\partial t^2} = 0. \quad (1.45)$$

These are standard equations of wave motion and they suggest the existence of electromagnetic waves propagating with a velocity

$$v = c / \sqrt{\varepsilon_r \mu_r}. \quad (1.46)$$

According to the law of refraction, if a plane electromagnetic wave falls onto a plane boundary between two homogeneous media, the angle of incidence bears a constant ratio to the angle of refraction. This constant ratio being equal to the ratio of the velocities  $v_1$  and  $v_2$  of propagation in the two media, namely

$$\frac{\sin \theta_1}{\sin \theta_2} = \frac{v_1}{v_2}. \quad (1.47)$$

We also define an 'absolute refractive index'  $n$  of a medium; it is the refractive index for refraction from vacuum into that medium,

$$n = \frac{c}{v}. \quad (1.48)$$

If  $n_1$  and  $n_2$  are the absolute refractive indices of two media, the (relative) refractive index  $n_{12}$  for refraction from the first into the second medium then is

$$n_{12} = \frac{n_2}{n_1} = \frac{v_1}{v_2}. \quad (1.49)$$

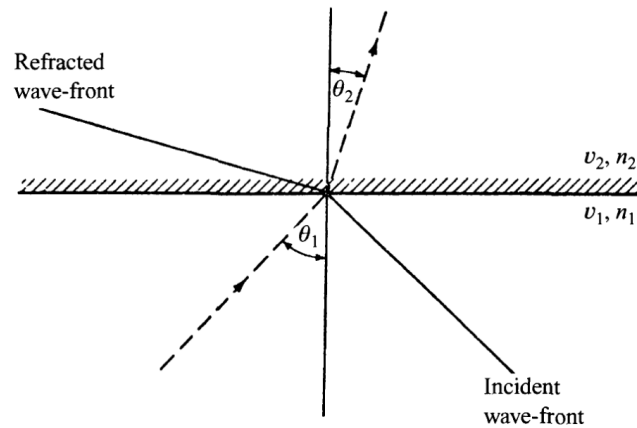


Figure 1.3. Illustrating of the refraction of a plane wave.

Comparison of Eq.(1.46) and Eq.(1.48) gives Maxwell's formula

$$n = \sqrt{\epsilon_r \mu_r}. \quad (1.50)$$

In a homogeneous medium in regions free of currents and charges, each rectangular component  $V(r, t)$  of the field vectors satisfies, according to Eq.(1.44), and Eq.(1.45) the homogeneous wave equation

$$\nabla^2 \vec{V} - \frac{1}{v^2} \frac{\partial^2 \vec{V}}{\partial t^2} = 0. \quad (1.51)$$

The simplest solution of this equation can be examined as follows; let  $\mathbf{r}(x, y, z)$  be a position vector of a point P in space and  $\mathbf{k}(k_x, k_y, k_z)$  a unit vector in a fixed direction. Any solution of equation (1.51) of the form

$$V = V(\vec{r} \cdot \vec{k}, t). \quad (1.52)$$

is said to represent a plane wave, since at each instant of time,  $\mathbf{V}$  is constant over each of the planes

$$\vec{r} \cdot \vec{k} = \text{constant} \quad (1.53)$$

which are perpendicular to the unit vector  $\mathbf{k}$ .

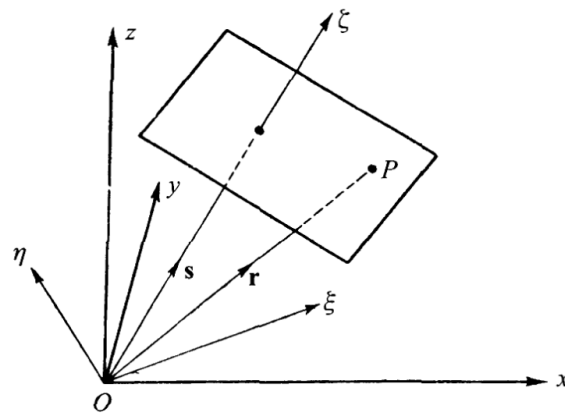


Figure 1.4. Propagation of a plane wave.

## 2.9. Polarization of light (TE and TM)

In transverse electric mode, the electric field has no longitudinal components ( $E_z=0$ ) but in the transverse direction ( $E_y \neq 0$ ). By definition, in the case of TE polarization

the electric intensity  $E$  is parallel to the interface. In the notation of Fig.1.5, the vector  $\vec{E}$  has only one component,  $E = (0, E_y, 0)$ , and vector  $\vec{H}$  has two components,  $H = (H_x, 0, H_z)$ . As shown in Fig. 1.5, each field contains components that propagate to the right (denoted by the superscript +) and components propagating to the left (denoted by the superscript -).

The boundary condition requires that the component of the electric field parallel to the interface is the same on both sides of the interface,

$$E_1^+ + E_1^- = E_2^+ + E_2^- . \quad (1.54)$$

The same holds for the magnetic field,

$$H_{1x}^+ + H_{1x}^- = H_{2x}^+ + H_{2x}^- . \quad (1.55)$$

Using Maxwell's equation

$$\vec{k} \times \vec{E} = \frac{\mu\omega}{c} \vec{H} . \quad (1.56)$$

to express the magnetic field  $\vec{H}$  in Eq. (1.55) in terms of  $\vec{E}$ ,

$$\frac{\mu_1\omega}{c} H_{1x}^+ = -k_{1z} E_1^+ \quad , \quad \frac{\mu_1\omega}{c} H_{1x}^- = k_{1z} E_1^- . \quad (1.57)$$

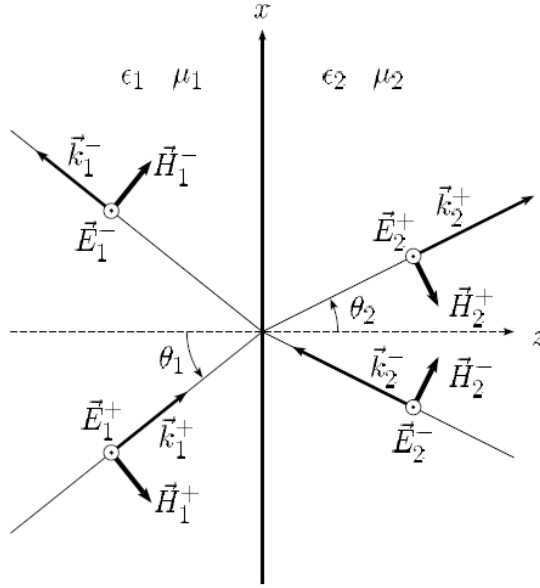


Figure 1.5. Scattering of electromagnetic waves at an interface: TE case.

and similar relations for the field in the second medium. Here,  $k_{1z}$  is the z-component of the wave vector in medium 1. Note that, the right-hand side of the second part of Eq.(1.57) has the opposite sign because the wave  $E_1^-$  propagates in the opposite direction. Inserting Eq.(1.57) into the Eq.(1.55), we obtain

$$-\frac{k_{1z}c}{\mu_1\omega}E_1^+ + \frac{k_{1z}c}{\mu_1\omega}E_1^- = -\frac{k_{2z}c}{\mu_2\omega}E_2^+ + \frac{k_{2z}c}{\mu_2\omega}E_2^-. \quad (1.58)$$

Equation (1.58) together with Eq.(1.54) can be written in a matrix form as

$$\begin{pmatrix} 1 & 1 \\ -\frac{k_{1z}}{\mu_1} & +\frac{k_{1z}}{\mu_1} \end{pmatrix} \begin{pmatrix} E_1^+ \\ E_1^- \end{pmatrix} = \begin{pmatrix} 1 & 1 \\ -\frac{k_{2z}}{\mu_2} & +\frac{k_{2z}}{\mu_2} \end{pmatrix} \begin{pmatrix} E_2^+ \\ E_2^- \end{pmatrix}, \quad (1.59)$$

which expresses the electric field on one side of the interface in terms of the electric field on the other side of the interface. Eq.(1.67) can be written as

$$\begin{pmatrix} E_2^+ \\ E_2^- \end{pmatrix} = M^{(s)} \begin{pmatrix} E_1^+ \\ E_1^- \end{pmatrix}, \quad (1.60)$$

with the transfer matrix  $M^{(s)}$  is given by [1]



$$M^{(s)} = \frac{1}{2} \begin{pmatrix} 1 + \frac{\mu_2 k_{1z}}{\mu_1 k_{2z}} & 1 - \frac{\mu_2 k_{1z}}{\mu_1 k_{2z}} \\ 1 - \frac{\mu_2 k_{1z}}{\mu_1 k_{2z}} & 1 + \frac{\mu_2 k_{1z}}{\mu_1 k_{2z}} \end{pmatrix}. \quad (1.61)$$

For transverse magnetic polarization, shown in Fig.1.6, we have the magnetic field vector  $\vec{H}$  parallel to the interface and, therefore, it has only one component  $\vec{H} = (0, H_y, 0)$ .

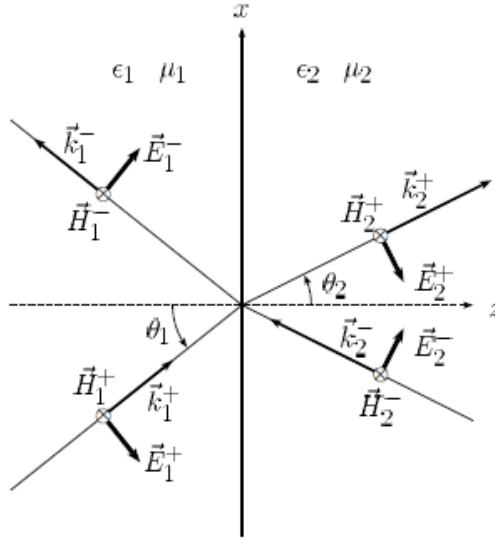


Figure 1.6.Scattering of an electromagnetic wave at an interface: TM case.

The electric field vector  $\vec{E}$  has two components  $\vec{E} = (E_x, 0, E_z)$ . Following the same procedure used for the TE polarization, we get

$$\tilde{M}^{(p)} = \frac{1}{2} \begin{pmatrix} 1 + \frac{\varepsilon_2 k_{1z}}{\varepsilon_1 k_{2z}} & 1 - \frac{\varepsilon_2 k_{1z}}{\varepsilon_1 k_{2z}} \\ 1 - \frac{\varepsilon_2 k_{1z}}{\varepsilon_1 k_{2z}} & 1 + \frac{\varepsilon_2 k_{1z}}{\varepsilon_1 k_{2z}} \end{pmatrix}, \quad (1.62)$$

where  $\tilde{M}^{(p)}$  is the transfer matrix for TM-polarization[1].

## 2.10. Transmission and reflection of a plane wave at an interface

### 2.10.1. Plane wave at an interface

Consider a plane wave striking the interface between two media as shown in Fig. 1.7. The electric and magnetic fields are given by the

$$\vec{E}(\vec{r}, t) = \vec{E}_o e^{i(\vec{k} \cdot \vec{r} - \omega t)}, \quad (1.63)$$

$$\vec{H}(\vec{r}, t) = \vec{H}_o e^{i(\vec{k} \cdot \vec{r} - \omega t)}, \quad (1.64)$$

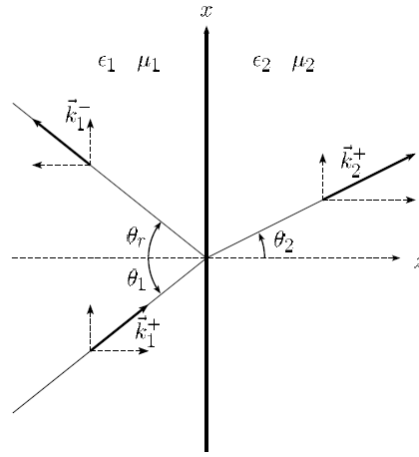


Figure 1.7. Wave vectors for an electromagnetic wave incident on a boundary separating two different media.

where  $\vec{E}_o$  and  $\vec{H}_o$  are the vectors that define the absolute value and the direction of  $\vec{E}(\vec{r}, t)$  and  $\vec{H}(\vec{r}, t)$ , respectively. The two media are characterized by different permittivities  $\epsilon_1$  and  $\epsilon_2$  and permeabilities  $\mu_1$  and  $\mu_2$ .

The coordinate system is chosen such that the interface between the two media is perpendicular to the  $z$ -axis and the plane of incidence. The geometry of the problem is shown in Fig. 1.7. Thus, the wave vector has only two components,

$$\vec{k} = (k_x, 0, k_z). \quad (1.65)$$

The conditions

$$\vec{E}_{1t} = \vec{E}_{2t}, \quad \text{and} \quad \vec{H}_{1t} = \vec{H}_{2t}, \quad (1.66)$$

must be satisfied at any point  $x$  of the interface and the tangential component of the vector  $\vec{k}$ ,  $k_x$ , must be the same for both media

$$k_{1x} = k_{2x} = k_x. \quad (1.67)$$

The explicit form of the dispersion relation  $n^2\omega^2/c^2 = k^2$  between the frequency and wave vector is given by

$$\frac{n_1^2\omega^2}{c^2} = k_1^2 = k_x^2 + k_{1z}^2, \quad n_1 = \sqrt{\mu_1\varepsilon_1}, \quad (1.68)$$

$$\frac{n_2^2\omega^2}{c^2} = k_2^2 = k_x^2 + k_{2z}^2, \quad n_2 = \sqrt{\mu_2\varepsilon_2}, \quad (1.69)$$

for media 1 and 2, respectively. Here,  $k_1$  and  $k_2$  are the absolute values of vectors  $\vec{k}_1$  and  $\vec{k}_2$ , respectively. In the case of planar waves, both components of the wave vector are real, thus an angle of incidence  $\theta_1$  and angle of refraction  $\theta_2$  can be defined as

$$\tan \theta_1 = \frac{k_x}{k_{1z}}, \quad (1.70)$$

$$\tan \theta_2 = \frac{k_x}{k_{2z}}, \quad (1.71)$$

From equation (1.67) we also have that

$$k_x = k_1 \sin \theta_1 = k_2 \sin \theta_2. \quad (1.72)$$

Using Eqs. (1.68), and (1.69) we finally obtain that

$$k_x = n_1 \frac{\omega}{c} \sin \theta_1 = n_2 \frac{\omega}{c} \sin \theta_2. \quad (1.73)$$

Taking the ratio of the two equations in (1.73), we obtain a relation between angles of incidence and reflection, known as Snell's law ,

$$\frac{\sin \theta_1}{\sin \theta_2} = \frac{n_2}{n_1}. \quad (1.74)$$

For the reflected wave, we have from Eqs.(1.68), and (1.69)  $k_1^{-2} = k_1^{+2}$ . As the x-component of the wave vector is preserved, we obtain that

$$k_{1z}^- = -k_{1z}^+. \quad (1.75)$$

The negative sign is due to the opposite direction of propagation of the reflected wave. Consequently, the angle of the propagation of the reflected wave,  $\theta_r = \tan^{-1} \left( k_x / k_{1z}^- \right)$  equals in absolute value the incident angle  $\theta_1$

$$\theta_r = -\theta_1. \quad (1.76)$$

## 2.10.2. Transmission and reflection coefficients

The aim of this subsection is to determine the transmission and reflection coefficients for both TE and TM polarizations.

### 2.10.2.1. The TE Polarization

The transfer matrix  $M^{(s)}$  given by Eq.(1.61) has been derived for the general case when the electromagnetic waves are coming from the left and the right of the interface. Consider now the case when the electromagnetic wave  $E_1^+$  is incident from the left and is scattered on the interface. Part of the wave,  $E_1^-$ , is reflected back, and another

part,  $E_2^+$ , is transmitted through the barrier. Since no wave is incident from medium 2, we designate  $E_2^- = 0$ . Then, we obtain from Eq.(1.60) that

$$E_2^+ = M_{11}^{(s)} E_1^+ + M_{12}^{(s)} E_1^-, \quad (1.77)$$

$$E_2^- = M_{21}^{(s)} E_1^+ + M_{22}^{(s)} E_1^- = 0. \quad (1.78)$$

The transmission and the reflection amplitudes for the electric field are defined as

$$t_s = \frac{E_2^+}{E_1^+}, \quad \text{and} \quad r_s = \frac{E_1^-}{E_1^+}. \quad (1.79)$$

Using the explicit form of the matrix  $M^{(s)}$ , given by Eq.(1.61), we can solve Eqs.(1.77), and (1.78) to obtain

$$t_s = \frac{|M^{(s)}|}{M_{22}^{(s)}} = \frac{2\mu_2 k_{1z}}{\mu_1 k_{2z} + \mu_2 k_{1z}}, \quad (1.80)$$

where  $|M^{(s)}| = \mu_2 k_{1z} / \mu_1 k_{2z}$ , and

$$r_s = -\frac{M_{21}^{(s)}}{M_{22}^{(s)}} = \frac{\mu_2 k_{1z} - \mu_1 k_{2z}}{\mu_1 k_{2z} + \mu_2 k_{1z}}. \quad (1.81)$$

The transmission coefficient is given by the ratio of the energy flows in the two media. Using the relations between  $\vec{E}$  and  $\vec{H}$ , we can express the energy flow perpendicular to the surface can be expressed as

$$S_1 = \frac{c}{8\pi} \text{Re}[\vec{E}_1^+ \times \vec{H}_1^{+*}] = \frac{c}{8\pi} \text{Re}[E_1^+ H_{1x}^{+*}] = \frac{c}{8\pi} \frac{\text{Re } k_{1z}}{\mu_1 \omega} |E_1^+|^2, \quad (1.82)$$

and

$$S_2 = \frac{c}{8\pi} \text{Re}[\vec{E}_2^+ \times \vec{H}_2^{+*}] = \frac{c}{8\pi} \text{Re}[E_2^+ H_{2x}^{+*}] = \frac{c}{8\pi} \frac{\text{Re } k_{2z}}{\mu_2 \omega} |E_2^+|^2. \quad (1.83)$$

Since  $E_2^+ = t_s E_1^+$ , we finally obtain the transmission and reflection coefficients as

$$T_s = \frac{S_2}{S_1} = \frac{\mu_1 \operatorname{Re} k_{2z}}{\mu_2 \operatorname{Re} k_{1z}} |t_s|^2. \quad (1.84)$$

$$R_s = |r_s|^2. \quad (1.85)$$

### 2.10.2.2. The TM Polarization

Following the same procedure used for the TE polarization, the transmission and reflection amplitude can be written as

$$\tilde{t}_p = \frac{|\tilde{M}^{(p)}|}{\tilde{M}_{22}^{(p)}} = \frac{2\varepsilon_2 k_{1z}}{\varepsilon_2 k_{1z} + \varepsilon_2 k_{2z}}, \quad (1.86)$$

$$\tilde{r}_p = -\frac{\tilde{M}_{21}^{(p)}}{\tilde{M}_{22}^{(p)}} = \frac{\varepsilon_2 k_{1z} - \varepsilon_1 k_{2z}}{\varepsilon_2 k_{1z} + \varepsilon_1 k_{2z}}, \quad (1.87)$$

where the transfer matrix  $\tilde{M}^{(p)}$  is given by Eq.(1.62). The tilde was used to emphasize that  $\tilde{t}$  is the transmission amplitude for the magnetic field. The Poynting vectors in this case are given by

$$S_1 = \frac{c}{8\pi} \operatorname{Re}[\vec{E}_1^+ \times \vec{H}_1^{+*}] = \frac{c}{8\pi} \operatorname{Re}[E_{1x}^+ H_1^{+*}] = \frac{c}{8\pi} \frac{\operatorname{Re} k_{1z}}{\varepsilon_1 \omega} |H_1^+|^2, \quad (1.88)$$

with a similar expression for  $S_2$ . The Poynting vector represents the directional energy flux density i.e. the rate of energy transfer per unit area, in units of watts per square meter ( $\text{W}/\text{m}^2$ ) of an electromagnetic field.

The transmission coefficient, given as the ratio of  $S_2/S_1$ , is given by

$$T_p = \frac{\varepsilon_1 \operatorname{Re} k_{2z}}{\varepsilon_2 \operatorname{Re} k_{1z}} |\tilde{t}_p|^2 \quad (1.89)$$

and the reflection coefficient is given by

$$R_p = |\tilde{r}_p|^2 \quad (1.90)$$

It is easy to prove that, in the absence of absorption ( $\text{Re } k_{1z} = k_{1z}$  and  $\text{Re } k_{2z} = k_{2z}$ ), we have

$$T + R = 1. \quad (1.91)$$

for both TE and TM polarizations.

### **2.10.3. Total transmission and total reflection**

#### **2.10.3.1. Total Transmission**

Formulas for the transmission and reflection coefficients can be applied to find the conditions under which the interface is totally transparent. In the absence of absorption

$$T + R = 1. \quad (1.92)$$

The parameters for which the total transmission appears can be obtained by solving the Equations

$$r_s = 0, \quad (1.93)$$

for the TE mode, and

$$r_p = 0, \quad (1.94)$$

for the TM mode.

First, we calculate the conditions of zero reflectance of an interface between two regular dielectrics. The usual result for the Brewster angle will be recovered, where only the p polarization(TM) gives zero reflection. However, if we have an interface between a dielectric and a left-handed medium with negative refractive index, we can have zero reflection for both the TE and TM polarizations. This is a very important result, since we have perfect transmission for both polarizations of electromagnetic waves.

### 2.10.3.2. Brewster Angles

There are special angles of incidence for which the reflection amplitudes

$$r_s = \frac{z_{21} \cos \theta_1 - \cos \theta_2}{z_{21} \cos \theta_1 + \cos \theta_2} = 0 \quad \text{or} \quad \tilde{r}_p = \frac{z_{12} \cos \theta_1 - \cos \theta_2}{z_{12} \cos \theta_1 + \cos \theta_2} = 0 \quad (1.95)$$

where  $z_{21}$  and  $z_{12}$  are defined as

$$z_{21} = \frac{\mu_2 k_1}{\mu_1 k_2} = \sqrt{\frac{\mu_2 \varepsilon_1}{\mu_1 \varepsilon_2}}, \quad z_{12} = \sqrt{\frac{\mu_1 \varepsilon_2}{\mu_2 \varepsilon_1}} \quad (1.96)$$

These angles that satisfy the conditions of Eq.(1.95) are called Brewster angles. The wave incident on an interface with Brewster angle( $\theta_{Bs}$  for TE and  $\theta_{Bp}$  for TM) is totally transmitted through the interface.

It is easy to find analytical expressions for the Brewster angles for both TE and TM polarizations. For instance, for the TE polarization, the Brewster angle  $\theta_{Bs}$  satisfies the equation

$$z_{21} \cos \theta_1 - \cos \theta_2 = 0 \quad (1.97)$$

Squaring and using Snell's law



$$\frac{\mu_2 \varepsilon_1}{\mu_1 \varepsilon_2} \cos^2 \theta_1 + \frac{\mu_1 \varepsilon_1}{\mu_2 \varepsilon_2} \sin^2 \theta_1 = 1. \quad (1.98)$$

If  $\mu_1 = \mu_2$ , then Eq.(1.98) has only trivial solution where  $\varepsilon_1 \equiv \varepsilon_2$  (absence of the interface). Thus, it is clear that for the TE polarization no Brewster angle exists for an interface of two identical dielectrics. However, if  $\mu_2 \neq \mu_1$ , Eq.(1.98) can be solved to give the Brewster angle  $\theta_{Bs}$  as

$$\cos^2 \theta_{Bs} = \frac{\varepsilon_2/\varepsilon_1 - \mu_1/\mu_2}{\mu_2/\mu_1 - \mu_1/\mu_2} \quad (1.99)$$

In a similar manner the Brewster angle  $\theta_{Bp}$  for the p polarized (TM) wave is given by

$$\cos^2 \theta_{Bp} = \frac{\mu_2/\mu_1 - \varepsilon_1/\varepsilon_2}{\varepsilon_2/\varepsilon_1 - \varepsilon_1/\varepsilon_2} \quad (1.100)$$

For nonmagnetic materials,  $\mu_1 = \mu_2$ , the Eq. (1.100) reduces to the well-known result

$$\tan \theta_{Bp} = \frac{n_2}{n_1} \quad (1.101)$$

### 2.10.3.3. Total Reflection

Consider an interface between two dielectrics with  $\mu_1 = \mu_2 = 1$ . If the refractive index  $n_2$  of the second medium is smaller than that of the first medium,  $n_1 > n_2$ . Any incident wave with angle  $\theta_1 > \theta_{crit}$  is totally reflected. One of the most important applications of total internal reflection is the propagation of light through fibers.

Total reflection, however, does not mean that the field is exactly zero on the opposite side of the interface. To calculate the field in the second medium, we start with the dispersion relations. In the first medium we have the following dispersion relation

$$\frac{\omega^2}{c^2} \varepsilon_1 = k_x^2 + k_{1z}^2, \quad (1.102)$$

where

$$k_x = \frac{\omega}{c} \sqrt{\varepsilon_1} \sin \theta_1. \quad (1.103)$$

In the second medium, we have

$$k_{2z} = i\kappa_2, \quad \kappa_2 > 0. \quad (1.104)$$

and the dispersion relation is given by

$$\frac{\omega^2}{c^2} \varepsilon_2 = k_x^2 - \kappa_2^2. \quad (1.105)$$

By solving Eqs.(1.102) and (1.105) for  $\kappa_2$  and substituting Eq.(1.103), we obtain

$$\kappa_2^2 = \frac{\omega^2}{c^2} [\varepsilon_1 \sin^2 \theta_1 - \varepsilon_2] \quad (1.106)$$

It might be more suitable to express  $\kappa_2$  in units of the wavelength of the incident wave as

$$\kappa_2 = \frac{2\pi}{\lambda_1} \sqrt{\sin^2 \theta_1 - \frac{\varepsilon_2}{\varepsilon_1}}, \quad \lambda_1 = \frac{2\pi}{k_1} = \frac{2\pi c}{\omega \sqrt{\varepsilon_1}} \quad (1.107)$$

Alternatively, we have

$$\kappa_2 = \frac{2\pi}{\lambda_1} \sqrt{\frac{\varepsilon_1}{\varepsilon_2} \sin^2 \theta_1 - 1}, \quad \lambda_1 = \frac{2\pi}{k_2} = \frac{2\pi c}{\omega \sqrt{\varepsilon_2}} \quad (1.108)$$

Note that  $\kappa_2$  is indeed real for  $\theta_1 > \theta_{crit}$ .

The transmission and reflection amplitudes of the total reflection can be calculated using the general form of the transfer matrix given by Eq.(1.61) with  $k_{2z} = i\kappa_2$ .

$$t_s = \frac{2i\kappa}{k_{1z} + i\kappa}, \quad (1.109)$$

and

$$r_s = \frac{k_{1z} - i\kappa_2}{k_{1z} + i\kappa_2}. \quad (1.110)$$

We can also show that

$$R_s = |r_s|^2 = 1 \quad (1.111)$$

#### 1.6.3.4. State of the Art

Sina Khorasani and Bizhan Rashidian studied in 2001 the propagation of guided light in dielectric slab waveguides in the presence of interface free charge layer. They show that the density and conductivity of interface free charges can be controlled by a transverse voltage [5].

Feasibility of a new integrated amplitude modulator/switch operation up to the visible spectrum was investigated in 2002 by Sina Khorasani, Alireza Nojeh, and Bizhan Rashidian. Plasma layers are suggested to be generated via the Muller effect at the waveguide's interfaces [6].

The transfer matrix method was modified for studying of optical wave propagation in layered media with conducting interfaces in 2002 by Sina Khorasani and Bizhan Rashidian [7].

Novel optical devices based on surface wave excitation at conducting interfaces were presented in a scientific paper by Khashayar Mehrany, Sina Khorasani, and Bizhan Rashidian in 2003 [8].

The effect of two-dimensional electron plasma formed on the surface of a semiconductor on the surface of a semiconductor on the refraction phase of an optical beam is presented in a scientific paper by Elham Darabi, Sina Khorasani, and Bizhan Rashidian and is published in December 2003 [9].

## Chapter Two

### Analysis of multilayer structure

#### 2.1. Transmission and reflection coefficients for a slab

Consider a slab of thickness  $l$  with permittivity  $\epsilon_2$  and permeability  $\mu_2$ , located between two semi-infinite media with electromagnetic parameters  $(\epsilon_1, \mu_1)$  and  $(\epsilon_3, \mu_3)$  as shown in Fig. 2.1. The transmission and reflection amplitudes for a plane wave arriving from the left for both TE and TM polarizations are investigated here. Transmission through a planar slab is schematically shown in Fig. 2.1. Fortunately, the transfer matrix technique accounts for all the contributions of multiple scattering very efficiently. On the other hand, multiple scattering inside the slab gives some interesting phenomena, such as the Fabry-Pérot resonances in dielectric slabs. First a general formula for the transfer matrix for a slab is derived. Then the transmission of an electromagnetic wave through a dielectric slab is studied. That the problem of transmission through a dielectric slab is very similar to the problem of propagation of a quantum particle through a rectangular potential. This analogy can be used to explain various interesting phenomena, such as resonant transmission and tunneling of an electromagnetic wave through a slab of material which has permittivity smaller than that of the embedding medium.

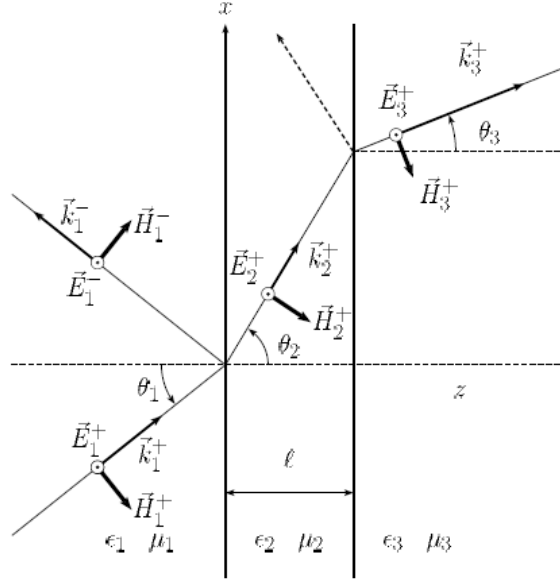


Figure 2.1. Schematic description of the transmission of an electromagnetic wave through a slab with width  $\ell$ .

### 2.1.1. Transmission and Reflection Amplitudes: TE polarization

To find the transfer matrix for the propagation of waves through the slab, the transfer matrix  $\mathbf{M}$  for a single interface is used which was derived in chapter one, where the composition law for transfer matrices is  $\mathbf{M}_{12} = \mathbf{M}_2 \mathbf{M}_1$ . In particular, for the TE polarization, one can write [1]

$$\begin{pmatrix} E_3^+ \\ E_3^- \end{pmatrix} = M_{12} \begin{pmatrix} e^{ik_{2z}\ell} & 0 \\ 0 & e^{-ik_{2z}\ell} \end{pmatrix} M_{23} \begin{pmatrix} E_1^+ \\ E_1^- \end{pmatrix}, \quad (2.1)$$

where the matrices  $M_{12}$  and  $M_{23}$  are given by equation (1.61) and the diagonal matrix

$$\begin{pmatrix} e^{ik_{2z}\ell} & 0 \\ 0 & e^{-ik_{2z}\ell} \end{pmatrix} \quad (2.2)$$

is the transfer matrix for a homogeneous medium  $(\epsilon_2, \mu_2)$  between two interfaces.

Multiplication of the matrices leads to the relation

$$\begin{pmatrix} E_3^+ \\ E_3^- \end{pmatrix} = M_{slab}^{(s)} \begin{pmatrix} E_1^+ \\ E_1^- \end{pmatrix}. \quad (2.3)$$

Explicit expressions for the elements of the matrix  $M_{slab}^{(s)}$  are given by

$$M_{11}^{(s)} = \frac{1}{2} \left[ 1 + \frac{\mu_3 k_{1z}}{\mu_1 k_{3z}} \right] \cos k_{2z} \ell + \frac{i}{2} \left[ \frac{\mu_3 k_{2z}}{\mu_2 k_{3z}} + \frac{\mu_2 k_{1z}}{\mu_1 k_{2z}} \right] \sin k_{2z} \ell, \quad (2.4)$$

$$M_{12}^{(s)} = \frac{1}{2} \left[ 1 - \frac{\mu_3 k_{1z}}{\mu_1 k_{3z}} \right] \cos k_{2z} \ell + \frac{i}{2} \left[ \frac{\mu_3 k_{2z}}{\mu_2 k_{3z}} - \frac{\mu_2 k_{1z}}{\mu_1 k_{2z}} \right] \sin k_{2z} \ell, \quad (2.5)$$

$$M_{22}^{(s)} = \frac{1}{2} \left[ 1 + \frac{\mu_3 k_{1z}}{\mu_1 k_{3z}} \right] \cos k_{2z} \ell - \frac{i}{2} \left[ \frac{\mu_3 k_{2z}}{\mu_2 k_{3z}} + \frac{\mu_2 k_{1z}}{\mu_1 k_{2z}} \right] \sin k_{2z} \ell, \quad (2.6)$$

$$M_{21}^{(s)} = \frac{1}{2} \left[ 1 - \frac{\mu_3 k_{1z}}{\mu_1 k_{3z}} \right] \cos k_{2z} \ell - \frac{i}{2} \left[ \frac{\mu_3 k_{2z}}{\mu_2 k_{3z}} - \frac{\mu_2 k_{1z}}{\mu_1 k_{2z}} \right] \sin k_{2z} \ell. \quad (2.7)$$

The transmission and reflection amplitudes can be obtained as

$$t_s = \frac{E_3^+}{E_1^+} = \frac{|M^{(s)}|}{M_{22}^{(s)}}, \quad r_s = \frac{E_1^-}{E_1^+} = -\frac{M_{21}^{(s)}}{M_{22}^{(s)}}, \quad (2.8)$$

and the corresponding transmission coefficient is given by

$$T_s = \frac{S_3}{S_1} = \frac{\mu_1 \operatorname{Re} k_{3z}}{\mu_3 \operatorname{Re} k_{1z}} |t_s|^2, \quad (2.9)$$

and the reflection coefficient

$$R_s = |r_s|^2. \quad (2.10)$$

### 2.1.2. Transmission and Reflection Amplitudes: TM polarization

Similarly, for the TM mode it is straightforward to show that the elements of the matrix  $M_{slab}^{(p)}$  are given by

$$\tilde{M}_{11}^{(p)} = \frac{1}{2} \left[ 1 + \frac{\varepsilon_3 k_{1z}}{\varepsilon_1 k_{3z}} \right] \cos k_{2z} \ell + \frac{i}{2} \left[ \frac{\varepsilon_3 k_{2z}}{\varepsilon_2 k_{3z}} + \frac{\varepsilon_2 k_{1z}}{\varepsilon_1 k_{2z}} \right] \sin k_{2z} \ell, \quad (2.11)$$

$$\tilde{M}_{12}^{(p)} = \frac{1}{2} \left[ 1 - \frac{\varepsilon_3 k_{1z}}{\varepsilon_1 k_{3z}} \right] \cos k_{2z} \ell + \frac{i}{2} \left[ \frac{\varepsilon_3 k_{2z}}{\varepsilon_2 k_{3z}} - \frac{\varepsilon_2 k_{1z}}{\varepsilon_1 k_{2z}} \right] \sin k_{2z} \ell, \quad (2.12)$$

$$\tilde{M}_{22}^{(p)} = \frac{1}{2} \left[ 1 + \frac{\varepsilon_3 k_{1z}}{\varepsilon_1 k_{3z}} \right] \cos k_{2z} \ell - \frac{i}{2} \left[ \frac{\varepsilon_3 k_{2z}}{\varepsilon_2 k_{3z}} + \frac{\varepsilon_2 k_{1z}}{\varepsilon_1 k_{2z}} \right] \sin k_{2z} \ell, \quad (2.13)$$

$$\tilde{M}_{21}^{(p)} = \frac{1}{2} \left[ 1 - \frac{\varepsilon_3 k_{1z}}{\varepsilon_1 k_{3z}} \right] \cos k_{2z} \ell - \frac{i}{2} \left[ \frac{\varepsilon_3 k_{2z}}{\varepsilon_2 k_{3z}} + \frac{\varepsilon_2 k_{1z}}{\varepsilon_1 k_{2z}} \right] \sin k_{2z} \ell. \quad (2.14)$$

Expressions (2.4)—(2.7) and (2.11)—(2.14) solve the problem of the transmission through a finite planar slab completely.

## 2.2. Multilayer media

Multilayered structures are built up by several thin films which thickness is of the same order of the wavelength of interest. A first approach, to understand the optical properties of these structures, is based on the multiple interferences which a light beam sustains when is reflected by several interfaces. Different transmission spectra can be obtained by changing the thickness and the refractive index of different layers. A second approach to understand the properties consists of inserting a periodic refractive index in the Maxwell equations. Multilayered structure can be considered as a subcase of a wider class of complex structures called Photonic Crystals. A set of approaches will be discussed in this chapter in order to explain the properties of multilayered structures.

### **2.3. Mathematical methods for the analysis and simulation of multilayers**

The development of methods for analyzing multilayer structures is essential to understand their fundamental properties. Any experimental exploration of the multilayers must be accompanied by a quantitative theoretical analysis so that the most interesting cases can be identified, the experimental measurements interpreted, and stable designs for successfully operating devices be found. This section provides an outline of the most widely used numerical techniques that make it possible to determine the optical properties of multilayers. The first, the Transfer Matrix method is the method used for the analysis of the multilayers presented in this work, for this reason it is presented in detail whereas the rest of methods are briefly explained.

#### **2.3.1. Transfer Matrix Method (TMM)**

This is the most widely used method for the mathematical study of one-dimensional structures because it allows the calculation of band diagrams , reflectivity and transmission spectra , emission spectra , guided modes and the modelization of porosity and thickness gradients.

To study the reflection and transmission of electromagnetic waves through a multilayer structure with the TMM method, we consider a one dimensional structure as shown in Fig. 2.2. in which  $n_1$  and  $n_2$  are the layers refractive index,  $h_1$  and  $h_2$  are the thicknesses of the respective layers and  $\Lambda$  is the period of the structure ( $\Lambda = h_1 + h_2$ ).



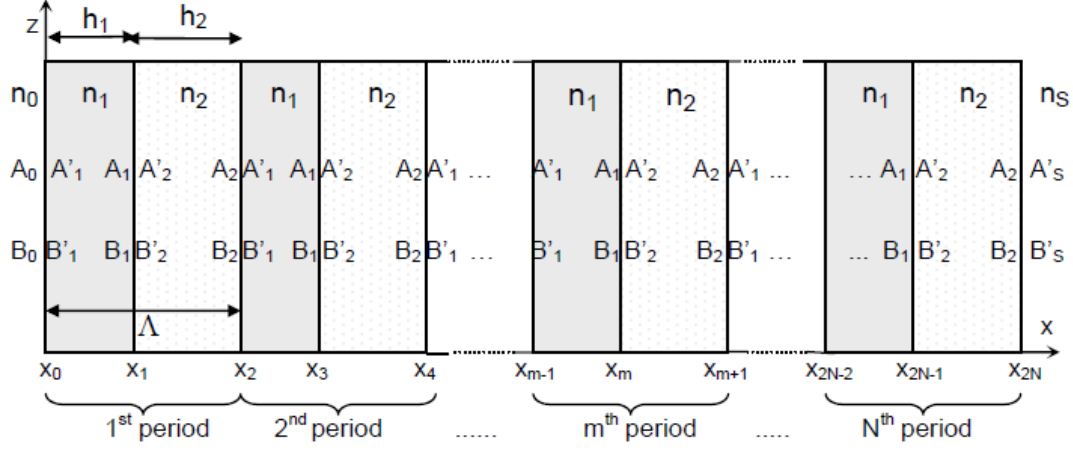


Figure 2.2. Schematic of a multilayer system.  $A_i$  represent the amplitude of the right traveling wave and  $B_i$  that of the left-traveling one. Note that  $A_i$  and  $B_i$  are not continuous at the interfaces.

The dielectric structure is defined by[10]

$$n(x) = \begin{cases} n_0, & x < x_0, \\ n_1, & x_0 < x < x_1 \text{ with } x_1 = x_0 + h_1, \\ n_2, & x_1 < x < x_2 \text{ with } x_2 = x_0 + \Lambda = x_1 + h_2, \\ \vdots & \\ n_s, & x_{2N} < x \text{ with } x_{2N} = x_0 + N\Lambda = x_{2N-1} + h_2, \end{cases} \quad (2.15)$$

with  $n(x) = n(x + \Lambda)$ .  $n_s$  is the substrate refractive index,  $n_0$  is that of the incident medium and  $n_m$  is the refractive index of the  $m$  layer. Layer thicknesses are related to  $x_m$  by  $h_m = x_m - x_{m-1}$  ( $m = 1 \dots 2N$ ), where  $N$  is an integer.

The electric field of a general ++plane-wave solution can be written as  $E = E(x)e^{i(\omega t - \beta z)}$ , where the electric field distribution  $E(x)$  can be written as

$$E(x) = \begin{cases} A_0 e^{-ik_{0x}(x-x_0)} + B_0 e^{ik_{0x}(x-x_0)}, & x < x_0, \\ A_m e^{-ik_{mx}(x-x_m)} + B_m e^{ik_{mx}(x-x_m)}, & x_{m-1} < x < x_m, \\ A'_s e^{-ik_{sx}(x-x_{2N})} + B'_s e^{ik_{sx}(x-x_{2N})}, & x_{2N} < x, \end{cases} \quad (2.16)$$

where  $k_{mx}$  is the  $x$  component of the wave vectors  $k_{mx} = \omega n_m \cos \theta_m / c$  and  $\theta_m$  is the ray angle in each layer.  $A_m$  and  $B_m$  represent the amplitude of the plane waves at interface  $x = x_m$ .

If the two general amplitudes of  $E(x)$  are represented as column vectors,

the plane waves at different layers can be related by

$$\begin{pmatrix} A_{m-1} \\ B_{m-1} \end{pmatrix} = D_{m-1}^{-1} D_m \begin{pmatrix} A'_m \\ B'_m \end{pmatrix} = D_{m-1}^{-1} D_m P_m \begin{pmatrix} A_m \\ B_m \end{pmatrix}, m = 1, 2, \dots, 2N + 1, \quad (2.17)$$

where matrices  $D_m$  are the dynamical matrices given by

$$D_m = \begin{cases} \begin{pmatrix} 1 & 1 \\ n_m \cos \theta_m & -n_m \cos \theta_m \end{pmatrix} & \text{for TE wave} \\ \begin{pmatrix} \cos \theta_m & \cos \theta_m \\ n_m & -n_m \end{pmatrix} & \text{for TM wave} \end{cases} \quad (2.18)$$

and  $P_m$  is the propagation matrix, that can be written as

$$P_m = \begin{pmatrix} e^{ik_{mx}h_m} & 0 \\ 0 & e^{-ik_{mx}h_m} \end{pmatrix}. \quad (2.19)$$

The relation between  $A_0$ ,  $B_0$  and  $A_s$ ,  $B_s$  can thus be written as

$$\begin{pmatrix} A_o \\ B_o \end{pmatrix} = D_o^{-1} [D_1 P_1 D_1^{-1} D_2 P_2 D_2^{-1}]^N D_s = \begin{pmatrix} M_{11} & M_{12} \\ M_{21} & M_{22} \end{pmatrix} \begin{pmatrix} A'_s \\ B'_s \end{pmatrix}, \quad (2.20)$$

where  $N$  is the number of periods in the structure, and  $D_o$  is giving by Eq.(2.18) with  $m=0$ .

The reflectance and transmittance of monochromatic plane waves through the multilayer structure are calculated from the matrix elements. If the light is incident from medium 0, the reflection and transmission coefficients are defined as

$$r = \left( \frac{B_o}{A_o} \right)_{B_s=0}, \quad (2.21)$$

$$t = \left( \frac{A_s}{A_o} \right)_{B_s=0}. \quad (2.22)$$

Using the matrix equation (2.20) and following the definitions in Eqs.(2.21), and (2.22) we obtain

$$r = \frac{M_{21}}{M_{11}}, \quad (2.23)$$

$$t = \frac{1}{M_{11}}. \quad (2.24)$$

Reflectance is given by

$$R = |r|^2 = \left| \frac{M_{21}}{M_{11}} \right|^2, \quad (2.25)$$

provided medium 0 is lossless.

If the bounding media (0,s) are both pure dielectric with real  $n_0$  and  $n_s$ , transmittance T is given by

$$T = \frac{n_s \cos \theta_s}{n_o \cos \theta_o} |t|^2 = \frac{n_s \cos \theta_s}{s_o \cos \theta_o} \left| \frac{1}{M_{11}} \right|^2. \quad (2.26)$$

### 2.3.2. Polynomial approach

In this approach the transfer matrix  $[M]$  can be expressed as the product of interface matrices and layer matrices. The matrix  $[r_j^\alpha]$  of the  $j^{\text{th}}$  interface located at the plane  $z_j$  between two layers of refractive indices  $n_j$  and  $n_{j+1}$  relates the fields on both sides of the interface, i.e.,

$$E^\alpha(z_j - \varepsilon) = [r_j^\alpha] E^\alpha(z_j + \varepsilon), \quad (2.27)$$

where  $\alpha$  stands for either p in p-polarization or for s in s-polarization and  $\varepsilon$  is an infinitely small distance. The interface matrix is given by [11-13]

$$[r_j^\alpha] = \frac{1}{t_{j,j+1}^\alpha} \begin{bmatrix} 1 & r_{j,j+1}^\alpha \\ r_{j,j+1}^\alpha & 1 \end{bmatrix}. \quad (2.28)$$

The propagation of the fields across the same layer with refractive index  $n_j$  between two interfaces located at  $z_{j-1}$  and  $z_j = z_{j-1} + d_j$  is given by the  $j^{\text{th}}$  layer matrix  $[\beta_j]$ , i.e.,

$$E^\alpha(z_{j-1} + \varepsilon) = [\beta_j] E^\alpha(z_j - \varepsilon), \quad (2.29)$$

where the matrix  $[\beta_j]$  is given by

$$[\beta_j] = \begin{bmatrix} e^{i\beta_j} & 0 \\ 0 & e^{-i\beta_j} \end{bmatrix}, \quad (2.30)$$

and  $\beta_j = k_0 n_j \cos \theta_j d_j$  with  $k_0$  is the free space wave number.

The  $M$ -matrix of such a system can be written as the product

$$[M_N^\alpha] = [\beta_1][r_1^\alpha][\beta_2][r_2^\alpha] \dots [\beta_n][r_n^\alpha] \quad (2.31)$$

In this approach, the  $M$ -matrix is then defined in terms of the elementary symmetric functions of the mathematical theory of polynomials [14,15].

### 2.3.3. BCITL Model

Traditionally, the propagation matrix approach is employed to solve problems related to planar multilayer structures rigorously. Alternatively, it is well known that these problems can also be solved readily by modeling these structures using multi-section transmission lines with appropriate characteristic impedances and propagation constants, where each transmission line possesses the same length as of the corresponding layer [16-19].

Recently, it has been shown that lossless multi-section transmission lines can be analyzed successfully using an equivalent model based on the conjugate characteristic-impedance transmission line (CCITL) [17]. By definition, CCITLs are lossless, and possess conjugate characteristic impedances of wave

propagating in opposite directions. CCITLs can be practically implemented using finite lossless periodically loaded transmission lines operated in pass bands. However, CCITLs cannot be used to model lossy multi-section transmission lines. Thus, one needs to resort to more general model for these cases. Anequivalent model based on the bi-characteristic impedance transmission line (BCITL) was employed to model planar multilayer structures effectively for both lossless and lossy cases [17,18]. In general, BCITLs are lossy, and possess different characteristic impedances  $Z_{ob}^{\pm}$   $Z_{ob}^{\pm}$  of wave propagating in opposite directions. Note that BCITLs can be practically implemented using finite lossy periodically loaded transmission lines, and a graphical tool, known as a generalized T-chart, has been recently developed for solving problems associated with BCITLs. It should be pointed out that CCITLs are a special case of BCITLs when associated losses of BCITLs disappear and the pass band operation is assumed.

## 2.4. Applications of multilayer structures

The first applications of multilayer structures were demonstrated more than 50 years ago for such uses as optical interference filters and reflection coatings. During the 1970s, "macro" multilayer films became essential to the semiconductor industry for making everything from computer chips to hard disk drives. In the late 1970s, Barbee pioneered significant advances in the fabrication technology of multilayers for a wide variety of applications in the x-ray, soft (lower energy) x-ray, and extreme ultraviolet regions of the electromagnetic spectrum [20]. For example, high-reflectivity multilayer mirrors have made possible a new class of telescopes for solar physics and astronomical research. Multilayer optics also have found applications in electron microprobes, scanning electron microscopes, x-ray lasers (especially in laser-fusion diagnostic systems), and particle beam lines in accelerators.

Multilayers were used as ultra-compact, high-energy storage, and extremely cost-effective capacitors made up of alternating metal and dielectric layers. Power electronic "snubber" capacitors, normally made of ceramic or polymer dielectrics, and

similar in size to a C battery, are usually connected to much smaller solid-state switching devices. These capacitors typically store 0.1 to 0.2 joules per cubic centimeter capacitor volume and are widely considered the limiting factor in many applications. In contrast, multilayer capacitors would store 10 joules per cubic centimeter while costing perhaps one-twentieth that of ceramic ones.

New application for multilayer structures emerges in the field of thermo-electricity. Current applications of thermoelectric devices include temperature-sensing thermocouples, electric power generators for spacecraft, and portable food and beverage coolers. The development of multilayers has attracted interest that multilayer thermo-electric materials may be the key to taking these devices into the commercial mainstream.

## Chapter Three

### Transmission and reflection in multilayer structures with conducting interfaces

#### 3.1 Basic relations

Before discussing multilayer structure, some basic relations should be introduced.

Maxwell's equations for a plane wave can be written in the following form [1]

$$\vec{k} \times \vec{E} = \frac{\mu\omega}{c} \vec{H}, \quad (3.1)$$

$$\vec{k} \times \vec{H} = -\frac{\varepsilon\omega}{c} \vec{E}, \quad (3.2)$$

$$\vec{k} \cdot \vec{E} = 0, \quad (3.3)$$

$$\vec{k} \cdot \vec{H} = 0. \quad (3.4)$$

Employing Eq. (3.1) to find  $(\vec{k} \times \vec{E}) \cdot (\vec{k} \times \vec{E})$ , the following relation can be obtained

$$|\vec{k}|^2 |\vec{E}|^2 = \left(\frac{\mu\omega}{c}\right)^2 |\vec{H}|^2. \quad (3.5)$$

In a similar manner, Eq. (3.2) gives

$$|\vec{k}|^2 |\vec{H}|^2 = \left(\frac{\varepsilon\omega}{c}\right)^2 |\vec{E}|^2. \quad (3.6)$$

Dividing Eq. (3.5) by Eq. (3.6) gives

$$|\vec{E}| = \sqrt{\frac{\mu}{\epsilon}} |\vec{H}| = \eta |\vec{H}|, \quad (3.7)$$

where  $\eta$  is the intrinsic impedance of the medium which defined as  $\eta = \frac{|\vec{E}|}{|\vec{H}|} = \sqrt{\frac{\mu}{\epsilon}}$ .

### 3.2 Reflection and transmission of a polarized electromagnetic wave at a conducting interface

In this section, the reflection and transmission coefficients at a conducting interface between two media, when illuminated by a polarized TM or TE wave, are studied by direct solution of Maxwell's equations. It is shown that the reflection and transmission behave in a similar manner as when the interface is non-conducting, e.g. obey Fresnel's expression of reflection and transmission coefficient, while having different expressions for the corresponding coefficients.

#### 3.2.1 Reflection and transmission of plane TM polarized light at a conducting interface

The arrangement of two adjacent dielectric semi-infinite slabs is illustrated in Fig.3.1. Here, the y axis is normal and outwards, and the  $z = 0$  or x-y plane represents the interface between medium 1 ( $z < 0$ ) and medium 2 ( $z > 0$ ).

Consider P-polarized wave is incident from media 1 to the interface with an angle of incidence  $\theta_i$ , the incident electric field  $\vec{E}_i(x, z)$  can be expressed as

$$\vec{E}_i(x, z) = \vec{E}_{oi} e^{-i[\vec{k}_i \cdot \vec{r} - \omega t]} \quad (3.8)$$



For TM mode, the electric field has two components (x and z), and at  $t=0$ , Eq. (3.8) becomes

$$\vec{E}_i(x, z) = E_{oi} \{ \cos \theta_i \hat{x} - \sin \theta_i \hat{z} \} e^{-i[\vec{k}_i \cdot \vec{r}]} \quad (3.9)$$

But

$$\vec{k}_i \cdot \vec{r}_i = k_1 \{ x \sin \theta_i + z \cos \theta_i \}, \quad (3.10)$$

where

$$k_1 = \frac{2\pi}{\lambda_1} \equiv \text{wave number in medium 1.} \quad (3.11)$$

So Eq. (3.9) becomes [5]

$$\vec{E}_i(x, z) = E_{oi} \{ \cos \theta_i \hat{x} - \sin \theta_i \hat{z} \} e^{-ik_1(x \sin \theta_i + z \cos \theta_i)}. \quad (3.12)$$

The magnitude of the incident electric field is given by

$$|\vec{E}_i(x, z)| = E_{oi}. \quad (3.13)$$

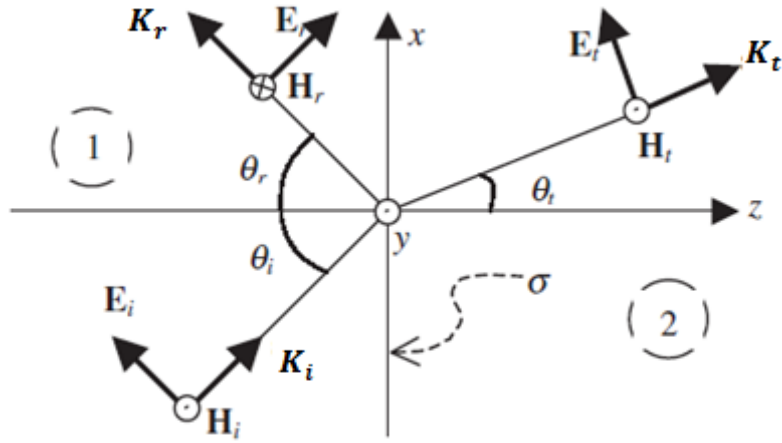


Figure 3.1. Configuration of reflected and refracted waves at an interface for TM mode.

Equation (3.1) can be expanded as

$$\begin{vmatrix} \hat{x} & \hat{y} & \hat{z} \\ k_x & 0 & k_z \\ E_x & 0 & E_z \end{vmatrix} = \frac{\mu_1 \omega}{c} \{H_x \hat{x} + H_y \hat{y} + H_z \hat{z}\}, \quad (3.14)$$

$$(k_z E_x - k_x E_z) \hat{y} = \left( \frac{\mu_1 \omega}{c} \right) H_y \hat{y}. \quad (3.15)$$

Using Eq. (3.7) the incident magnetic field can be written as

$$\vec{H}_i = \frac{|\vec{E}_i|}{\eta_1} \hat{y}, \quad (3.16)$$

$$\vec{H}_i(x, z) = \frac{E_{oi}}{\eta_1} e^{-ik_1(x \sin \theta_i + z \cos \theta_i)} \hat{y}. \quad (3.17)$$

The reflected electric field in medium 1 is given by

$$\vec{E}_r(x, z) = \vec{E}_{or} e^{-i[\vec{k}_r \cdot \vec{r}_r - \omega t]}. \quad (3.18)$$

At  $t=0$ , Eq. (3.18) can be written as

$$\vec{E}_r(x, z) = E_{or} \{\cos \theta_r \hat{x} + \sin \theta_r \hat{z}\} e^{-i[\vec{k}_r \cdot \vec{r}_r]}. \quad (3.19)$$

But

$$\vec{k}_r \cdot \vec{r}_r = k_1 \{x \sin \theta_r - z \cos \theta_r\}. \quad (3.20)$$

So that Eq. (3.19) becomes

$$\vec{E}_r(x, z) = E_{or} \{\cos \theta_r \hat{x} - \sin \theta_r \hat{z}\} e^{-ik_1(x \sin \theta_r - z \cos \theta_r)}. \quad (3.21)$$

The magnitude of reflected electric field will be

$$|\vec{E}_r(x, z)| = E_{or}. \quad (3.22)$$

The reflected magnetic field  $\vec{H}_r$  can be written as

$$\vec{H}_r = \frac{|\vec{E}_r|}{\eta_1} (-\hat{y}), \quad (3.23)$$

$$\vec{H}_r(x, z) = \frac{-E_{or}}{\eta_1} e^{-ik_1(x \sin \theta_r - z \cos \theta_r)} \hat{y}. \quad (3.24)$$

In a similar manner, the transmitted electric field can be written

$$\vec{E}_t(x, z) = E_{ot} \{ \cos \theta_t \hat{x} - \sin \theta_t \hat{z} \} e^{-ik_2(x \sin \theta_t + z \cos \theta_t)}. \quad (3.25)$$

The magnitude of transmitted electric field will be

$$|\vec{E}_t(x, z)| = E_{ot} \quad (3.26)$$

Using Eq. (3.7) yields

$$\vec{H}_t = \frac{|\vec{E}_t|}{\eta_2} \hat{y} \quad (3.27)$$

$$\vec{H}_t(x, z) = \frac{-E_{ot}}{\eta_2} e^{-ik_2(x \sin \theta_t - z \cos \theta_t)} \hat{y} \quad (3.28)$$

Applying the continuity of the tangential components of electric field at  $z = 0$ , gives that [21]

$$(\vec{E}_1 - \vec{E}_2) \times \hat{n}_{12} = 0, \quad (3.29)$$

$$\{(\vec{E}_i + \vec{E}_r - \vec{E}_t) \times \hat{z}\}|_{z=0} = 0 \quad (3.30)$$

$$\begin{aligned} & \left( E_{oi} e^{-ik_1(x \sin \theta_i + 0)} (\cos \theta_i \hat{x} - \sin \theta_i \hat{z}) \right) \times \hat{z} \\ & + \left( E_{or} e^{-ik_1(x \sin \theta_r + 0)} (\cos \theta_r \hat{x} + \sin \theta_r \hat{y}) \right) \times \hat{z} \\ & - \left( E_{ot} e^{-ik_2(x \sin \theta_t + 0)} (\cos \theta_t \hat{x} - \sin \theta_t \hat{y}) \right) \times \hat{z} = 0, \end{aligned} \quad (3.31)$$

and making use of

$$\theta_i = \theta_r, \quad (3.32)$$

$$n_1 \sin \theta_i = n_2 \sin \theta_t, \quad (3.33)$$

the following relations can be obtained

$$(-E_{oi} \cos \theta_i - E_{or} \cos \theta_i) e^{-ik_1 x \sin \theta_i} = -E_{ot} \cos \theta_t e^{-k_2 x \sin \theta_t}. \quad (3.34)$$

Equation (3.34) can be simplified as

$$(E_{oi} + E_{or}) \cos \theta_i = E_{ot} \cos \theta_t = E^{\parallel} (x, 0). \quad (3.35)$$

The current density of a conducting medium is given by Ohm's law[2]

$$\vec{J} = \sigma[\vec{E} + \vec{v} \times \vec{B}] = \sigma \vec{f}, \quad (3.36)$$

where  $\vec{J}$ ,  $\sigma$ ,  $\vec{E}$ ,  $\vec{v}$ ,  $\vec{B}$ , and  $\vec{f}$  are current density, conductivity, electric field, velocity of charges, magnetic field, and the force per unit charge, respectively.

Since no charge motion  $\vec{v} = 0$ , so

$$\vec{J} = \sigma \vec{E}. \quad (3.37)$$

The surface current density for a conducting layer of an effective thickness is much smaller than the wavelength of light can be written as [5, 7, 21, and 22]

$$\vec{J}_s(x) = \sigma \vec{E}^{\parallel} (x, z = 0), \quad (3.38)$$

$$\vec{E}^{\parallel} (x, 0) = \vec{E}_1 \times \hat{n}_{12} = \vec{E}_2 \times \hat{n}_{12}, \quad (3.39)$$

where

$$|\vec{E}^{\parallel} (x, 0)| = (|\vec{E}_i| + |\vec{E}_r|) \cos \theta_i = |\vec{E}_t| \cos \theta_t. \quad (3.40)$$

The magnetic field  $\vec{H}$  at ( $z=0$ ) can also be written as

$$(\vec{H}_1 - \vec{H}_2) \times \hat{n}_{12} = \vec{J}_s(x), \quad (3.41)$$

$$\vec{H}_1 = \vec{H}_i + \vec{H}_r, \quad (3.42)$$

$$\vec{H}_2 = \vec{H}_t, \quad (3.43)$$

$$(\vec{H}_i + \vec{H}_r - \vec{H}_t) \times \hat{z} = \vec{J}_s(x, z = 0). \quad (3.44)$$

Equation (3.44) may be written as

$$\vec{H}_i^{\parallel} + \vec{H}_r^{\parallel} - \vec{H}_t^{\parallel} = J_s \hat{x} \quad (3.45)$$

Substituting (3.17), (3.24), and (3.28) into (3.45) gives

$$\begin{aligned} \frac{E_{oi}}{\eta_1} e^{-ik_1(x \sin \theta_i + z \cos \theta_i)} - \frac{E_{or}}{\eta_1} e^{-ik_1(x \sin \theta_r - z \cos \theta_r)} \\ - \frac{E_{ot}}{\eta_2} e^{-ik_2(x \sin \theta_t + z \cos \theta_t)} = J_s = \sigma |\vec{E}^{\parallel}|, \end{aligned} \quad (3.46)$$

which may be reduced to give

$$(E_{oi} - E_{or}) \frac{1}{\eta_1} = \left( \frac{1}{\eta_2} + \sigma \cos \theta_t \right) E_{ot} \quad (3.47)$$

The Fresnel's reflection and transmission coefficients are given by [4]

$$r = \frac{E_{or}}{E_{oi}}, \quad t = \frac{E_{ot}}{E_{oi}} \quad (3.48)$$

Substituting Eq.(3.35), and Eq.(3.47) into Eq.(3.48) gives[5,21].

$$t_{TM} = \frac{E_{ot}}{E_{oi}} = \frac{2 \cdot \eta_2 \cdot \cos \theta_i}{\eta_2 \cdot \cos \theta_t + \eta_1 \cdot \cos \theta_i (1 + \eta_2 \cdot \sigma \cdot \cos \theta_i \cdot \cos \theta_t)} \quad (3.49)$$

$$r_{TM} = \frac{E_{or}}{E_{oi}} = \frac{\eta_2 \cos \theta_t - \eta_1 \cos \theta_i (1 + \eta_2 \sigma \cos \theta_t)}{\eta_2 \cos \theta_t + \eta_1 \cos \theta_i (1 + \eta_2 \sigma \cos \theta_t)} \quad (3.50)$$

### 3.2.2 Reflection and transmission of plane TE polarized light at a conducting interface

The case of TE polarized light is similar to that of TM with the electric field has only one component (y-direction) and the magnetic field has two components in the x and z directions.

The incident field in medium 1 can be expressed as

$$\vec{E}_i(x, z) = \vec{E}_{oi} e^{-i[\vec{k}_i \cdot \vec{r}_i - \omega t]}, \quad (3.51)$$

with

$$\vec{k}_i \cdot \vec{r}_i = k_1 \{x \sin \theta_i + z \cos \theta_i\}. \quad (3.52)$$

So that Eq. (3.51) reads

$$\vec{E}_i(x, z) = E_{oi} e^{-ik_1[x \sin \theta_i + z \cos \theta_i]} \hat{y}. \quad (3.53)$$

Moreover, the magnitude of the incident electric field is given by

$$|\vec{E}_i(x, z)| = E_{oi}. \quad (3.54)$$

As mentioned above the magnetic field intensity has two components one at the x direction, and the other at the z direction, and at assuming that  $t=0$

$$\vec{H}_i(x, z) = \frac{E_{oi}}{\eta_1} (-\cos \theta_i \hat{x} + \sin \theta_i \hat{z}) e^{-ik_1(x \sin \theta_i + z \cos \theta_i)}, \quad (3.55)$$

with a magnitude

$$|\vec{H}_i(x, z)| = \frac{E_{oi}}{\eta_1} e^{-ik_1(x \sin \theta_i + z \cos \theta_i)} = \frac{|\vec{E}_i(x, z)|}{\eta_1}. \quad (3.56)$$

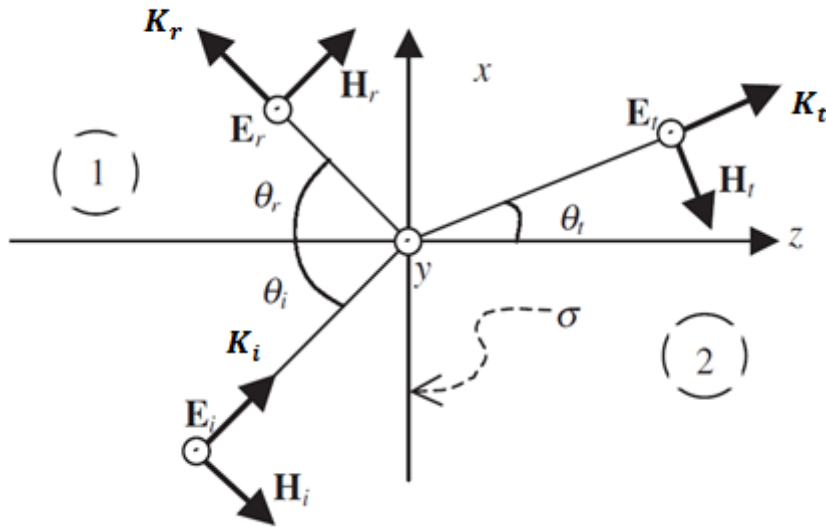


Figure 3.2. Configuration of reflected and refracted waves at an interface between two media for the TE mode.

For the reflected field ( $z < 0$ ) in medium 1, one can write

$$\vec{E}_r(x, z) = \vec{E}_{or} e^{-i[\vec{k}_r \cdot \vec{r}_r - \omega t]}, \quad (3.57)$$

with

$$\vec{k}_r \cdot \vec{r}_r = k_1 \{x \sin \theta_r - z \cos \theta_r\}. \quad (3.58)$$



At  $t=0$ , Eq. (3.57) becomes

$$\vec{E}_r(x, z) = E_{or} e^{-ik_1(x \sin \theta_r - z \cos \theta_r)} \hat{y}. \quad (3.59)$$

The magnitude of the reflected electric field is given by

$$|\vec{E}_r(x, z)| = E_{or}. \quad (3.60)$$

The reflected magnetic field intensity can be written as

$$\vec{H}_r(x, z) = \frac{E_{or}}{\eta_1} (\cos \theta_r \hat{x} + \sin \theta_r \hat{z}) e^{-ik_1(x \sin \theta_r - z \cos \theta_r)}. \quad (3.61)$$

$H_r$  is related to  $E_{or}(x, z)$  by [22]

$$|\vec{H}_r(x, z)| = \frac{|\vec{E}_r(x, z)|}{\eta_1} = \frac{E_{or}}{\eta_1}. \quad (3.62)$$

For the transmitted electric and magnetic fields in medium 2, the following relations are applicable

$$\vec{E}_t(x, z) = \vec{E}_{ot} e^{-i[\vec{k}_t \cdot \vec{r}_t - \omega t]}, \quad (3.63)$$

$$\vec{k}_t \cdot \vec{r}_t = k_2 \{x \sin \theta_t + z \cos \theta_t\}, \quad (3.64)$$

$$\vec{E}_t(x, z) = E_{ot} e^{-ik_2(x \sin \theta_t + z \cos \theta_t)} \hat{y}, \quad (3.65)$$

$$|\vec{E}_t(x, z)| = E_{ot} e^{-ik_2(x \sin \theta_t + z \cos \theta_t)}, \quad (3.66)$$

$$\vec{H}_t(x, z) = \frac{E_{ot}}{\eta_2} (-\cos \theta_t \hat{x} + \sin \theta_t \hat{z}) e^{-ik_2(x \sin \theta_t + z \cos \theta_t)}, \quad (3.67)$$

$$|\vec{H}_t(x, z)| = \frac{E_{ot}}{\eta_2} e^{-ik_2(x \sin \theta_t + z \cos \theta_t)} = \frac{|\vec{E}_t(x, z)|}{\eta_2}. \quad (3.68)$$

Making use of Eqs. (3.48), the Fresnel reflection and transmission coefficient for TE-polarization can be written as [5, 7, 21, and 22]

$$t_{TE} = \frac{2\eta_2 \cos \theta_i}{\eta_2 \cos \theta_i + \eta_1 \cos \theta_t \left(1 + \frac{\eta_2 \sigma}{\cos \theta_t}\right)}, \quad (3.69)$$

$$r_{TE} = \frac{\eta_2 \cos \theta_i - \eta_1 \cos \theta_t \left(1 + \frac{\eta_2 \sigma}{\cos \theta_t}\right)}{\eta_2 \cos \theta_i + \eta_1 \cos \theta_t \left(1 + \frac{\eta_2 \sigma}{\cos \theta_t}\right)} \quad (3.70)$$

### 3.3 Simulation of multilayer structures

#### 3.3.1 Simulation of Bragg reflector with three layers

To demonstrate the reflectance from Bragg reflector in the presence of conducting interfaces, three layer Bragg reflector is assumed. The layer of high refractive index is assumed to be titanium oxide (TiO<sub>2</sub>) and the one with low refractive index is taken to be magnesium fluoride (MgF<sub>2</sub>) on a substrate of glass- silicon dioxide- (SiO<sub>2</sub>)[23-25]. The optical parameters of these layers were taken from the handbook of optical constants of solids [23-25].

Figure 3.3 shows the proposed structure with A represents TiO<sub>2</sub> with high refractive index ( $n_H$ ) and B represents MgF<sub>2</sub> layers with low index of refraction ( $n_L$ ).

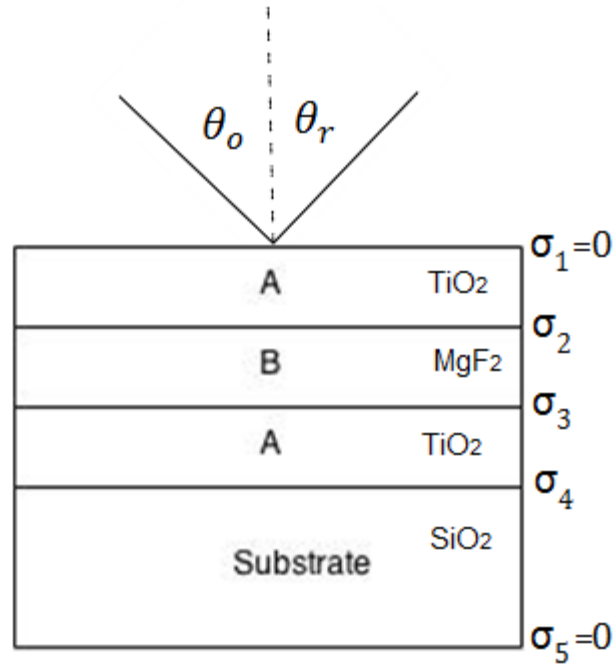


Figure 3.3 Schematic diagram of three-layer Bragg reflector.

To calculate the reflectance of the proposed structure, the transfer matrix, comprising the interface  $[r_i]$  and layer  $[\beta_i]$  matrices, is used [1]

$$M = [\beta_1][r_1][\beta_2][r_2][\beta_3][r_3], \quad (3.71)$$

where  $[\beta_i]$  is the layer matrix of the  $i^{\text{th}}$  layer, and  $[r_i]$  is the interface matrix between the  $(i-1)^{\text{th}}$  and  $i^{\text{th}}$  layer.

The layer matrix of the  $i^{\text{th}}$  layer can be defined as [1,26-28]

$$[\beta_i] = \begin{bmatrix} e^{i\beta_i} & 0 \\ 0 & e^{-i\beta_i} \end{bmatrix}, \quad (3.72)$$

where

$$\beta_i = \left(\frac{2\pi}{\lambda}\right) n_i(d_i) \cos \theta_i, \quad (3.73)$$

and  $d_i$  is the thickness of the  $i^{\text{th}}$  layer,  $n_i$  is the refractive index of the  $i^{\text{th}}$  layer,  $\theta_i$  is the incidence angle at the  $i^{\text{th}}$  layer.

Moreover, the interface matrix is given by [1, 27, and 28]

$$[r_i] = \begin{pmatrix} 1 \\ t_{i,i+1} \end{pmatrix} \begin{pmatrix} 1 & r_{i,i+1} \\ r_{i,i+1} & 1 \end{pmatrix}, \quad (3.74)$$

where  $r_{i,i+1}$  and  $t_{i,i+1}$  are Fresnel's reflection and transmission coefficients between layer  $i$  and layer  $i+1$  respectively.

The reflection from the proposed structure can be calculated from transfer matrix element as [1]

$$r = \frac{M_{2,1}}{M_{1,1}}. \quad (3.75)$$

### 3.3.1.1 Results of simulation of three-layer Bragg reflector

As mentioned before, a three-layer Bragg reflector is assumed where  $\text{TiO}_2$  and  $\text{MgF}_2$  are taken to be the high and low refractive index materials. MATLAB program was used to multiply the interface and layer matrices and to find the elements of the transfer matrix.

The reflection coefficient for p- and s- polarizations are calculated using Eq. (3.50), and Eq. (3.70) respectively. The reflectivity for both polarizations is calculated as [24]

$$R = \frac{R_p + R_s}{2} = \frac{|r_p|^2 + |r_s|^2}{2} \quad (3.76)$$

Moreover we calculate the ellipsometric parameters  $\psi$  and  $\Delta$ , where  $\psi$  measures the amplitude ratio between p- and s- reflection coefficient, and  $\Delta$  measures the phase difference between p- and s- polarization.  $\psi$  and  $\Delta$  are given by [24]:

$$\psi = \tan^{-1} \left( \frac{|r_p|}{|r_s|} \right) \quad (3.77)$$

$$\Delta = \arg \left( \frac{r_p}{r_s} \right) \quad (3.78)$$

A dielectric mirror (Bragg reflector) usually consists of identical alternating layers of high and low refractive indices, as shown in Fig. 3.3. The optical thicknesses are typically chosen to be quarter-wavelength long at some center wavelength  $\lambda_o$ , that is,  $n_H d_H = n_L d_L = \lambda_o/4$ , where  $n_H$  and  $n_L$  are the indices of refraction of the high- and low-index layers, respectively,  $d_H$  and  $d_L$  are the thicknesses of the high- and low-index layers, respectively. Incident angle was taken to be  $18^\circ$ .

The behavior of the reflectivity from three-layer Bragg reflector is studied using the transfer matrix method (TMM) approach.

Figure 3.4 shows the reflectivity for three different values of  $\sigma$ . As can be seen from the figure, increasing the value of  $\sigma$  leads to a slight shift of the reflectivity profile towards higher values of  $\lambda$ .

To study the ellipsometric parameters  $\psi$  and  $\Delta$  for the three-layer Bragg reflector, we consider  $\theta_0 = 18^\circ$ . The importance of  $\psi$  and  $\Delta$  comes from the fact that once they are determined during a measurement at a given wavelength one can invert Fresnel equations to extract the optical parameters of a bulk sample. For a multilayer structure one must perform a spectroscopic ellipsometric scan over a certain spectrum to determine the thickness, the refractive index, and the extinction factor for each layer. Figures 3.5 and 3.6 show respectively  $\psi$  and  $\Delta$  for the three-layer Bragg reflector in the spectral range 350-850 nm. As the figures reveal,  $\psi$  ranges between  $35 - 44^\circ$  whereas  $\Delta$  ranges between  $-5 - 5^\circ$ . Both of them changes slightly with increasing the conductivity of the interface between layers constituting Bragg reflector. As can be seen from Fig. 3.5, the behavior of  $\psi$  with the wavelength for the 3 layer Bragg reflector is opposite of that of the reflectivity. As the conductivity of layers increase  $\psi$  decreases and becomes less flatter within some bandwidth. Also it has sharper edges and tends to  $43^\circ$  which means the complex Fresnel reflection coefficients for p- and s-polarized lights have equal magnitudes. In the spectral region  $\lambda < 400\text{nm}$ , the ellipsometric parameter  $\psi$  oscillates between  $39^\circ$  and  $43^\circ$ .

Figure 3.6 shows that the phase difference  $\Delta$  between p- and s- polarized lights is enhanced with increasing of  $\sigma$ . This enhancement is barely detected for  $\sigma = 0.1$  and it is relatively observable for  $\sigma = 0.3$ .

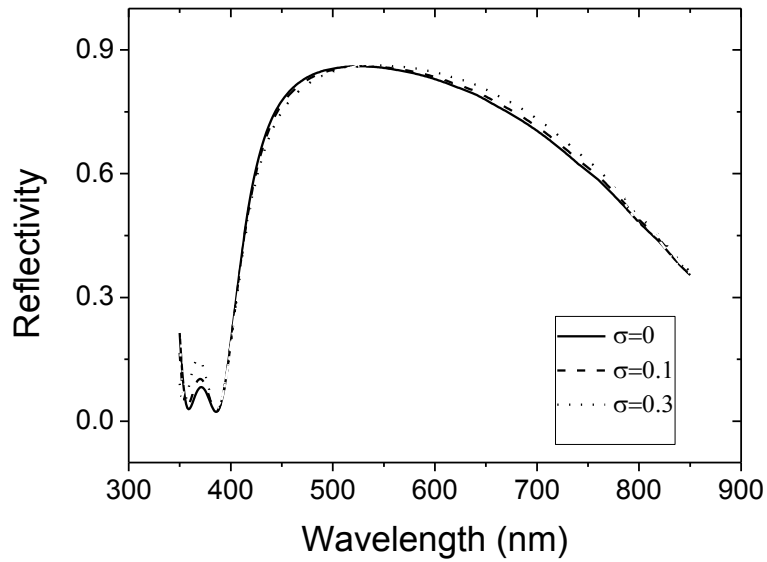


Figure 3.4. Calculated reflectivity of three-layer-quarter-wavelength Bragg reflector, at  $\theta_o = 18^\circ$  in the spectral range of 350-850 nm for different values of  $\sigma$ .

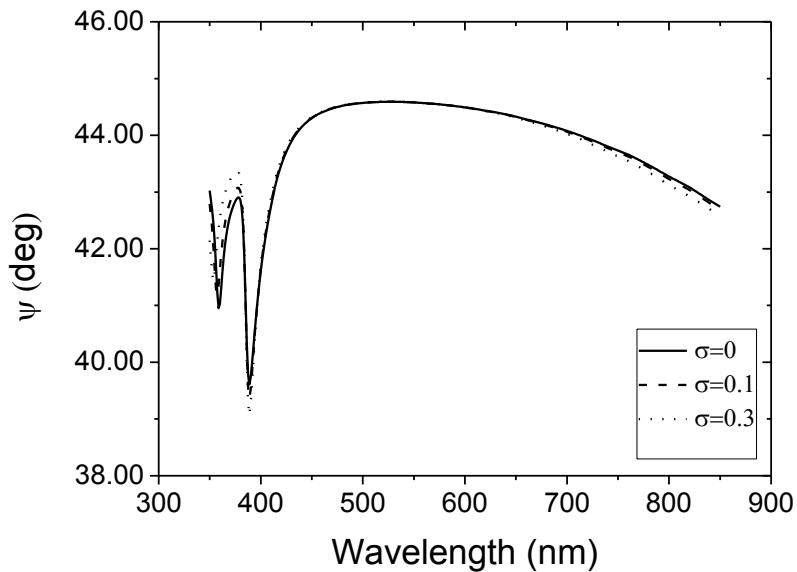


Figure 3.5. The ellipsometric parameter  $\psi$  of three-layer-quarter-wavelength Bragg reflector, at  $\theta_o = 18^\circ$  in the spectral range of 350-850 nm for different values of  $\sigma$ .

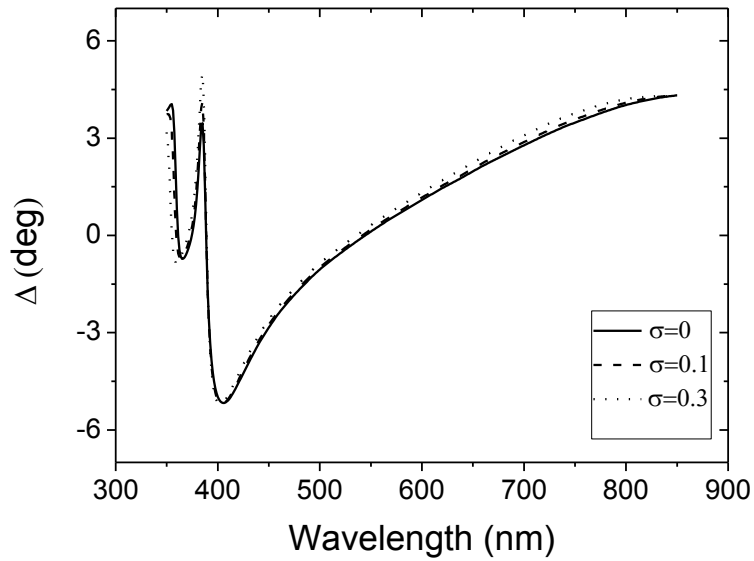


Figure 3.6. The ellipsometric parameter  $\Delta$  of three-layer-quarter-wavelength Bragg reflector, at  $\theta_o = 18^\circ$  in the spectral range of 350-850 nm for different values of  $\sigma$ .

### 3.3.2 Simulation of a Bragg reflector with five layers

It is considered that we have five-layers Bragg reflector. The first, the third, and the fifth layers are made of  $\text{TiO}_2$  which have high refractive index compared with the second and fourth layers which are made of  $\text{MgF}_2$  which have low refractive index. The substrate is made of  $\text{SiO}_2$ .

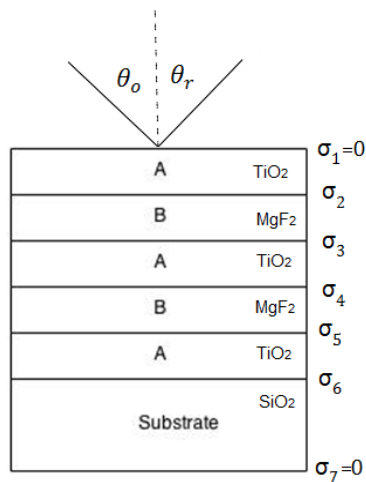


Figure 3.7. Structure of Bragg reflector of five layers

As same as three-layers Bragg reflector , to calculate the reflectance for this structure, the transfer matrix for the structure is given by [1]

$$M = [\beta_1][r_1][\beta_2][r_2][\beta_3][r_3][\beta_4][r_4][\beta_5][r_5] \quad (3.79)$$

### 3.3.2.1 Result of simulation of Bragg reflector with five layers

The behavior of the reflectivity from Brag reflector for the case of 5layer Bragg reflectoris investigated using the TMM approach as shown in Fig. 3.8. The reflectivity rises and becomes flatter as the conductivity between the layers increases within the bandwidth  $\Delta\lambda$ . Figures 3.9 and 3.10 show respectively  $\psi$  and  $\Delta$  for the 5-layer Bragg reflector in the spectral range 350-850 nm. As the figures reveal,  $\psi$  ranges between  $31.5^\circ - 48.7^\circ$  whereas  $\Delta$  ranges between  $-15^\circ - 25^\circ$ .

The effect of increasing  $\sigma$  on  $\psi$  is not significant except in the IR region for  $\lambda > 840$  nm. However considerable effect of increasing  $\sigma$  on  $\Delta$  can be seen from Fig. 3.10 for  $\lambda > 700$  nm.

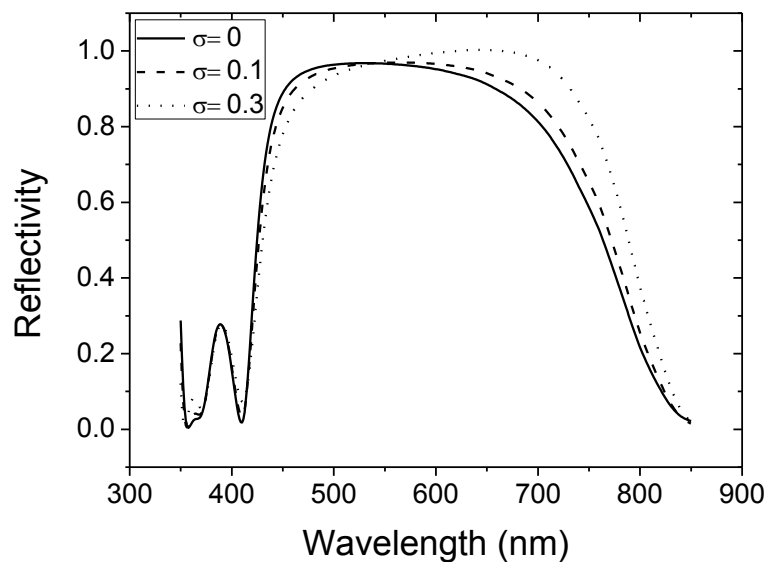


Figure 3.8. Calculated reflectivity of five-layer-quarter-wavelength Bragg reflector, at  $\theta_o = 18^\circ$  in the spectral range of 350-850 nm for different values of  $\sigma$ .



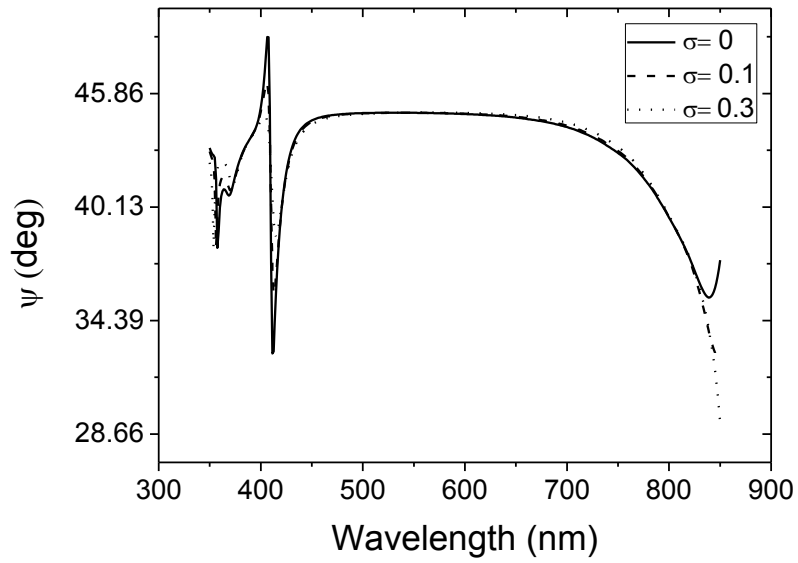


Figure 3.9. The ellipsometric parameter  $\psi$  of five-layer-quarter-wavelength Bragg reflector, at  $\theta_o = 18^\circ$  in the spectral range of 350-850 nm for different values of  $\sigma$ .

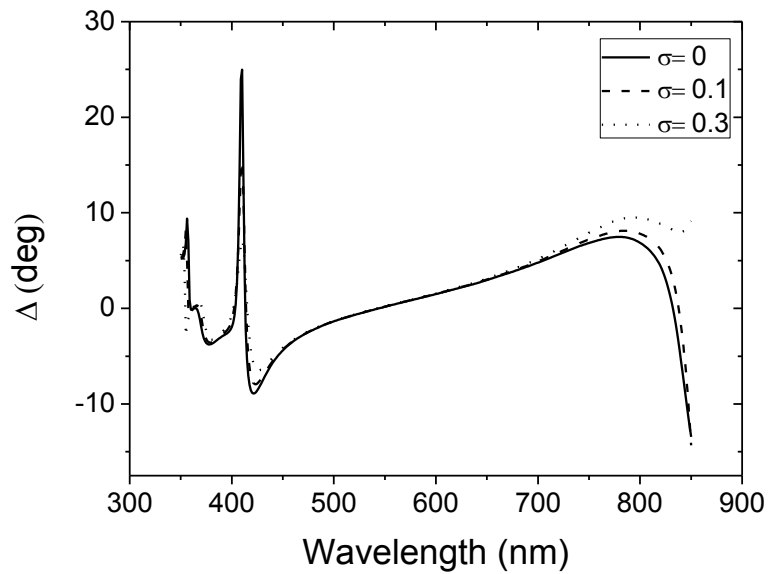


Figure 3.10. The ellipsometric parameter  $\Delta$  of five-layer-quarter-wavelength Bragg reflector, at  $\theta_o = 18^\circ$  in the spectral range of 350-850 nm for different values of  $\sigma$ .

## Chapter Four

### Manipulation of the conducting interfaces in multilayer structures

In this chapter, Bragg reflector is considered with conducting interfaces. Sina Khorasani a Persian professor discussed in many research papers the behavior of light with conducting interfaces. He explains the accumulation of surface charges which comes either from misbalance between Fermi levels of the adjacent dielectrics or from trapped electrons or holes in the quantum wells across the valence and conducting bands, or from trapping of charge due to lattice imperfections[5,7,8]. Many Bragg reflector configurations are assumed. For each configuration the transfer matrix is derived to find the reflectivity and phase angle. These parameters are studied in details with the wavelengths of the incident light, angle of incidence and the applied voltage.

#### 4.1 Three-layer Bragg reflector with conducting interfaces and transverse voltage

A dc voltage is considered to be applied to a three-layer Bragg reflector with a conducting interface between the last high index layer and the substrate. The interface conductivity can be calculated according to the following expression[5,24]

$$\sigma = -i \frac{e|q_s|}{m^* \omega}, \quad (4.1)$$

where  $\sigma$ ,  $e$ ,  $|q_s|$ ,  $m^*$  and  $\omega$  are interface conductivity, electron charge, charge density, effective mass of electron, and angular frequency of light respectively.

This conducting interface is generated due to interface charge of two dielectrics, and is generally composed of the depletion layer, which results from the initial misbalance between the Fermi levels of the adjacent dielectrics. The depletion layer charge is formed by the ionized impurities and thus it is not mobile. Therefore, its contribution to the interface conductivity should be described by a positive sign, resulting in a net increment in local permittivity [5, 7, and 8].

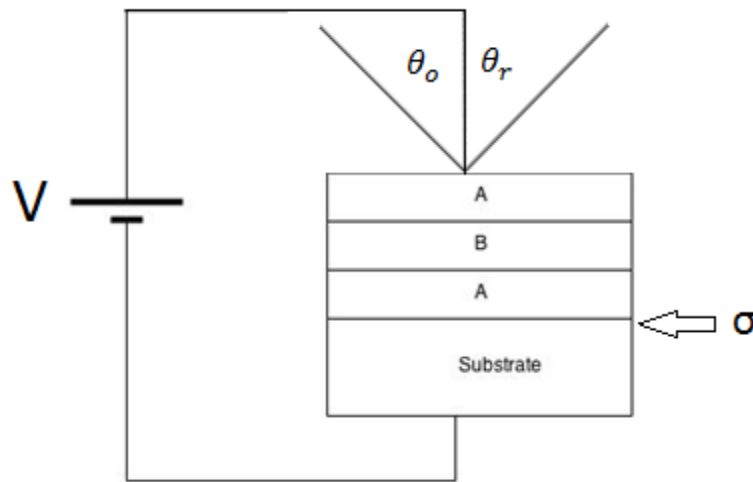


Figure 4.1. Three-layer Bragg reflector with an applied voltage V.

The charge density in the  $i^{\text{th}}$  layer can be calculated using the following expression [5, 7, 8, and 25]

$$|q_{i,i+1}| = \left| \frac{\varepsilon_{i+1}\rho_{i+1} - \varepsilon_i\rho_i}{d_s\rho_s + d_i\rho_i + d_{i+1}\rho_{i+1}} \right| V, \quad (4.2)$$

where  $\varepsilon_i$ ,  $\rho_i$ , and  $d_i$  represent permittivity, resistivity, and thickness of the  $i^{\text{th}}$  layer respectively. V is the transverse voltage that is applied to the multi-layer structure.

Electric resistivity quantifies how strongly a given material opposes the flow of electric current. A low resistivity indicates a material that readily allows the movement of electric charge.

Substituting from Eq. (4.2) into Eq. (4.1), gives

$$\sigma_i = -i \frac{e V}{m^* \omega} \left| \frac{\epsilon_{i+1} \rho_{i+1} - \epsilon_i \rho_i}{d_s \rho_s + d_i \rho_i + d_{i+1} \rho_{i+1}} \right|. \quad (4.3)$$

In a similar manner to the mathematical treatment developed in chapter three, the transfer matrix of the three-layer structure shown in Fig. 4.1 is given in terms of the layer and interface matrices as

$$M = [\beta_1][r_1][\beta_2][r_2][\beta_3][r_3], \quad (4.4)$$

where

$$[\beta_i] = \begin{bmatrix} e^{i\beta_i} & 0 \\ 0 & e^{-i\beta_i} \end{bmatrix}, \quad (4.5)$$

$$\beta_i = \left( \frac{2\pi}{\lambda} \right) n_i(d_i) \cos \theta_i, \quad (4.6)$$

and

$$[r_i] = \begin{pmatrix} 1 \\ t_{i,i+1} \end{pmatrix} \begin{pmatrix} 1 & r_{i,i+1} \\ r_{i,i+1} & 1 \end{pmatrix}, \quad (4.7)$$

$r_{i,i+1}$  is a Fresnel's reflection coefficient, and  $t_{i,i+1}$  is the Fresnel's transmission coefficient. Thus the reflectance,  $\psi$ , and  $\Delta$  can be calculated from transfer matrix as the following

$$r_p = \frac{M_{2,1}^p}{M_{1,1}^p}, \quad r_s = \frac{M_{2,1}^s}{M_{1,1}^s}, \quad R = \frac{|r_p|^2 + |r_s|^2}{2}, \quad (4.8)$$

$$\psi = \tan^{-1} \left( \frac{\left| \frac{M_{2,1}^p}{M_{1,1}^p} \right|}{\left| \frac{M_{2,1}^s}{M_{1,1}^s} \right|} \right), \quad (4.9)$$

$$\Delta = \tan^{-1} \left( \frac{\operatorname{img} \left( \frac{M_{2,1}^p / M_{1,1}^p}{M_{2,1}^s / M_{1,1}^s} \right)}{\operatorname{real} \left( \frac{M_{2,1}^p / M_{1,1}^p}{M_{2,1}^s / M_{1,1}^s} \right)} \right). \quad (4.10)$$

#### 4.2 Five-layer Bragg reflector with conducting interfaces and transverse voltage

The argument mentioned above is now extended to five-layer Bragg reflector.

Figure 4.2 shows the five-layer structure with the applied transverse voltage.

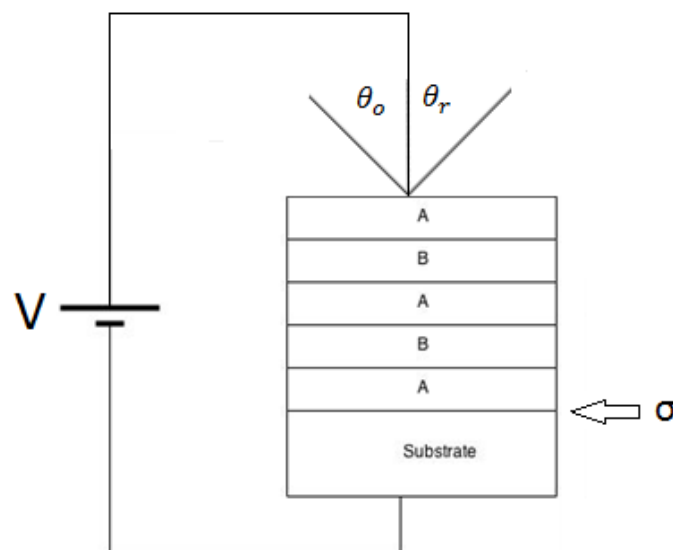


Figure 4.2. Five-layer Bragg reflector with an applied voltage V.

The transfer matrix of the five-layer Bragg reflector can be written in terms of the layer matrix  $[\beta]$ , and interface matrix  $[r]$  as

$$M = \prod_{i=1}^n [\beta_i][r_i], \quad (4.11)$$

where  $n$  is the number of Bragg reflector layers.

After performing the product of matrices given by Eq.(4.11) and obtaining the four-elements of the transfer matrix, the reflectivity,  $\psi$ , and  $\Delta$  can be obtained using Eqs (4.8), (4.9), and (4.10) respectively. And any number of layers can be treated in the same manner.

### 4.3 Simulation results for Bragg reflector

The simulated results of a Bragg reflector with different configurations were performed using MATLAB program, and are discussed in this section. The silicon (Si) is taken as a high refractive index layer, and copper (Cu) is taken as a low refractive index layer. The optical parameters of these layers were taken from the handbook of optical constants of solids [29-31].

The electric resistivity of silicon and copper are taken to be 0.0100 ohm-cm , and 0.00000170 ohm-cm respectively [32-37].

The spectral range is taken to be 400 nm – 850 nm, with a step of 1 nm so the program takes the previous spectral range with 450 points.

Indexing in MATLAB starts with 1, so wavelength of 400 nm is taken as wavelength of index 1, and wavelength of 850 nm is taken as wavelength of index 450.

Thus the center wavelength is with index of  $450/2 + 1$ , which equals 226.

The wavelength corresponding to the index 226 is  $\lambda_o = 625nm$ .

The thicknesses of Si, and SiO<sub>2</sub> are taken depending on the condition of Bragg reflector  $n_H d_H = \lambda_o/4$ , while the thickness of Cu is taken to be 5 nm. The thickness of Cu layer is considered to be very small in order to form a thin conducting layer and at the same time to be penetrable such light can reach the other layers.

Transverse voltages of 0, 1000, and 5000 volt will be applied to the structure. Three-layer, five-layer, nine layer, and fifteen layer structures will be discussed.

### **4.3.1 Investigation of the effect of wavelength and voltage**

#### **4.3.1.1 Results of a three-layer structure**

Three-layer Bragg reflector is assumed in which Si is used as the low index layer, and Cu is used as the high index layer. Transverse voltages of 0V and 1000 V are applied across the three-layer Bragg reflector. Silicon dioxide (SiO<sub>2</sub>) is taken as a substrate layer.

The reflectivity,  $\psi$ , and  $\Delta$  are studied as a function of wavelength in the spectral range from 400nm to 850 nm for an angle of incidence of 20°.

The following figures show the result obtained for the reflectivity,  $\psi$ , and  $\Delta$  using Eqs. (4.8),(4.9),and (4.10).

Figure 4.3.shows the reflectivity from three layer Bragg reflector as a function of the wavelength of the incident light for a transverse voltages of zero, and 1000 volt, and an incidence angle of 20° in the spectral range of 400 nm to 850 nm.

As can be seen from the Fig 4.3, the reflectivity decreases as the wavelength increases of the incident light with a small dip is observed at about 600nm. When a potential difference of 1000 V is applied to the three-layer structure, the shape of curve remains unchanged with a small enhancement in the reflectivity. Moreover there is a small

shift in the dip position towards shorter wavelength with increasing the applied voltage.

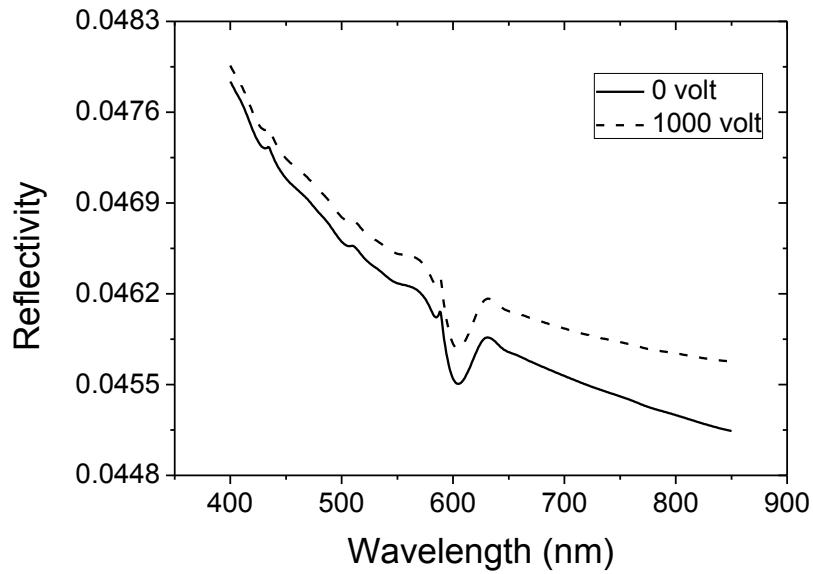


Figure 4.3. Reflectivity from three-layer Bragg reflector for Si-Cu structure for different values of voltage and for  $\theta_i=20^\circ$ .

The difference between the reflectivity values at 1000 V, and 0 V for three-layer Bragg reflector is shown in Fig.4.4. It is clear that it is approximate a linear line with positive slope.

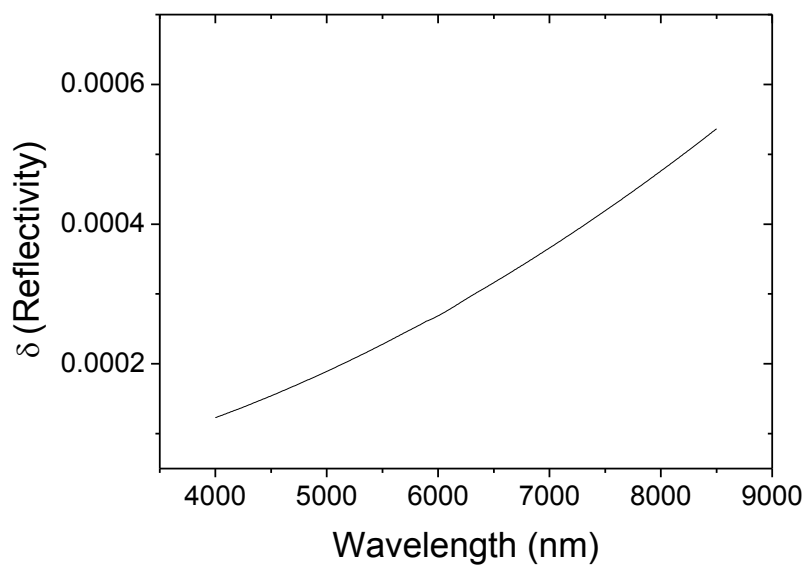


Figure 4.4. Reflectivity difference from three-layer Bragg reflector for Si-Cu



structure for different values of voltage and for  $\theta_i=20^\circ$ .

The ellipsometric parameter  $\psi$  of the three-layer Bragg reflector is shown as y-axis with the wavelength of the incident light as x-axis for two different transverse voltages; 0 and 1000 V in Fig. 4.5. Increasing of the transverse voltage enhances the  $\psi$  value in the spectral range 400 nm to 850 nm. A small dip appears around 600 nm, and it is noticed that there is a slight shift in the dip position towards shorter wavelengths when applying transverse voltage.

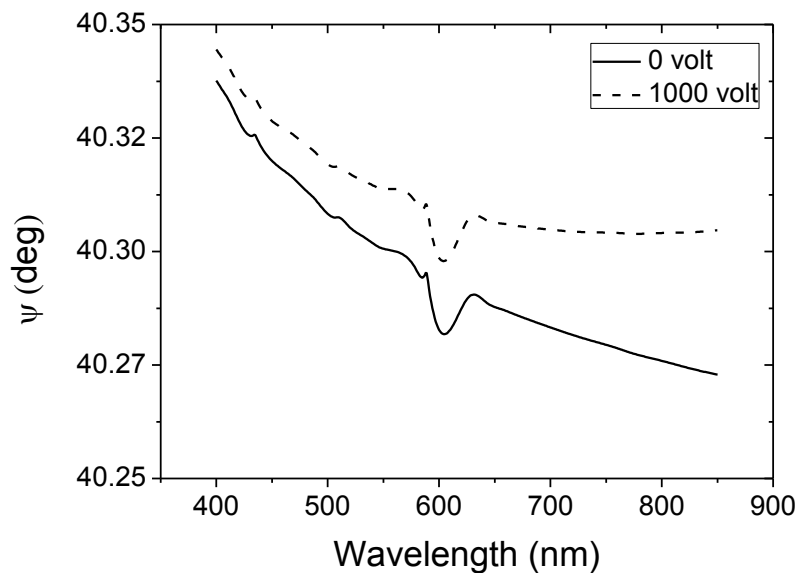


Figure 4.5.  $\psi$  of three-layer Bragg reflector for Si-Cu structure for different values of voltage and for  $\theta_i=20^\circ$ .

It is clear that the curve in Fig.4.6. is approximate a linear line with positive slope. The line represent the difference of values of  $\psi$  between 1000 V, and 0 V values of  $\psi$  for three-layer Bragg reflector.

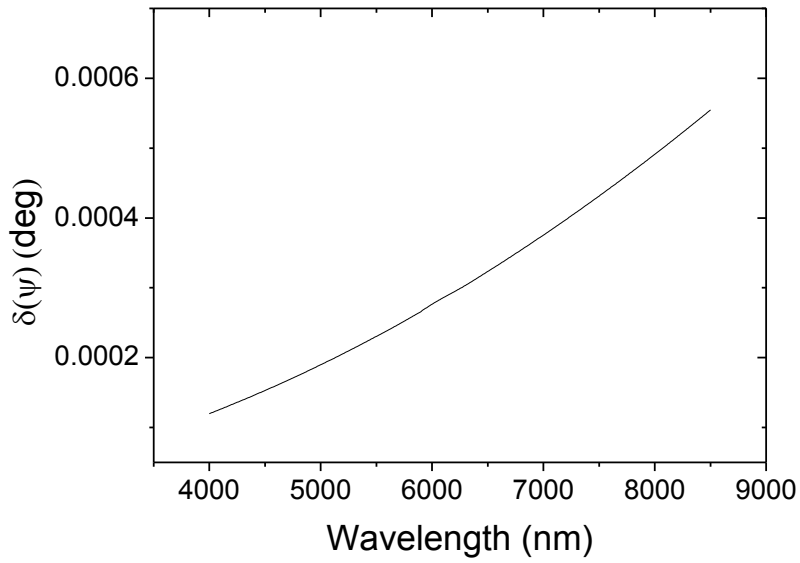


Figure 4.6.  $\psi$  difference of three-layer Bragg reflector for Si-Cu structure for different values of voltage and for  $\theta_i=20^\circ$ .

The Phase difference " $\Delta$ " between the two components of light equals zero when applying no transverse voltage, and it changes gradually from -0.1 degree to -0.7 degree when applying a transverse voltage of 1000 volt. This is shown in Fig. 4.7. in the spectral range of 400nm to 850 nm.

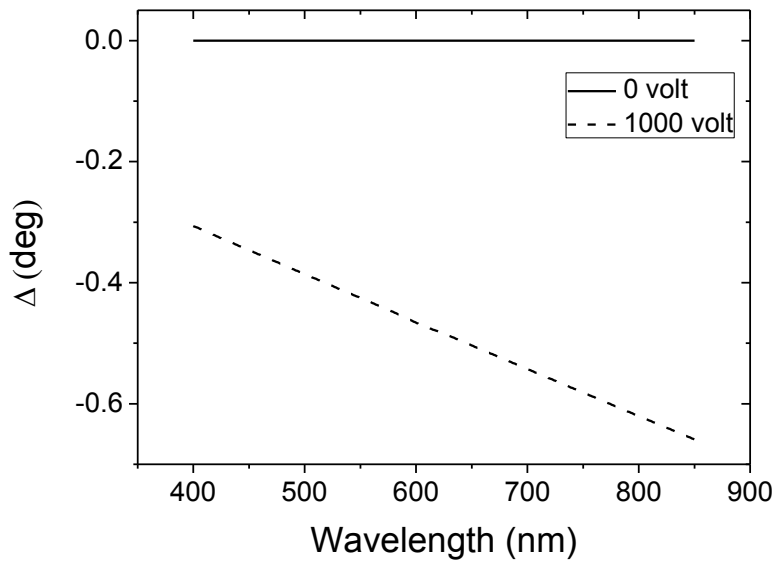


Figure 4.7.  $\Delta$  of three-layer Bragg reflector for Si-Cu structure for different values of voltage and for  $\theta_i=20^\circ$ .

The  $\Delta$  difference of values between 1000 V, and 0 V values of  $\Delta$  for three-layer Bragg reflector is shown in Fig.4.8. It is clear that it is approximate a linear line with negative slope.

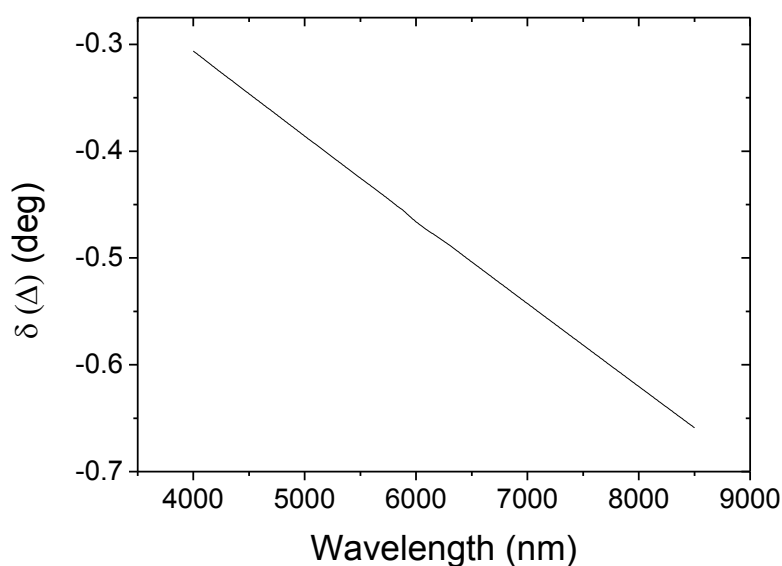


Figure 4.8.  $\Delta$  difference of three-layer Bragg reflector for Si-Cu structure for different values of voltage and for  $\theta_i=20^\circ$ .

#### 4.3.1.2 Results of a five-layer structure

In a similar manner, five-layer Bragg reflector is discussed in this subsection. The following figures show the results obtained for the reflectivity,  $\psi$ , and  $\Delta$ .

Figure 4.9. shows the reflectivity of five layer Bragg reflector versus the wavelength of the incident light for two different transverse voltages; 0 V and 1000 V. The reflectivity increases very fast from 400 nm to about 650 nm, then it becomes stable from 650 nm to 850 nm. The reflectivity value in the stable region is near one. It is clear that increasing of the transverse voltage will dampen the reflectivity in the spectral range 400 nm to 850 nm.

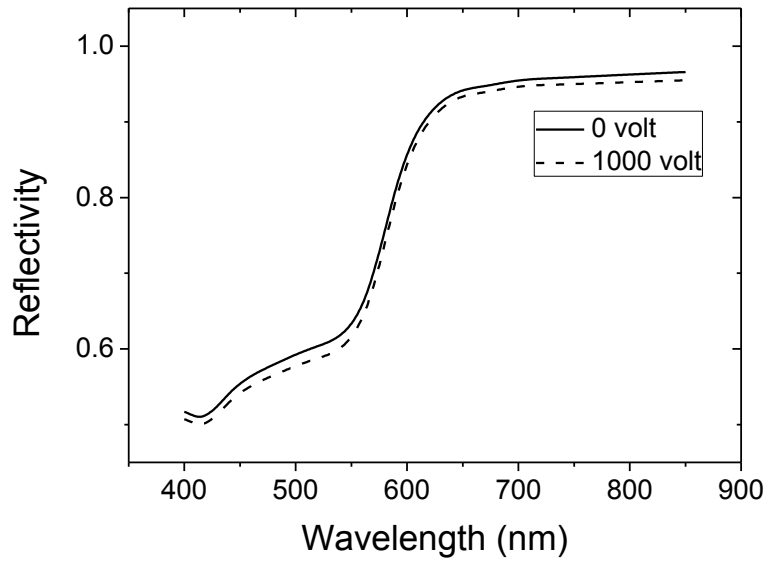


Figure 4.9. Reflectivity of five-layer Bragg reflector for Si-Cu structure for different values of the voltage and  $\theta_i=20^\circ$ .

Figure 4.10. illustrates the ellipsometric parameter  $\psi$  of the five layer Bragg reflector as a function of wavelength for two different transverse voltages; 0 V and 1000 V. It is clear that there is no change of  $\psi$  value when applying 1000 volt across the Bragg reflector in the spectral range 400 nm to 850 nm.

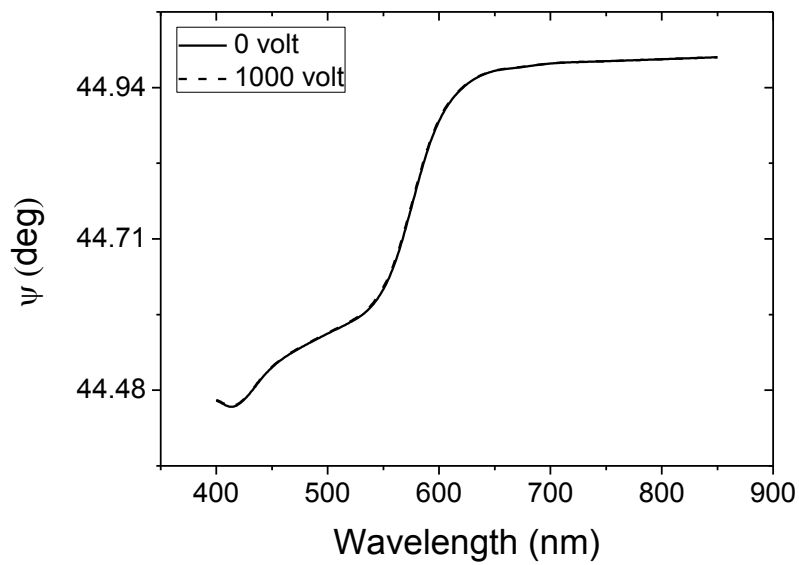


Figure 4.10.  $\psi$  of five-layer Bragg reflector for Si-Cu structure for different values of voltage and  $\theta_i=20^\circ$ .

On the other hand the Phase difference " $\Delta$ " dependence on the wavelength is shown in Fig. 4.11. and is slightly enhanced when applying a transverse voltage of 1000 volt across the five layer Bragg reflector.

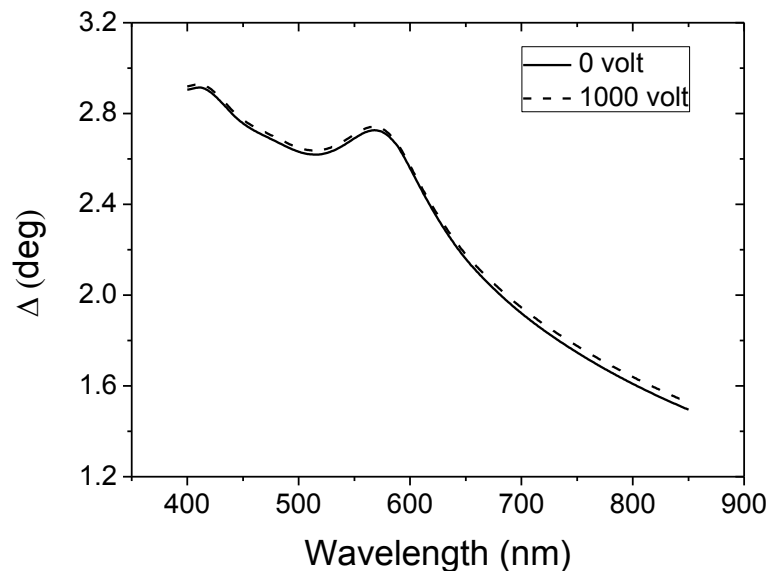


Figure 4.11.  $\Delta$  of five-layer Bragg reflector for Si-Cu structure for different values of voltage and  $\theta_i=20^\circ$ .

#### 4.3.1.3 Results of a nine-layer structure

Reflectivity,  $\psi$ , and  $\Delta$  of nine-layer Bragg reflector will be discussed in this subsection. The following figures show the result obtained for the reflectivity,  $\psi$ , and  $\Delta$ . Figure 4.12. illustrates the reflectivity of nine layer Bragg reflector versus the wavelength of the incident light for two different transverse voltages; 0 V and 1000 V. the variation of the reflectivity with the wavelength of the incident light for nine-layer Bragg reflector is similar to that of five-layer Bragg reflector. The reflectivity increases very fast from 400 nm to about 650 nm, then it becomes more stable from 650 nm to 850 nm as it approaches unity. It is clear that increasing of the transverse voltage will reduce very slightly the reflectivity in the spectral range under study.

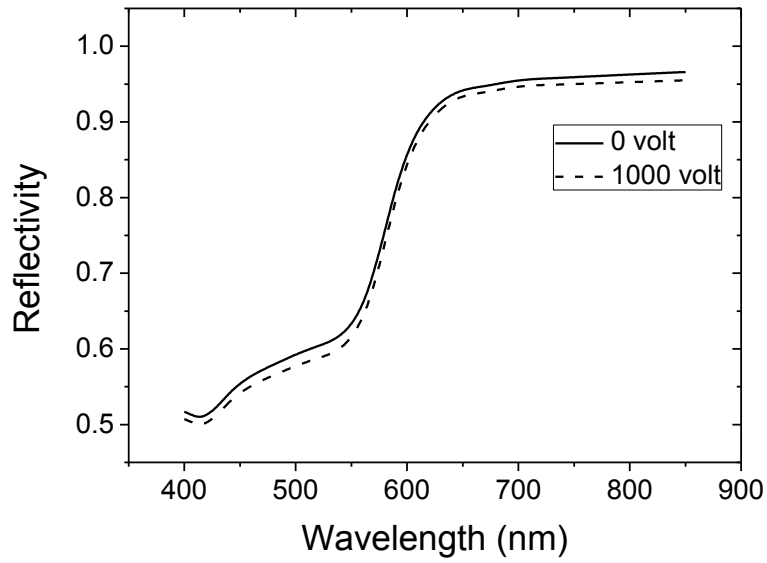


Figure 4.12. Reflectivity of nine-layer Bragg reflector for Si-Cu structure for different values of voltage and for  $\theta_i=20^\circ$ .

Figure 4.13. illustrates  $\psi$  of the nine-layer Bragg reflector as a function of wavelength for two different transverse voltages; 0 V and 1000 V obviously. There is no considerable change of  $\psi$  value when applying 1000 volt across the Bragg reflector in the spectral range under consideration.

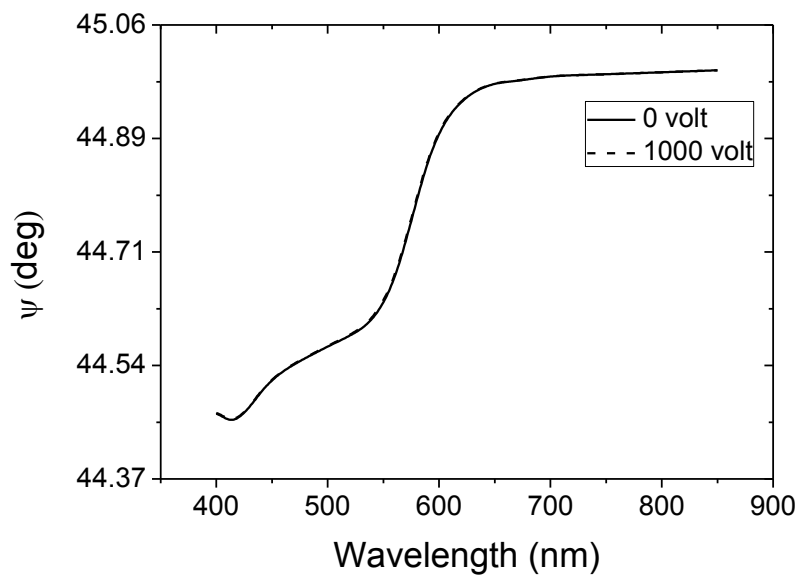


Figure 4.13.  $\psi$  of nine-layer Bragg reflector for Si-Cu structure for different values of voltage and for  $\theta_i=20^\circ$ .

Alternatively The Phase difference " $\Delta$ " is slightly enhanced when applying a transverse voltage of 1000 volt to a nine layer Bragg reflector which is shown in Fig.4.14.

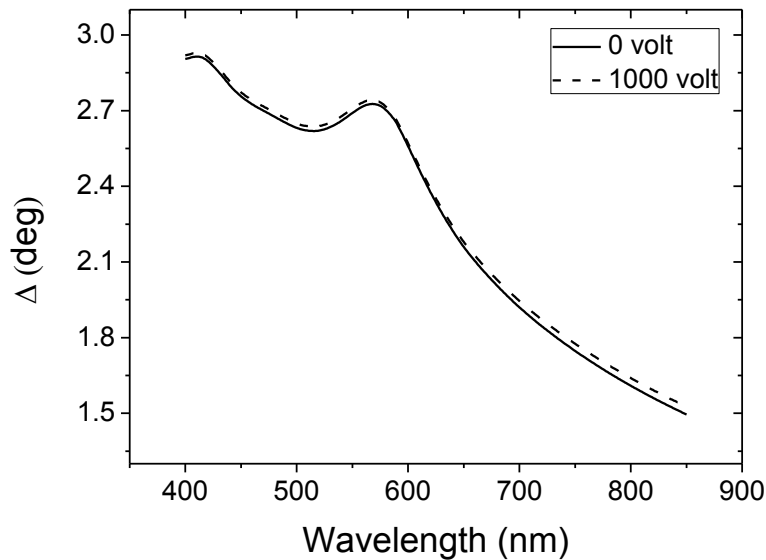


Figure 4.14.  $\Delta$  of nine-layer Bragg reflector for Si-Cu structure for different values of voltage and for  $\theta_i=20^\circ$ .

#### 4.3.1.4 Results for a fifteen-layer structure

The reflectivity versus the wavelength for fifteen-layer Bragg reflector is shown in Fig.4.15. for two values of V. The reflectivity curve for V=0 is similar to that of nine- and five- layer Bragg reflectors. When applying a voltage of 1000 V to the fifteen-layer Bragg reflector, a change in the reflectivity is observed. The reflectivity decreases when applying the voltage. This decrease in the reflectivity is dependent on the wavelengths.

The decrease in reflectivity is enhanced as the wavelength increases. The behavior of  $\psi$  with the wavelength and V is similar to that of the reflectivity as can be seen from Fig.4.16.

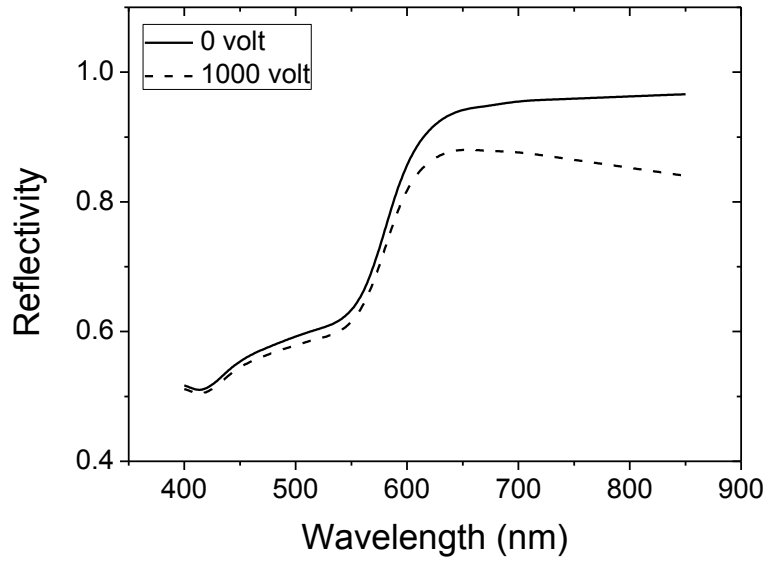


Figure 4.15. Reflectivity of fifteen-layer Bragg reflector for Si-Cu structure for  $\theta_i=20^\circ$ , and with 0, and 1000 volt.

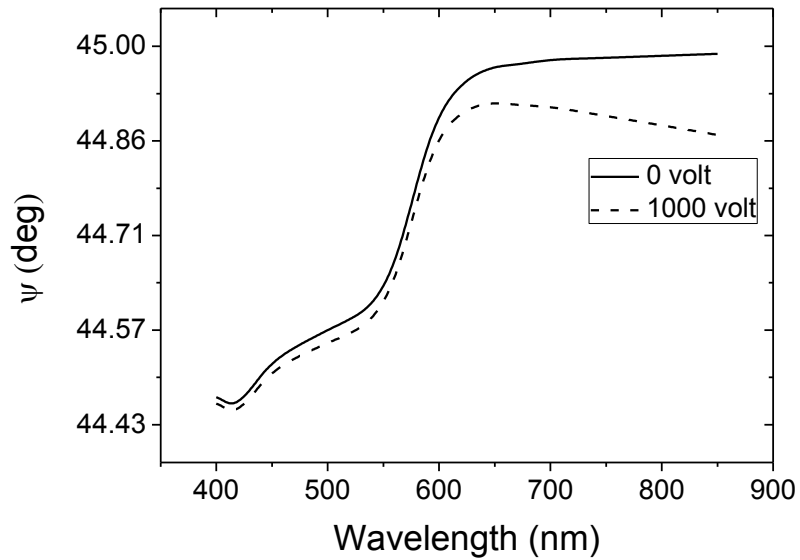


Figure 4.16.  $\psi$  of fifteen-layer Bragg reflector for Si-Cu structure for different values of voltage and for  $\theta_i=20^\circ$ .



The phase difference  $\Delta$  versus the wavelength for a fifteen-layer Bragg reflector is shown in Fig.4.17. for two values of  $V$ . the dependence on  $V$  is very small and it can be seen for  $\lambda > 650$  nm.

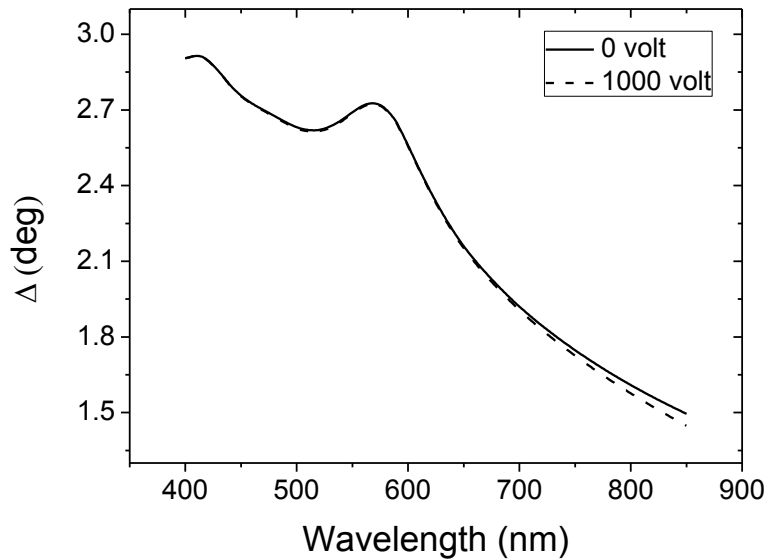


Figure 4.17.  $\Delta$  of fifteen-layer Bragg reflector for Si-Cu structure for different values of voltage and for  $\theta_i=20^\circ$ .

### 4.3.2 Investigation of Bragg reflector with the incident angle, and wavelength.

In this subsection, the effect of varying the applied potential, the angle of incidence, and the wavelength of light on  $R$ ,  $\psi$ , and  $\Delta$  of three Bragg structures will be studied. Three applied potentials will be used. The angle of incidence will be varied from  $0^\circ$  to  $80^\circ$  and four wavelengths of light will be considered.

#### 4.3.2.1 Results of a three-layer Bragg structure

Figures 4.18. and Fig.4.19. show the reflectivity and  $\psi$  as a function of the angle of incidence for different wavelength for a three layer Bragg reflector. The considered wavelengths are 550 nm, 600 nm, 633 nm, and 700 nm.

The light is incidence with different angles, with no transverse voltage. The reflectivity is taken as y-axis , while incidence angle is taken as x-axis in Fig.4.18, while  $\psi$  is taken as y-axis in Fig.4.19.

It can be noticed that the reflectivity increases from 0.045 to 0.394 as the incident angle is changed from  $0^\circ$  to  $80^\circ$ . Moreover, Fig. 4.18.shows no detectable change in the reflectivity with the change in wavelength.

The reflectivity increases remarkably with the angle of incidence. Changing the wavelength of the incident light does not affect the reflectivity profile.  $\psi$  decreases with the angle of incidence and reaches a minimum value at an angle of  $57^\circ$ . In a similar manner to the reflectivity profile, there is no effect of the wavelength of incident light on the  $\psi$  curve.

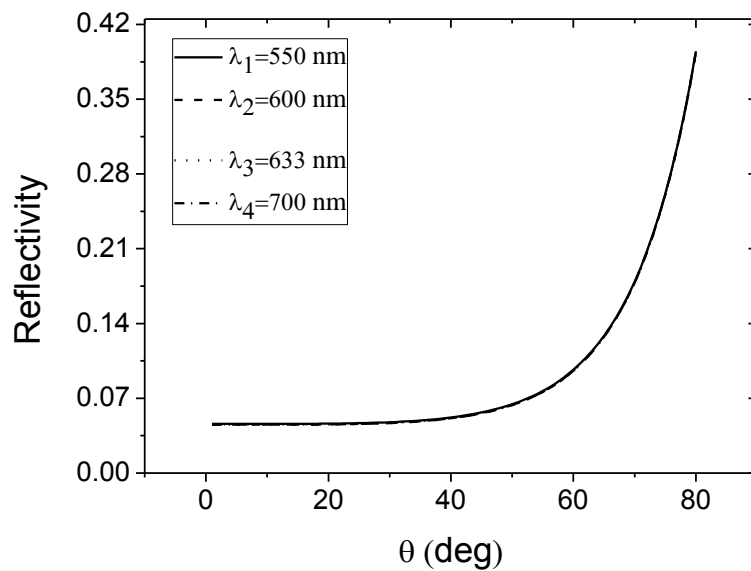


Figure 4.18. Reflectivity of three-layer Bragg reflector for Si-Cu structure versus the incident angle with transverse voltage of 0 volt.

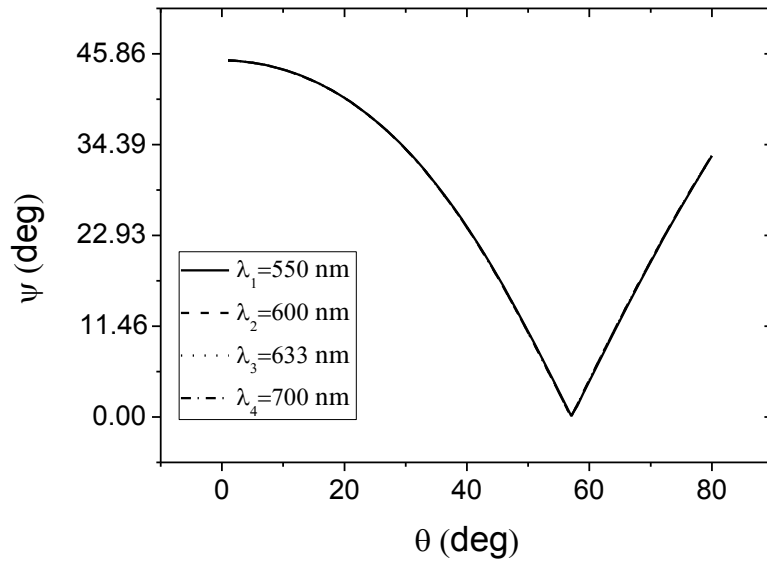


Figure 4.19.  $\psi$  of three-layer Bragg reflector for Si-Cu structure versus the incident angle with transverse voltage of 0 volt.

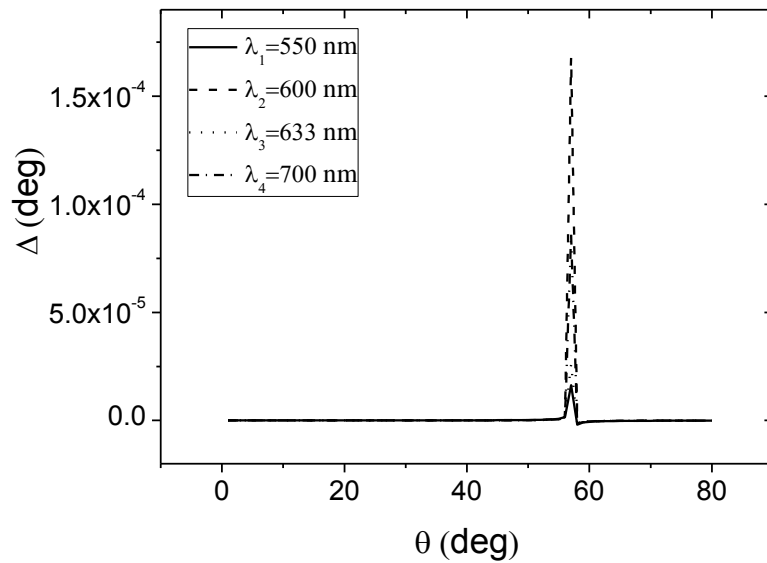


Figure 4.20.  $\Delta$  of three-layer Bragg reflector for Si-Cu structure versus the incident angle with transverse voltage of 0 volt for different values of  $\lambda$ .

Phase difference angle versus the angle of incidence is illustrated in Fig. 4.20. Different wavelengths of incident lights were examined when the transverse voltage equals zero. Figure 4.20 shows a notch behavior around  $\theta_i = 57^\circ$  which is the same

angle for the lowest value of  $\psi$  appears in Fig.4.19. A very slight change of order  $10^{-4}$  of  $\Delta$  with the wavelength of incident light. All other scanned incidence angles do not show a similar behavior.

The reflectivity and  $\psi$  versus the incidence angle for a transverse voltage of 1000 volt, of three layer Bragg reflector do not change with the wavelength except small deviation and curvature of  $\psi$  at the bottom near  $\theta_i = 57^\circ$ . This appears in Fig.4.21., and Fig.4.22.

The huge effect of transverse voltage of 1000 volt appears on the phase difference angle in Fig.4.23. A very rapid decreasing of the Phase difference before  $\theta_i = 57^\circ$ , then also a very rapid increasing after the same angle. The vertical line of  $\theta_i = 57^\circ$ , is as an asymptoting line. Phase difference angles of different wavelengths act in the same manner with very slight difference in values.

Where the applied voltage is zero to the three-layer Bragg reflector,  $\Delta$  is approximately zero for all incidence angles as can be seen in Fig.4.20. where a transverse voltage of 1000 volt is applied to the structure, a significant change in  $\Delta$  curve is observed in the region between  $\theta_i = 50^\circ - 70^\circ$ , especially at  $\theta_i = 57^\circ$  where  $\Delta$  ranges between  $50^\circ$  and  $80^\circ$ . Moreover there is a slight effect of  $\lambda$  on  $\Delta$  curves in the incidence angle range  $50^\circ-70^\circ$ .

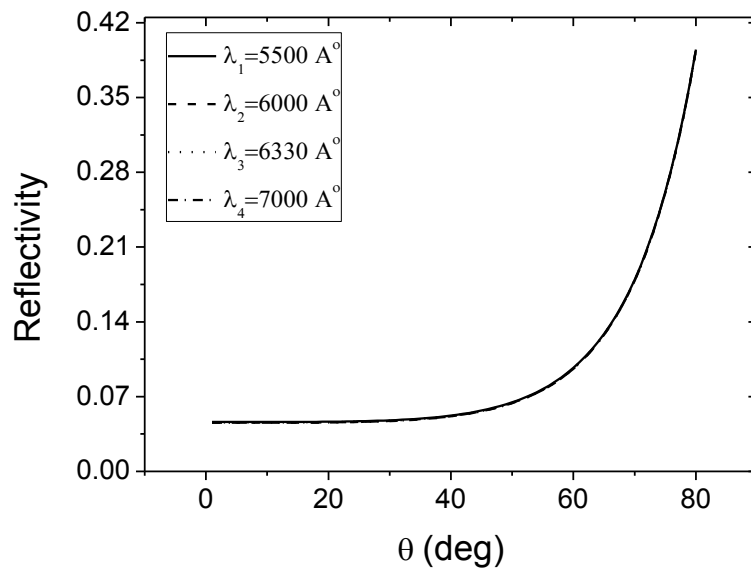


Figure 4.21. Reflectivity of three-layer Bragg reflector for Si-Cu structure versus the incident angle with transverse voltage of 1000 volt

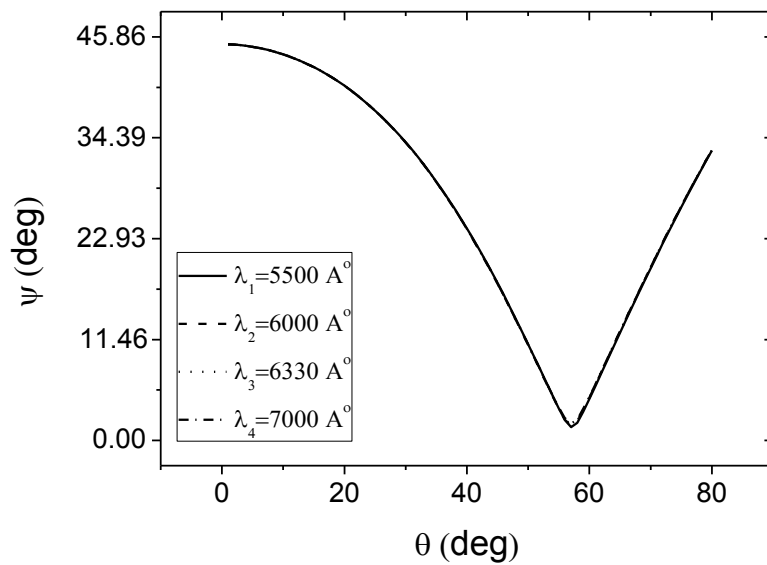


Figure 4.22.  $\psi$  of three-layer Bragg reflector for Si-Cu structure versus the incident angle with transverse voltage of 1000 volt

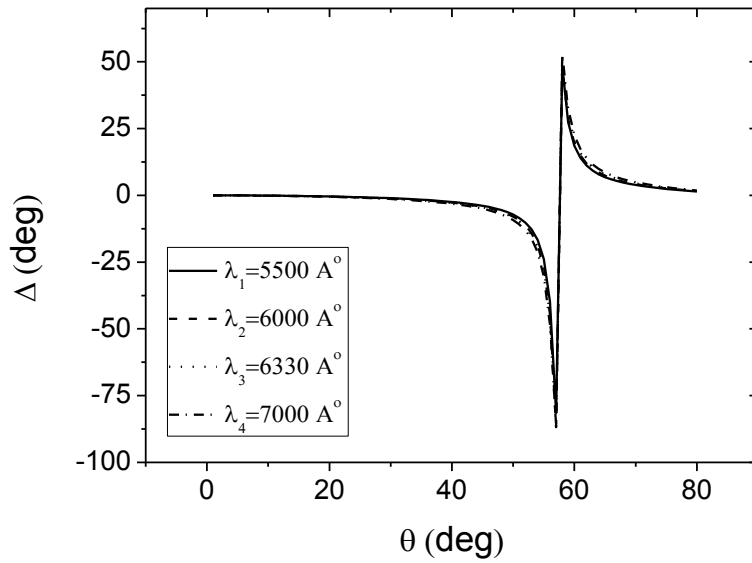


Figure 4.23.  $\Delta$  of three-layer Bragg reflector for Si-Cu structure versus the incident angle with transverse voltage of 1000 volt.

The same notation and discussion can be said for a three layer Bragg reflector with 5000 volt transverse voltage except more curvature at the bottom of  $\psi$  near  $\theta_i = 57^\circ$ , and less inclining negative slope of Phase difference angle about the asymptoting line  $\theta_i = 57^\circ$ . Applying a transverse voltage of 5000 V slightly enhances the effect of different wavelengths. All these can be seen in Fig.4.24., Fig.4.25., Fig.4.26.

Applying different values of transverse voltage does not change the critical value of  $\theta_i = 57^\circ$ .

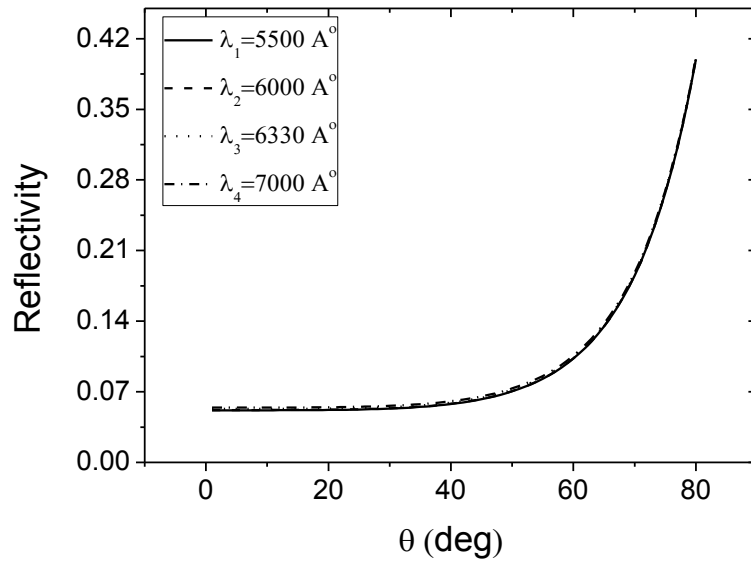


Figure 4.24. Reflectivity of three-layer Bragg reflector for Si-Cu structure versus the incident angle with transverse voltage of 5000 volt

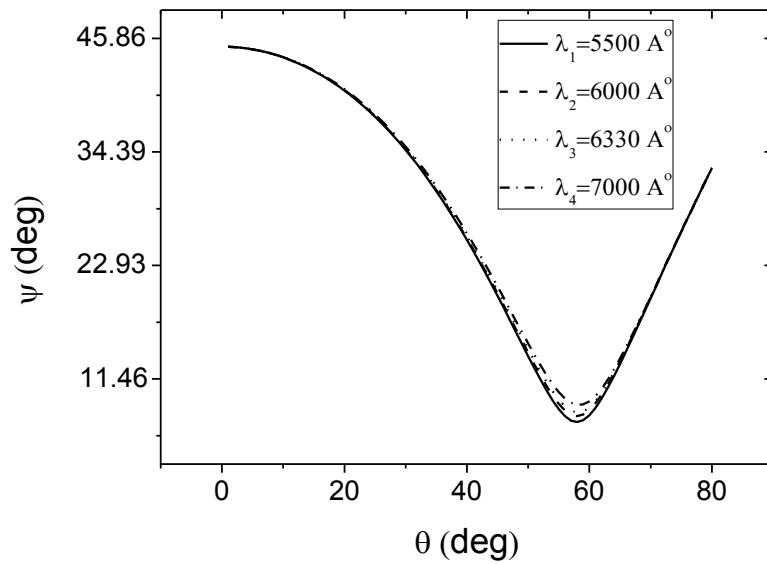


Figure 4.25.  $\psi$  of three-layer Bragg reflector for Si-Cu structure versus the incident angle with transverse voltage of 5000 volt

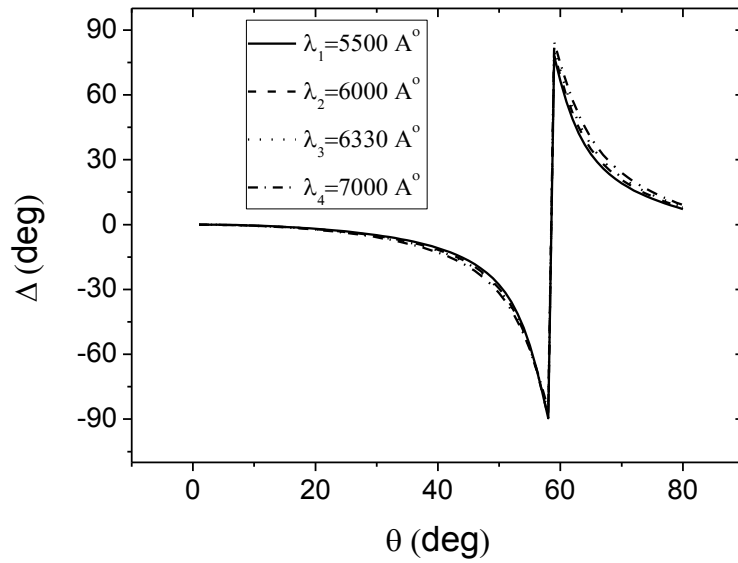


Figure 4.26.  $\Delta$  of three-layer Bragg reflector for Si-Cu structure versus the incident angle with transverse voltage of 5000 volt

#### 4.3.2.2 Results of a five-layer structure

Figure 4.27, and Fig 4.28. shows the reflectivity and  $\psi$  respectively as a function of incidence angle. Both reflectivity and  $\psi$  have different values when incident a light with different wavelengths, and applying no transverse voltage across five layer Bragg reflector.

The behavior of reflectivity versus the incidence angle with no transverse voltage, 100 V, and 5000 V is shown in Fig.4.27, 4.30, 4.32. respectively. Reflectivity curves – with different wavelengths- show a stable and nearly constant value when it is studied as a function of incidence angles in the range  $\theta_i = 0^\circ - 60^\circ$ , then suddenly increase in the incidence angles range  $60^\circ - 80^\circ$ .

The greater is the wavelength, the smaller is the difference between values of reflectivity and also between the  $\psi$ s.



The behavior of  $\psi$  as a function of incidence angle in five-layer Bragg reflector differ of that of three-layer in smoothness and a dipangle  $\theta_i$ . In five-layer Bragg reflector the curve of  $\psi$  decreases smoothly with increasing in  $\theta_i$  until reaches the lowest value of  $\theta_i = 77^\circ$ . Note that the dip angle  $\theta_i = 77^\circ$  shifts to the right – increases- with increases of wavelength. This discussion of  $\psi$  is true for a transverse voltage of 0 V, 1000 V, and 5000 V, which are shown in Fig.4.28, 4.31, 4.34.

Different-wavelength curves of " $\Delta$ " as a function of  $\theta_i$  is plotted in Fig.4.29. The curve of  $\Delta$  increases gradually with increasing of  $\theta_i$  until reaches critical value  $\theta_i = 77^\circ$ . The critical value  $\theta_i$  is shifted with the increasing of wavelength i.e. the same behavior of that of  $\psi$ .

Fig.4.33, 4.35 show the similar behavior of  $\Delta$  with respect of  $\theta_i$  with different wavelength in the presence of transverse voltage of 1000 V, and 5000 V respectively.

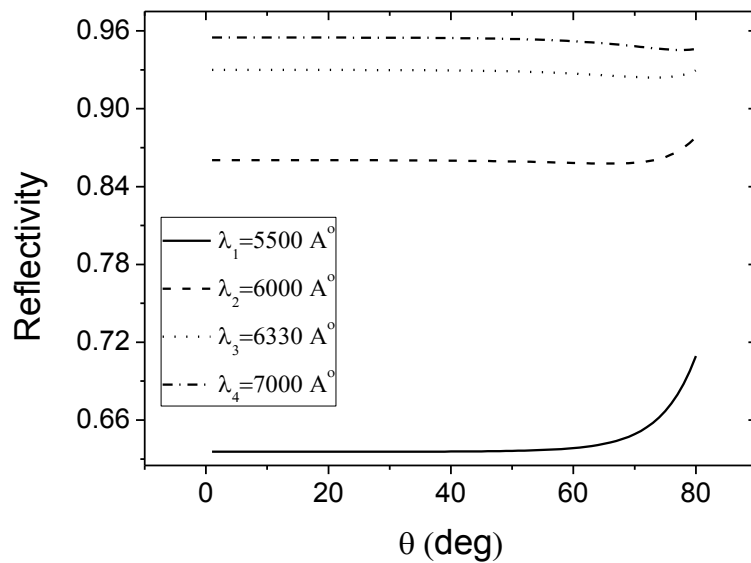


Figure 4.27. Reflectivity of five-layer Bragg reflector for Si-Cu structure versus the incident angle with transverse voltage of 0 volt

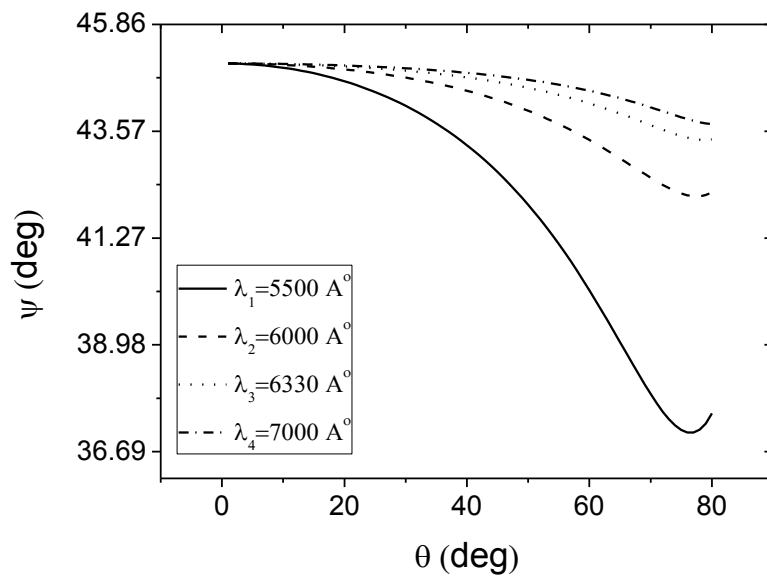


Figure 4.28.  $\psi$  of five-layer Bragg reflector for Si-Cu structure versus the incident angle with transverse voltage of 0 volt

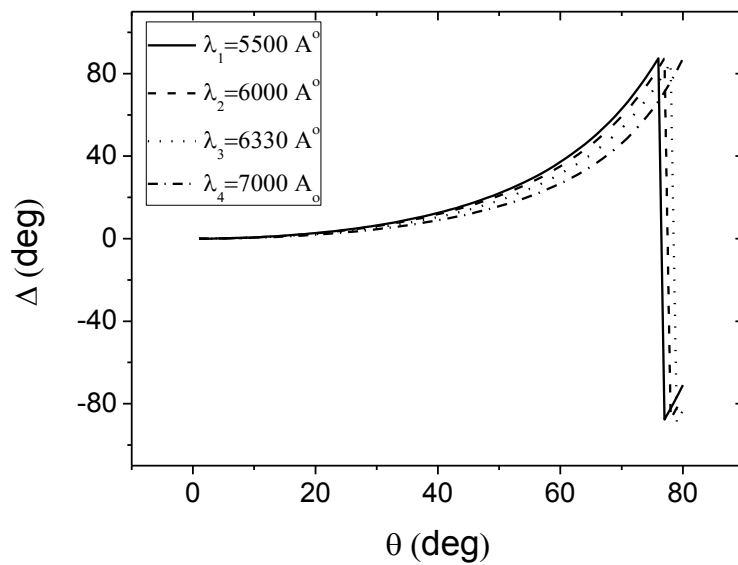


Figure 4.29.  $\Delta$  of five-layer Bragg reflector for Si-Cu structure versus the incident angle with transverse voltage of 0 volt

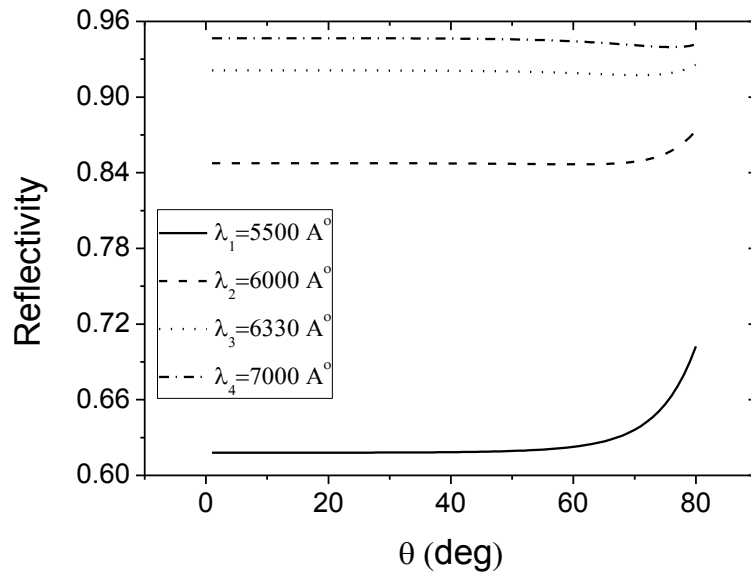


Figure 4.30. Reflectivity of five-layer Bragg reflector for Si-Cu structure versus the incident angle with transverse voltage of 1000 volt

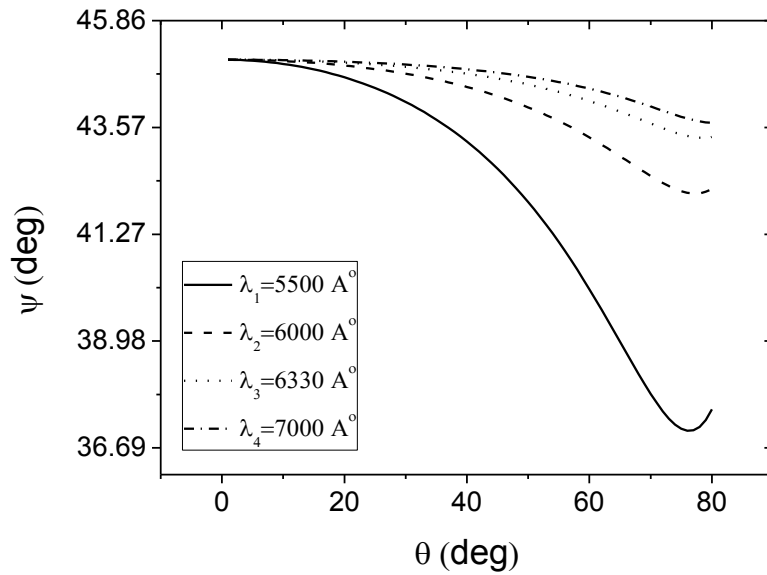


Figure 4.31.  $\psi$  of five-layer Bragg reflector for Si-Cu structure versus the incident angle with transverse voltage of 1000 volt

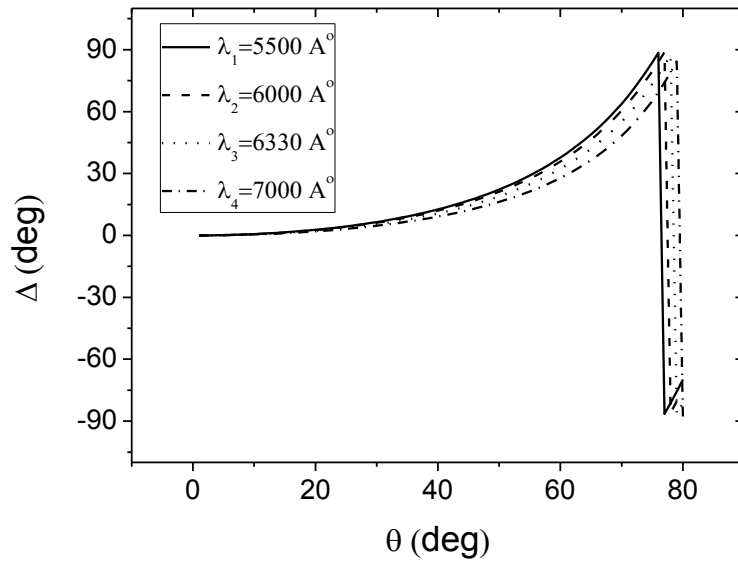


Figure 4.32.  $\Delta$  of five-layer Bragg reflector for Si-Cu structure versus the incident angle with transverse voltage of 1000 volt

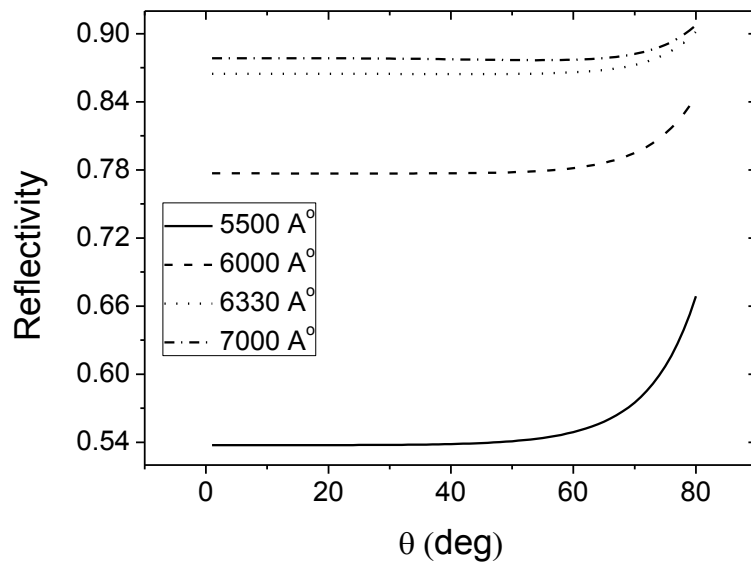


Figure 4.33. Reflectivity of five-layer Bragg reflector for Si-Cu structure versus the incident angle with transverse voltage of 5000 volt

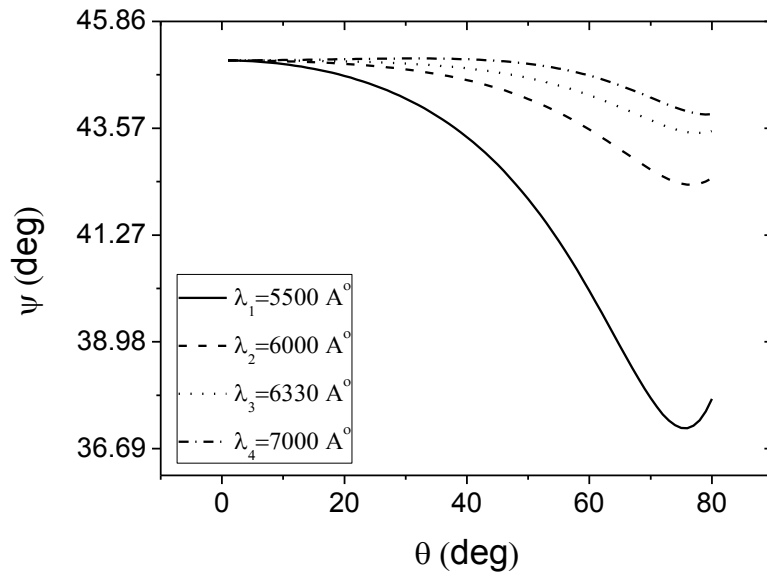


Figure 4.34.  $\psi$  of five-layer Bragg reflector for Si-Cu structure versus the incident angle with transverse voltage of 5000 volt

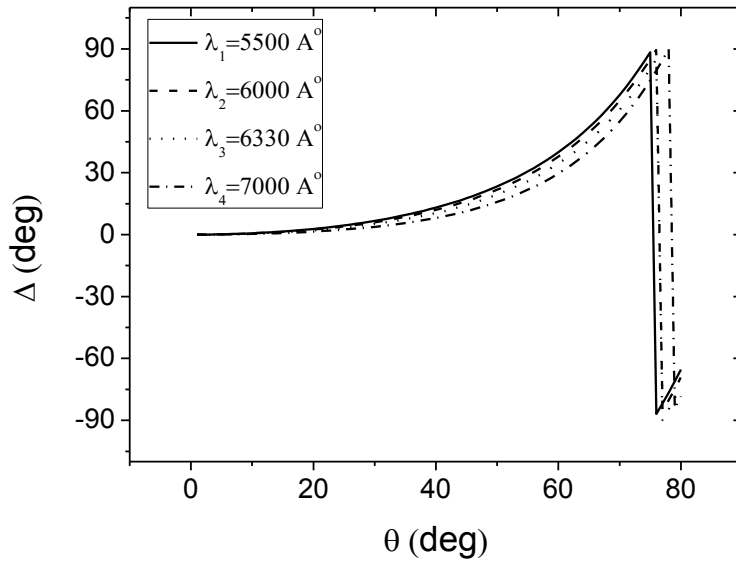


Figure 4.35.  $\Delta$  of five-layer Bragg reflector for Si-Cu structure versus the incident angle with transverse voltage of 5000 volt

### 4.3.2.3 Results for a nine-layer structure.

The reflectivity and  $\psi$  are plotted versus incidence angle in Fig.4.36, and Fig 4.37, respectively. Both reflectivity and  $\psi$  have varying values when a light is incident with different wavelengths, and applying no transverse voltage across nine-layer Bragg reflector. The greater is the wavelength, the smaller is the difference between values of reflectivity -with different wavelengths- and also between the  $\psi$ s.

Phase difference angles for different wavelengths of incident light with different angles are shown in Fig.4.38.

Regarding the critical valley angle  $\theta_i = 77^\circ$ , and the transverse voltage of 0 V, 1000 V, and 5000 V, the similar talk as which was said previously in five-layer structure can be said here.

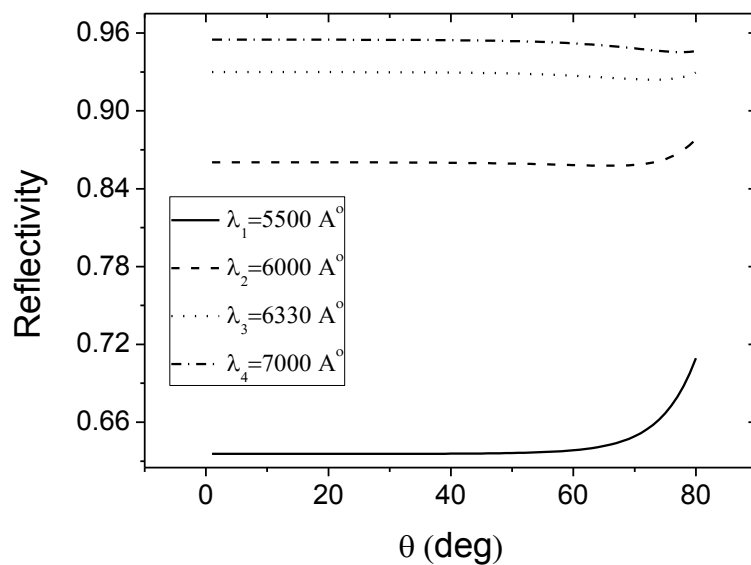


Figure 4.36. Reflectivity of nine-layer Bragg reflector for Si-Cu structure versus the incident angle with transverse voltage of 0 volt

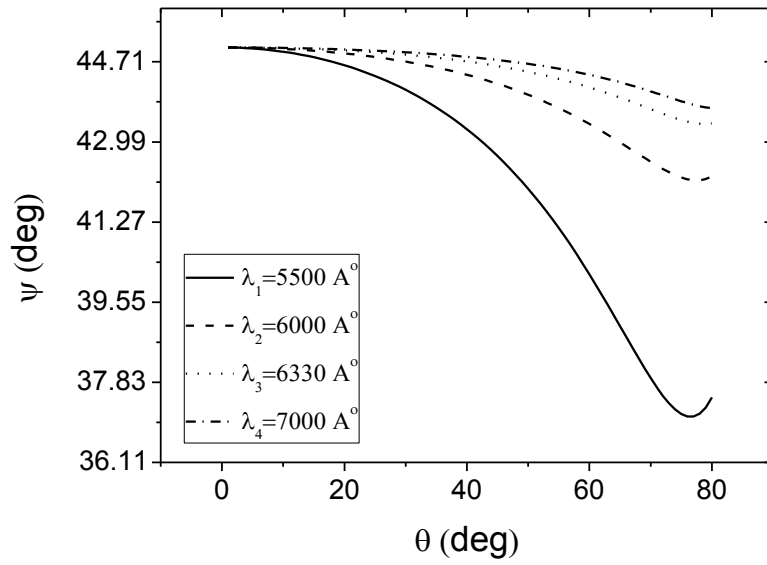


Figure 4.37.  $\psi$  of nine-layer Bragg reflector for Si-Cu structure versus the incident angle with transverse voltage of 0 volt

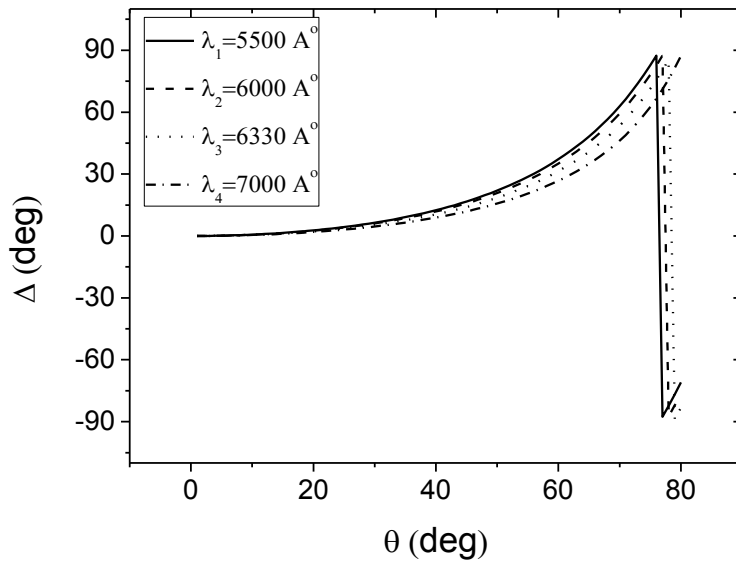


Figure 4.38.  $\Delta$  of nine-layer Bragg reflector for Si-Cu structure versus the incident angle with transverse voltage of 0 volt

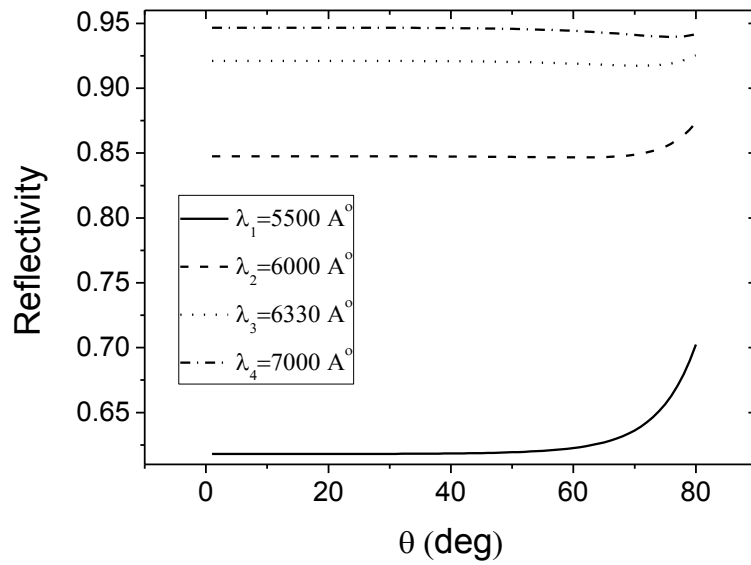


Figure 4.39. Reflectivity of nine-layer Bragg reflector for Si-Cu structure versus the incident angle with transverse voltage of 1000 volt

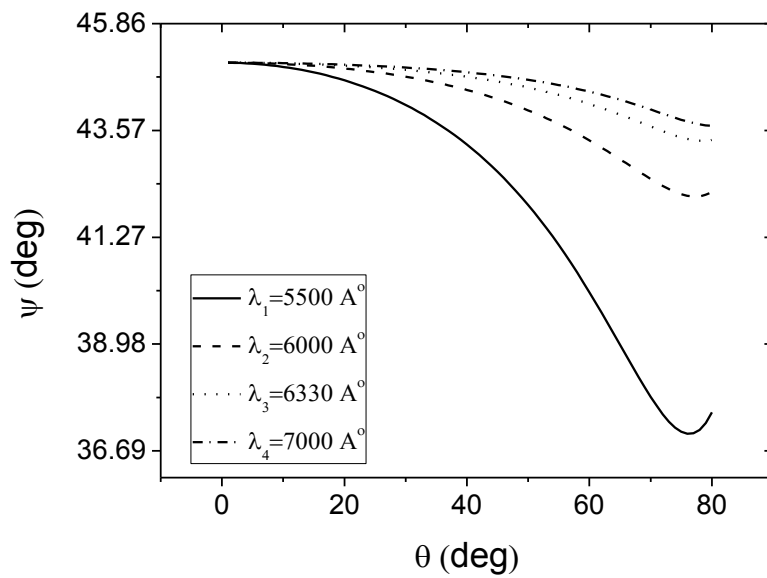


Figure 4.40.  $\psi$  of nine-layer Bragg reflector for Si-Cu structure versus the incident angle with transverse voltage of 1000 volt



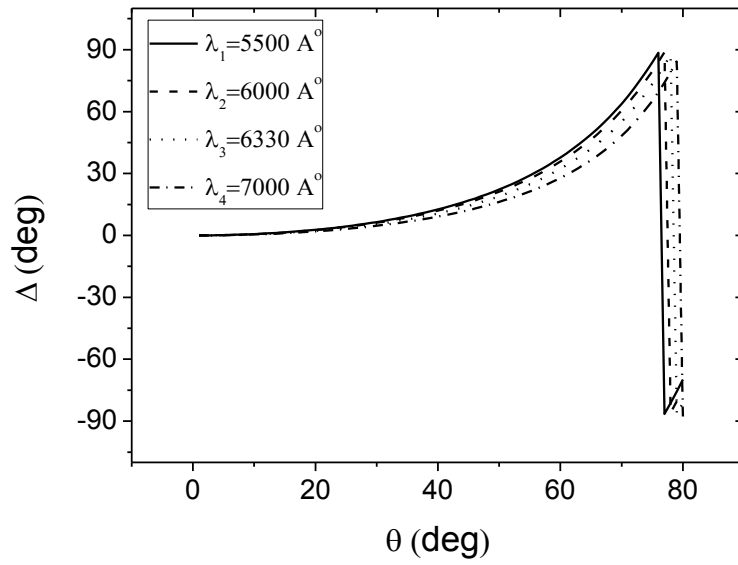


Figure 4.41.  $\Delta$  of nine-layer Bragg reflector for Si-Cu structure versus the incident angle with transverse voltage of 1000 volt

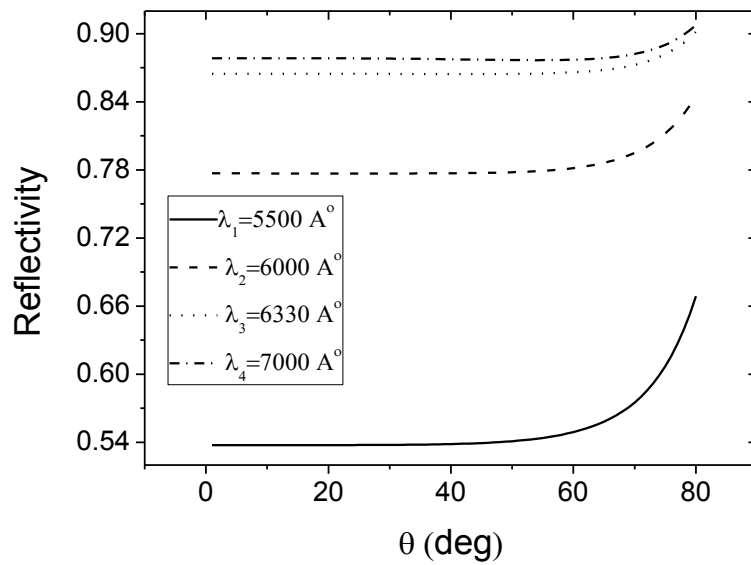


Figure 4.42. Reflectivity of nine-layer Bragg reflector for Si-Cu structure versus the incident angle with transverse voltage of 5000 volt

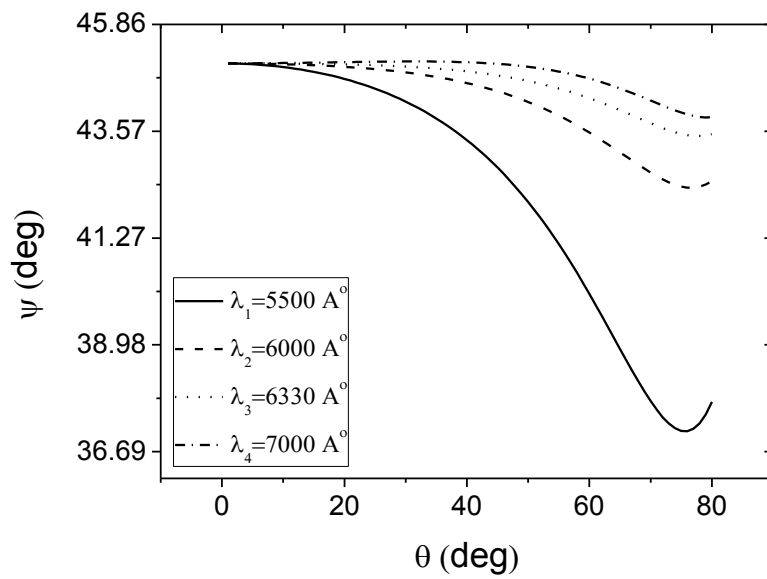


Figure 4.43.  $\psi$  of nine-layer Bragg reflector for Si-Cu structure versus the incident angle with transverse voltage of 5000 volt

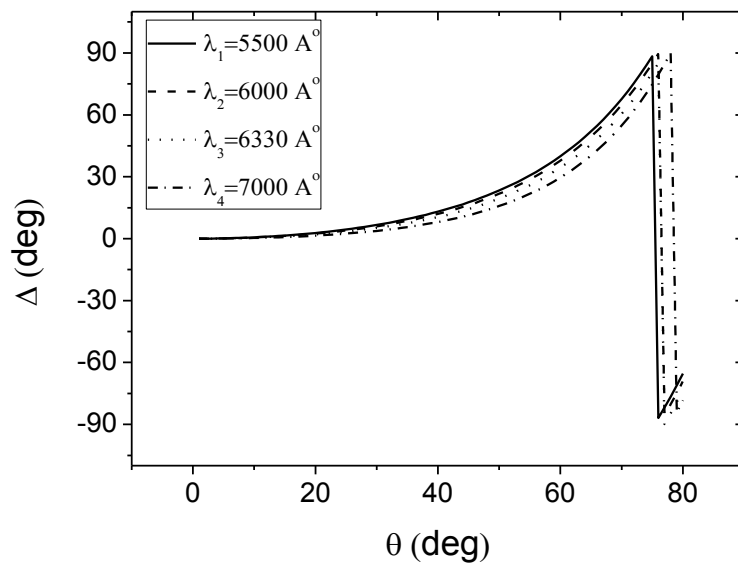


Figure 4.44.  $\Delta$  of nine-layer Bragg reflector for Si-Cu structure versus the incident angle with transverse voltage of 5000 volt

#### 4.3.2.4 Results of a fifteen-layer structure

Numerical talk is left until reach this subsection to clarify the similarity among five-, nine-, and fifteen-layer structure. The reflectivity for 0 V transverse voltage for fifteen-layer Bragg reflector is shown in Fig.4.45. The reflectivity curves for different wavelengths are stable and constant in the range between  $\theta_i = 0^\circ - 60^\circ$  and have the following values;  $R = 0.63533$  for wavelength of 550 nm,  $R = 0.86034$  for wavelength of 600 nm,  $R = 0.92992$  for wavelength of 633 nm, and  $R = 0.95488$  for wavelength of 700 nm. The previous values are true for nine-layer, and five-layer Bragg reflector.

While the values of  $\psi$  for 0 V, for wavelengths of 550 nm, 600 nm, 633 nm, and 700 nm are all start from  $45.02^\circ$  and decreasing gradually with different slope for each wavelength as shown in Fig.4.46. The  $\psi$  curve of wavelength 500 nm has the lowest value- valley angle- of  $37^\circ$  when the incidence angle has the value of  $76.80^\circ$ . Again the values of  $\psi$  for nine-, and five-layer are identical of those of fifteen-layer Bragg Reflector. The applying of a transverse voltage of 0 V across fifteen-layer Bragg reflector gives the following values of  $\Delta$  for the wavelength of 550 nm; see Fig.4.46. Maximum  $\Delta$  is  $86.35^\circ$  at  $\theta_i = 76^\circ$ , and minimum  $\Delta$  is  $-86.7^\circ$  at  $\theta_i = 77^\circ$ , which are the same values for nine-layer, and five-layer Bragg reflector.

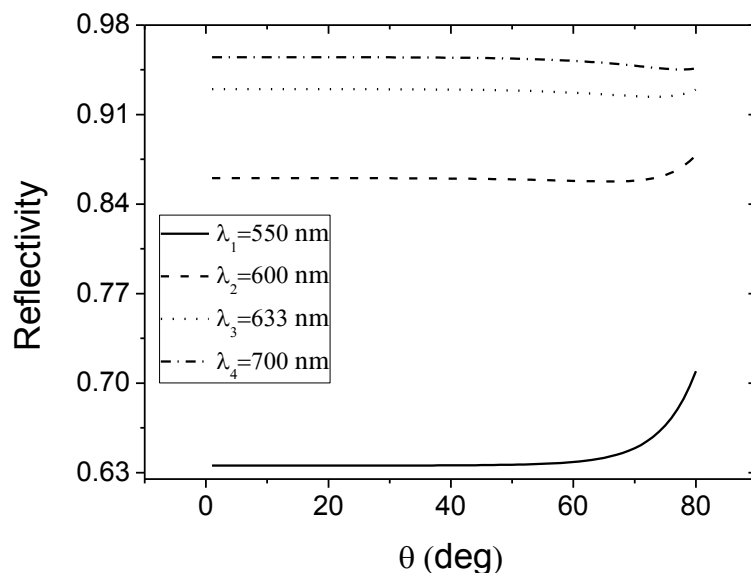


Figure 4.45. Reflectivity of fifteen-layer Bragg reflector for Si-Cu structure versus the incident angle with transverse voltage of 0 volt

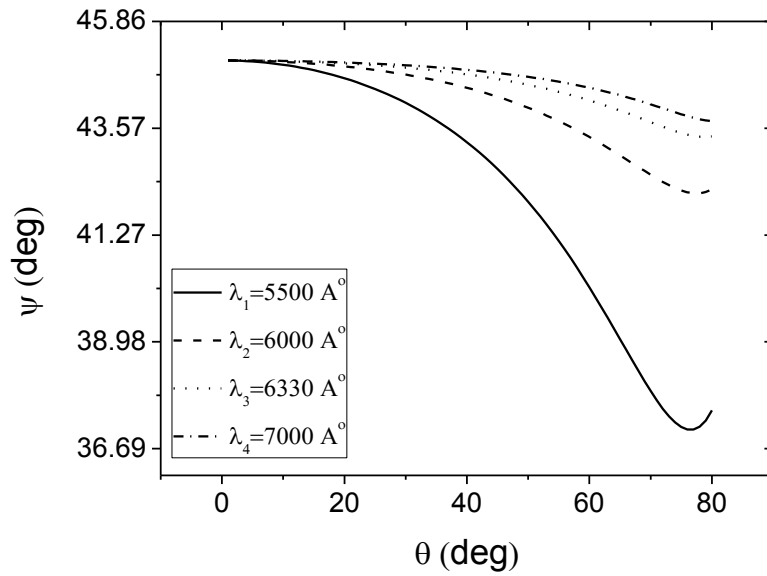


Figure 4.46.  $\psi$  of fifteen-layer Bragg reflector for Si-Cu structure versus the incident angle with transverse voltage of 0 volt

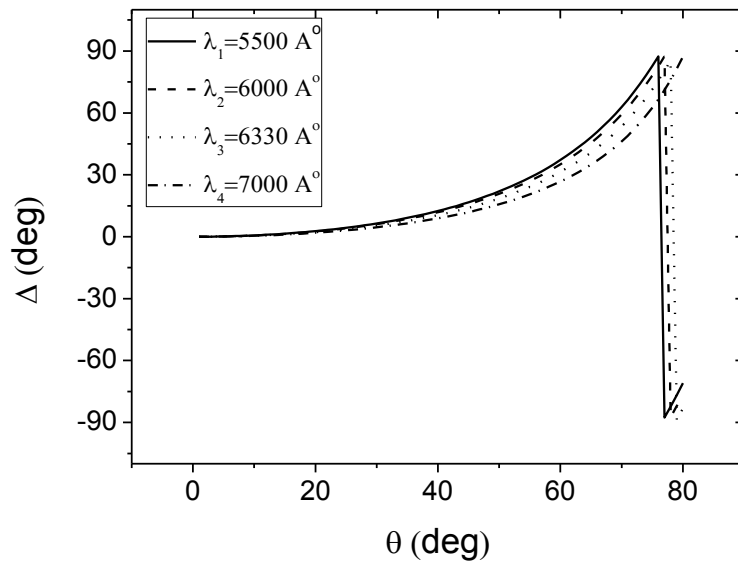


Figure 4.47.  $\Delta$  of fifteen-layer Bragg reflector for Si-Cu structure versus the incident angle with transverse voltage of 0 volt

The reflectivity values when applying a transverse voltage of 1000 V is shown in Fig.4.48. The different wavelength curves show a stable and constant behavior in the range between  $\theta_i = 0^\circ - 50^\circ$  and have the following values;  $R = 0.618042$  for wavelength of 550 nm,  $R = 0.847573$  for wavelength of 600 nm,  $R = 0.921143$  for

wavelength of 633 nm, and  $R = 0.946679$  for wavelength of 700 nm. The previous values are identical in case of nine-layer, and five-layer Bragg reflector.

The applying of a transverse voltage of 1000 V across fifteen-layer Bragg reflector gives the following values of  $\psi$  for the wavelength of 550 nm, 600 nm, 633 nm, and 700 nm are all start from  $45.02^\circ$  and decreasing gradually with different slope for each wavelength as shown in Fig.4.49. The  $\psi$  curve of wavelength 500 nm has the lowest value- valley angle- of  $37^\circ$  when the incidence angle has the value of  $76.01^\circ$ . Again the values of  $\psi$  for nine-, and five-layer are identical of those of fifteen-layer Bragg Reflector.

The values of  $\Delta$  for the wavelength of 550 nm is shown in Fig.4.50. when applying a transverse voltage of 0 V across fifteen-layer Bragg reflector gives the following; maximum  $\Delta$  is  $86.92^\circ$  at  $\theta_i = 76^\circ$ , and minimum  $\Delta$  is  $-85.69^\circ$  at  $\theta_i = 77.15^\circ$ , which are the same values for nine-layer, and five-layer Bragg reflector.

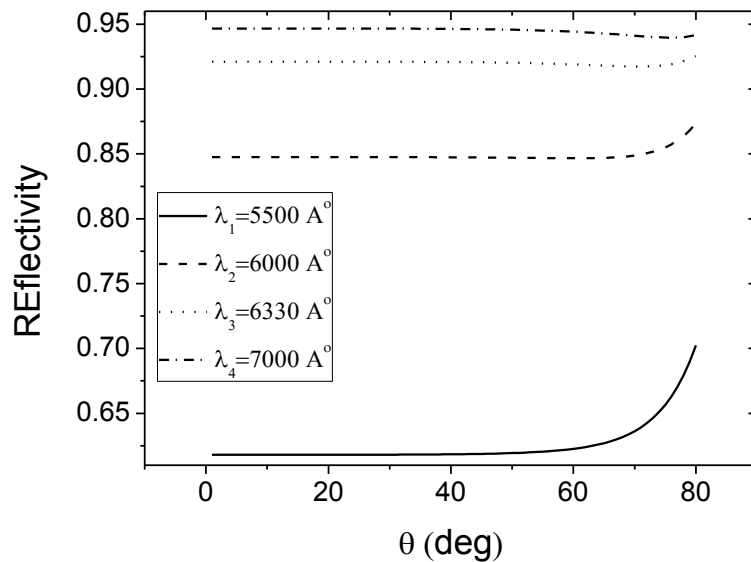


Figure 4.48. Reflectivity of fifteen-layer Bragg reflector for Si-Cu structure versus the incident angle with transverse voltage of 1000 volt

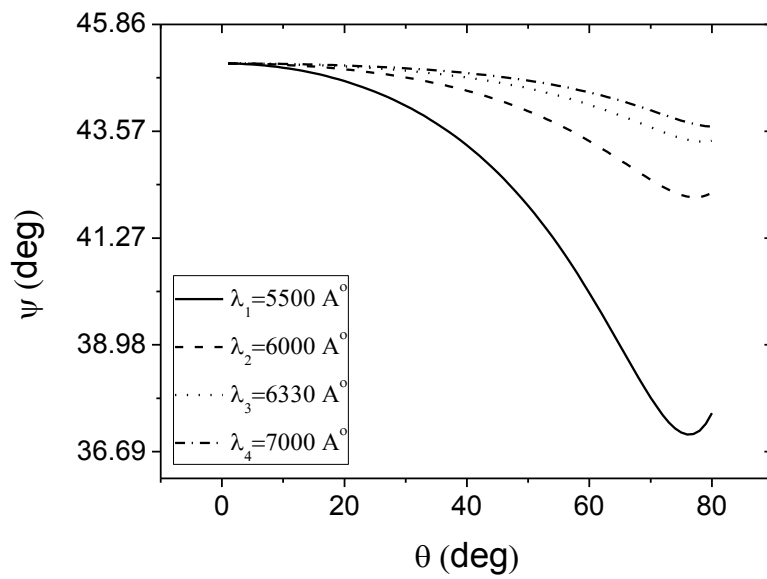


Figure 4.49.  $\psi$  of fifteen-layer Bragg reflector for Si-Cu structure versus the incident angle with transverse voltage of 1000 volt

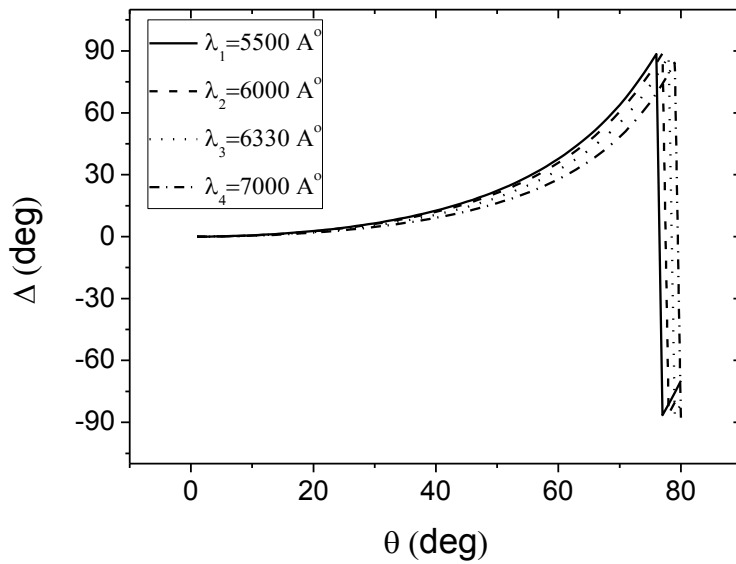


Figure 4.50.  $\Delta$  of fifteen-layer Bragg reflector for Si-Cu structure versus the incident angle with transverse voltage of 1000 volt

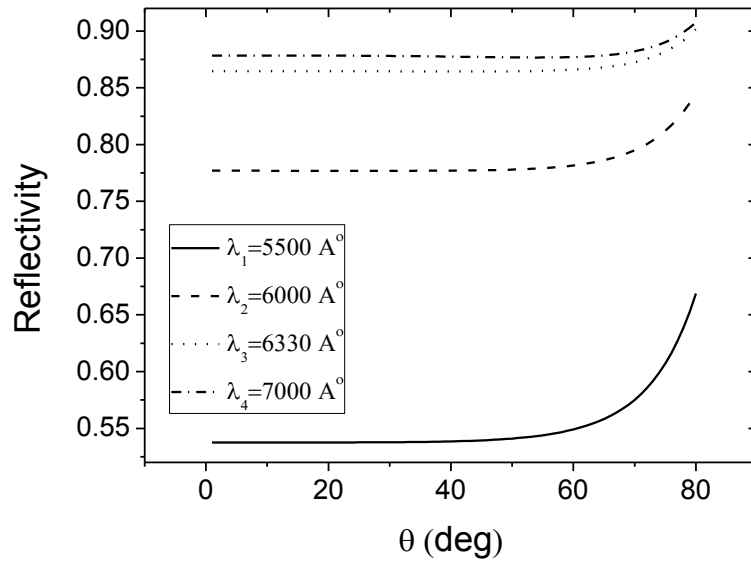


Figure 4.51. Reflectivity of fifteen-layer Bragg reflector for Si-Cu structure versus the incident angle with transverse voltage of 5000 volt

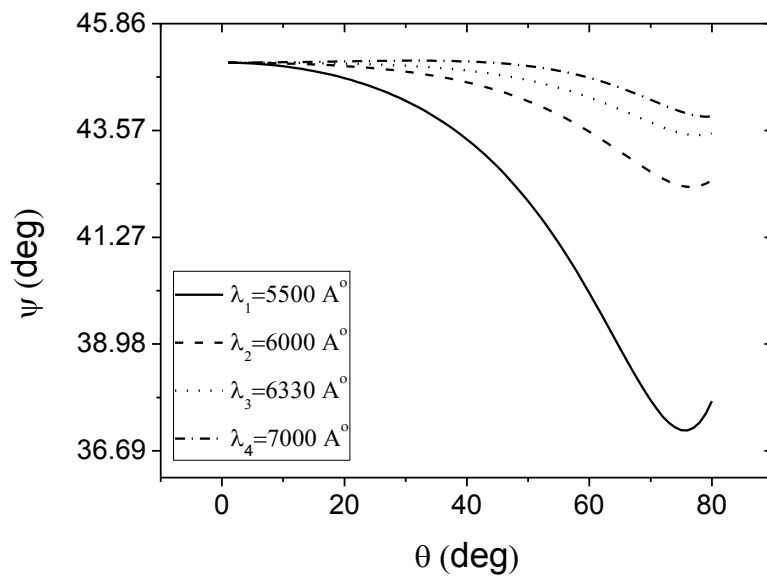


Figure 4.52.  $\psi$  of fifteen-layer Bragg reflector for Si-Cu structure versus the incident angle with transverse voltage of 5000 volt

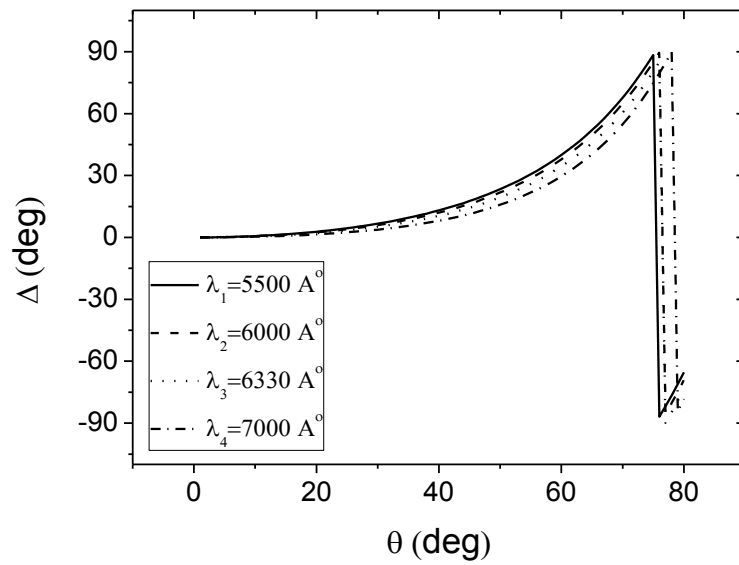


Figure 4.53.  $\Delta$  of fifteen-layer Bragg reflector for Si-Cu structure versus the incident angle with transverse voltage of 5000 volt

### 4.3.3 Investigation of Bragg reflector performance with the incident angle and transverse voltage.

#### 4.3.3.1 Results of a three-layer structure

Figure 4.54 shows the reflectivity for three layer Bragg reflector versus the incident angle, when applying a transverse voltage of 0 volt or 1000 volt the values are nearly identical, while applying 5000 volt will cause a slight enhancement of reflectivity.



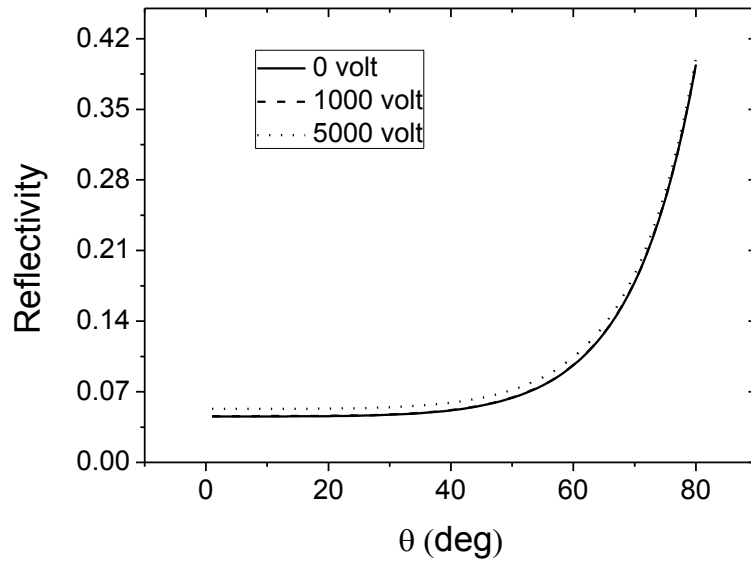


Figure 4.54. Reflectivity of three-layer Bragg reflector for Si-Cu structure versus the incident angle with transverse voltage of 0, 1000, and 5000 volt

Figure 4.55 shows  $\psi$  of three layer Bragg reflector as a function of incident angle. The figures shows a sharp cliff around  $\theta_i = 58^\circ$  with a no transverse voltage, the sharpness decreases when applying 1000 volt, and it becomes round curve when applying 5000 volt.

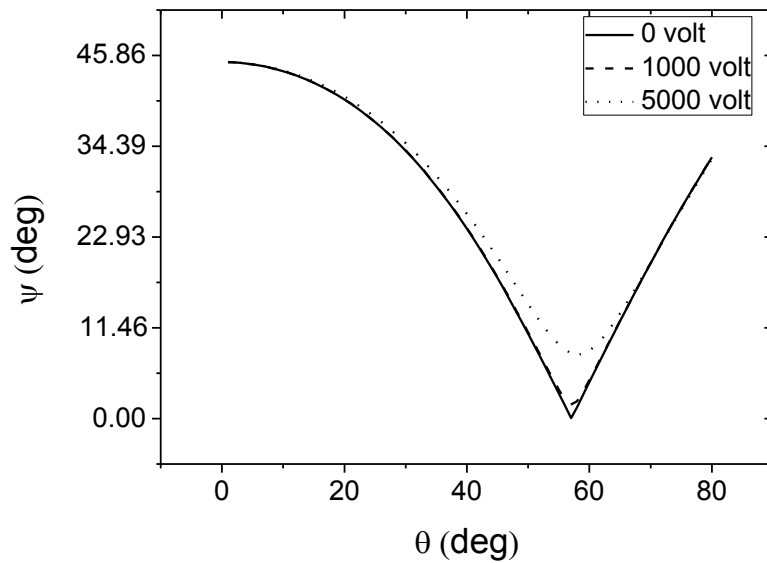


Figure 4.55.  $\psi$  of three-layer Bragg reflector for Si-Cu structure versus the incident angle with transverse voltage of 0, 1000, and 5000 volt

It is seen in Fig. 4.56. that with zero transverse voltage the Phase difference angle is zero degree, and with 1000, and 5000 volt there is an asymptoting around  $\theta_i = 58^\circ$ . The changing of Phase difference with 5000 volt becomes fast comparing with 1000 volt.

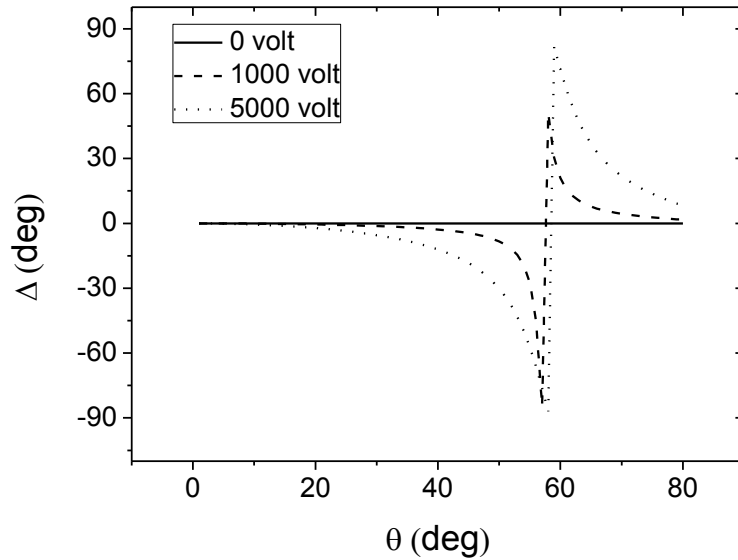


Figure 4.56.  $\Delta$  of three-layer Bragg reflector for Si-Cu structure versus the incident angle with transverse voltage of 0, 1000, and 5000 volt

#### 4.3.3.2 Results of a five-layer structure

Figure 4.57. shows the reflectivity as a function of angle of incidence for five layer Bragg reflector, while Fig.4.58. illustrates the  $\psi$  versus incident angle. More transverse voltage will cause a more dampen of reflectivity. Regarding the  $\psi$  when applying 1000 volt transverse voltage the  $\psi$  dampen while when applying 5000 volt  $\psi$  is enhanced.

Figure 4.59. presents Phase difference versus incidence angle for five layer Bragg reflector, more transverse voltage will cause a slight increase in Phase difference angle.

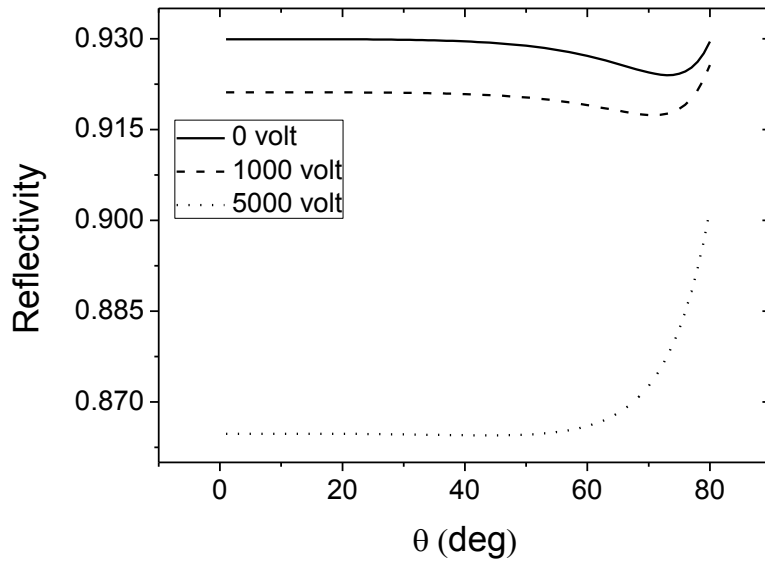


Figure 4.57. Reflectivity of five-layer Bragg reflector for Si-Cu structure versus the incident angle with transverse voltage of 0, 1000, and 5000 volt

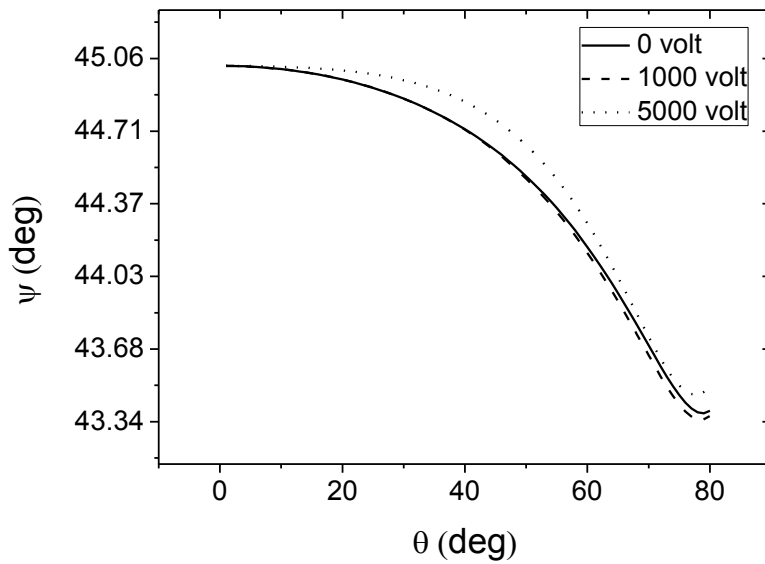


Figure 4.58.  $\psi$  of five-layer Bragg reflector for Si-Cu structure versus the incident angle with transverse voltage of 0, 1000, and 5000 volt

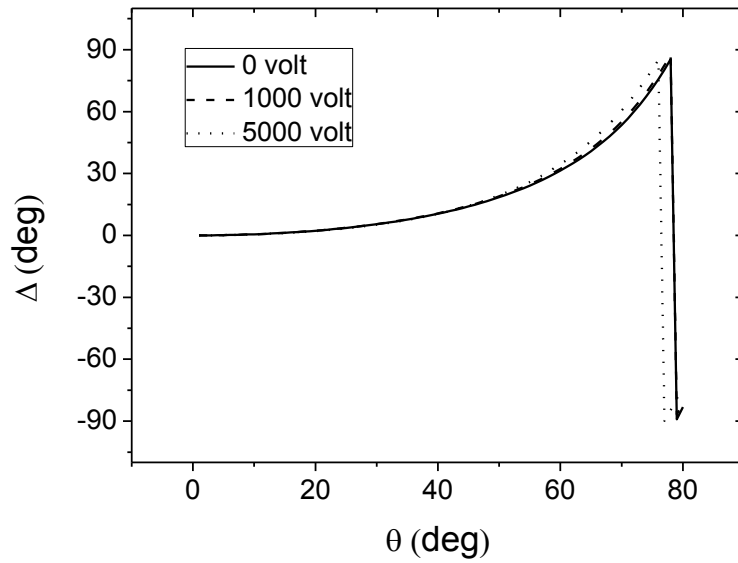


Figure 4.59.  $\Delta$  of five-layer Bragg reflector for Si-Cu structure versus the incident angle with transverse voltage of 0, 1000, and 5000 volt

#### 4.3.3.3 Results of a nine-layer structure

Figure 4.60 shows the nine layer Bragg reflector's reflectivity as a function of incident angle while Fig. 4.61 illustrates the  $\psi$  versus incidence angle. More transverse voltage will cause a more dampen of reflectivity. Regarding the  $\psi$  when applying 1000 volt transverse voltage the  $\Psi$  dampens while when applying 5000 volt  $\psi$  increases.

Figure 4.62 shows Phase difference versus incidence angle for five layer Bragg reflector, more transverse voltage will cause a slight increase in Phase difference angle.

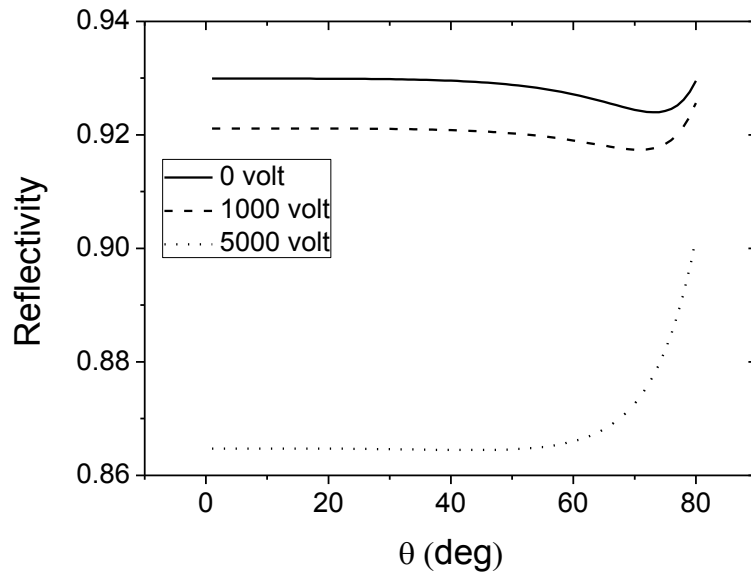


Figure 4.60. Reflectivity of nine-layer Bragg reflector for Si-Cu structure versus the incident angle with transverse voltage of 0, 1000, and 5000 volt

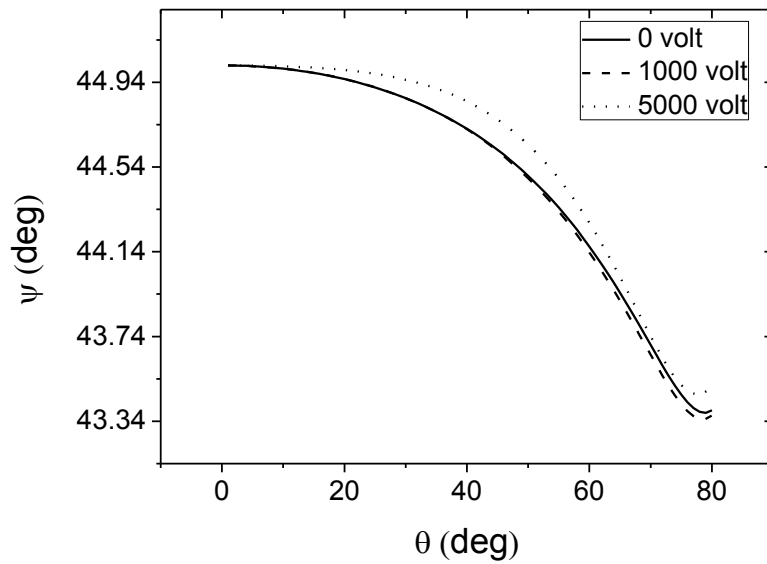


Figure 4.61.  $\psi$  of nine-layer Bragg reflector for Si-Cu structure versus the incident angle with transverse voltage of 0, 1000, and 5000 volt

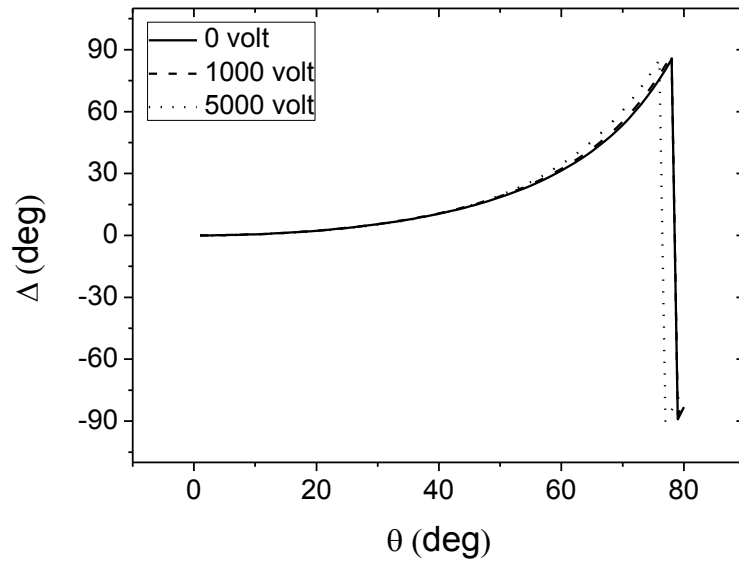


Figure 4.62.  $\Delta$  of nine-layer Bragg reflector for Si-Cu structure versus the incident angle with transverse voltage of 0, 1000, and 5000 volt

#### 4.3.3.4 Results of a fifteen-layer structure

Figure 4.63. shows the fifteen layer Bragg reflector's reflectivity as a function of incident angle while Fig.4.64. illustrates the  $\psi$  versus incidence angle. More transverse voltage will cause a more dampen of reflectivity and more increment of  $\psi$  when applying 5000 volt transverse voltage but more dampen when applying 5000 volt.

Figure 4.65. presents Phase difference versus incidence angle for fifteen layer Bragg reflector, more transverse voltage will cause a slight increase in Phase difference angle.

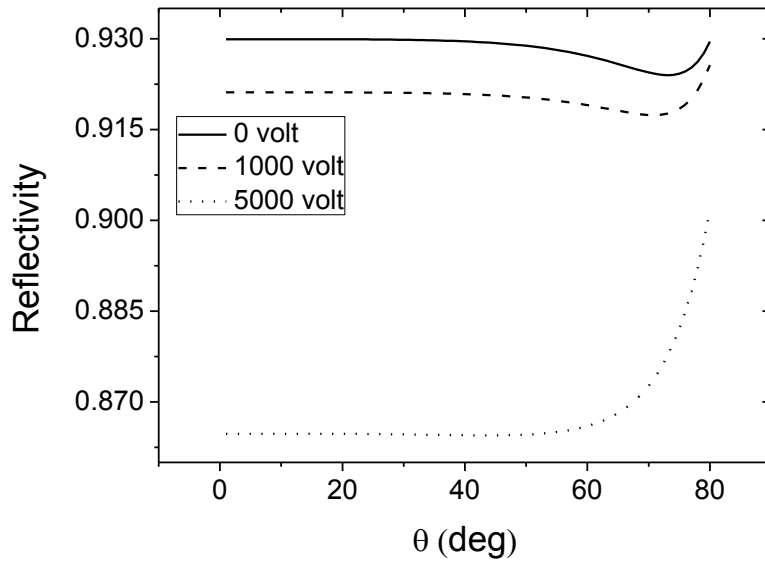


Figure 4.63. Reflectivity of fifteen-layer Bragg reflector for Si-Cu structure versus the incident angle with transverse voltage of 0, 1000, and 5000 volt

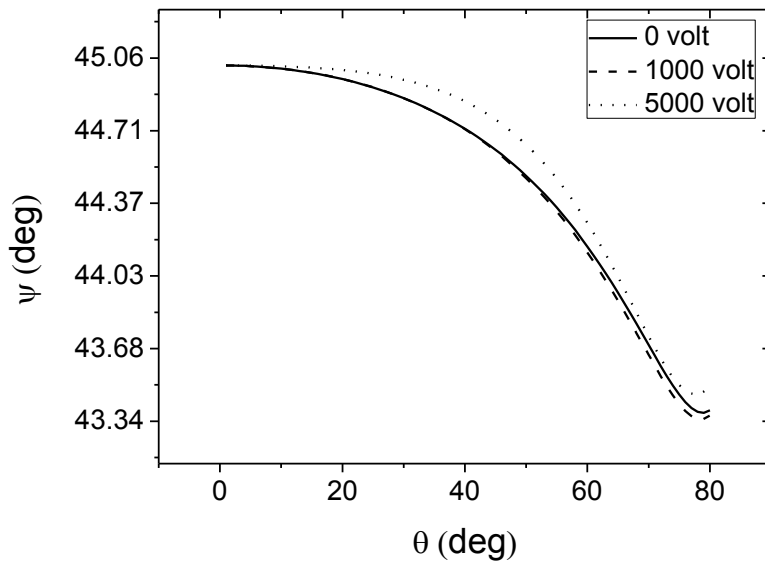


Figure 4.64.  $\psi$  of fifteen-layer Bragg reflector for Si-Cu structure versus the incident angle with transverse voltage of 0, 1000, and 5000 volt

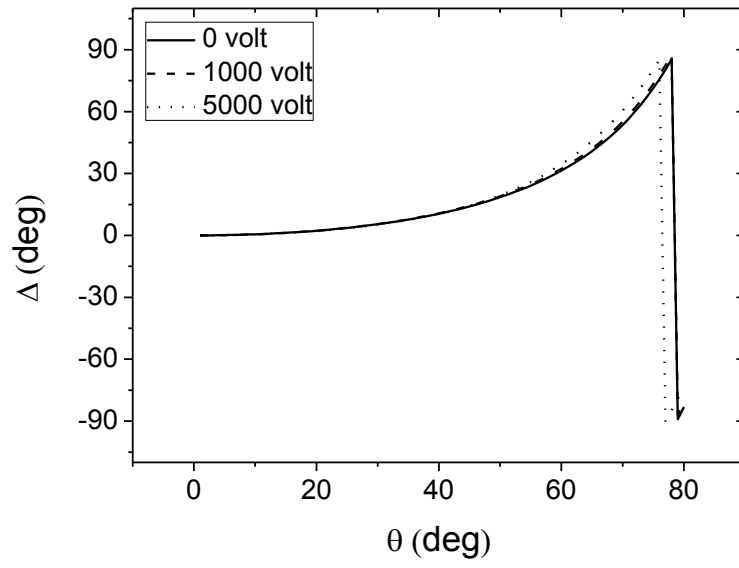


Figure 4.65.  $\Delta$  of fifteen-layer Bragg reflector for Si-Cu structure versus the incidence angle with transverse voltage of 0, 1000, and 5000 volt



## Chapter five

### General conclusion

In this thesis a reflection and transmission from a multilayer structure with interface free charge layer are studied in detail.

A famous semiconductor material, the Silicon (Si), is taken to be a high refractive index layer. While Copper (Cu) is taken to be a layer of low refractive index. The substrate is taken to be glass, Silicon dioxide ( $\text{SiO}_2$ ).

This Thesis studies three-layer, five-layer, nine-layer, and fifteen-layer structures. The study investigates the effect of wavelength and transverse voltage on a reflectivity ( $R$ ), ellipsometric parameters  $\psi$ , and  $\Delta$ .

The study clarifies the effect of incident angle and wavelength on the same parameters  $R$ ,  $\psi$ , and  $\Delta$ .

The thesis also studies the performance of reflectivity,  $\psi$ , and  $\Delta$  with the incident angle and transverse voltage.

The simulation revealed that the reflectivity decreases as the wavelength increases of the incident light, when a potential difference of 1000 V is applied to the three-layer structure, the shape of curve remains unchanged with a small enhancement in the reflectivity.

Which means that the reflectivity difference for three-layer Bragg reflector is approximate a linear line with positive slope.

Increasing of the transverse voltage will enhance the  $\psi$  value in the spectral range 400 nm to 850 nm for a three-layer Bragg reflector.

The Phase difference " $\Delta$ " between the two components of light equals zero when applying no transverse voltage, and it changes gradually from -0.1 degree to -0.7 degree when applying a transverse voltage of 1000 volt across a three-layer Bragg reflector

While for five-, and nine-layer Bragg reflector the reflectivity increases very fast from 400 nm to about 650 nm, then it becomes stable from 650 nm to 850 nm. The reflectivity value in the stable region is near one. It is clear that there is no change of  $\psi$  value when applying 1000 volt across the Bragg reflector in the spectral range 400 nm to 850 nm.

The Phase difference " $\Delta$ " dependence on the wavelength is slightly enhanced when applying a transverse voltage of 1000 volt across the five layer Bragg reflector.

When applying a voltage of 1000 V to the fifteen-layer Bragg reflector, a significant change in the reflectivity is observed. The reflectivity decreases when applying the voltage. This decrease in the reflectivity is critically dependent on the wavelengths. The behavior of  $\psi$  with the wavelength and V is similar to that of the reflectivity. The phase difference  $\Delta$  versus the wavelength for a fifteen-layer Bragg reflector is affected slightly by the voltage, and it can be seen for  $\lambda > 650$  nm.

The reflectivity for three layer Bragg reflector versus the incidence angle, when applying a transverse voltage of 0 volt or 1000 volt the values come nearly identical, while applying 5000 volt will cause a slight enhancement of reflectivity. The  $\psi$  of three layer Bragg reflector as a function of incident angle shows a sharp cliff around  $\theta_i = 58^\circ$  with a no transverse voltage, the sharpness decreases when applying 1000 volt, and it becomes round curve when applying 5000 volt. It is depicted. that with zero volt transverse voltage the Phase difference angle is zero degree, and with 1000, and 5000 volt there is an asymptoting around. The changing of Phase difference with 5000 volt becomes fast comparing with 1000 volt.

Regarding five-, nine, and fifteen-layer Bragg reflector the reflectivity as a function of incidence angle for five layer Bragg reflector is damped when applying a transverse voltage. The  $\psi$  is damped when applying 1000 volt transverse voltage, while when applying 5000 volt  $\psi$  is enhanced. Phase difference versus incidence angle for five layer Bragg reflector is slightly increased when applying transverse voltage.

The whole results which are gained in chapter four proposed a new photo-electric device. A new device allow manipulating of reflectivity,  $\psi$ , and  $\Delta$  as a function of transverse voltage. The device in general has two behaviors. The first when the

number of layers is three. The second behavior appears with large number of layers - five-layer, nine-layer, and fifteen-layer Bragg reflector-.

Note that the effect of conductivity appears clearly in case of three-layer because the varying conductivity is generated between the third layer – last layer of Bragg reflector- and the substrate. And when applying a transverse voltage across a device the reflectivity  $R$ , and  $\psi$  will be enhanced. The value of enhancement increases linearly with the increasing of the wavelength of incidence light in the spectral range 400 nm- 850 nm. While " $\Delta$ " the phase difference between p- polarized component of light and s- polarized component of light decreases linearly with increasing of wavelength in the spectral range 400 nm- 850 nm.

The opposite behavior of large number Bragg reflector can be concluded for five-layer, nine-layer, and fifteen-layer Bragg reflector. The effect of voltage appears clearly with the increasing of number of layers, so it is useful to focus on fifteen-layer Bragg reflector.

The reflectivity,  $R$  decrease when applying a transverse voltage across the fifteen-layer Bragg reflector. Reflectivity, and  $\psi$  are affected strongly with a transverse voltage when the wavelength increases, while the phase difference decreases slightly when applying a transverse voltage, the effect of a voltage increases with the increasing of wavelength.

The change of reflectivity with respect to voltage specially in high wavelength spectral range 650-850 nm can be dealt with as amplitude modulation.

Regarding the three-layer Bragg reflector, the applying of 1000 voltage will increase the amplitude. The incidence light can be considered as base band light or carrier light, the transverse voltage as modulating wave, and the reflected light can be considered as modulated light.

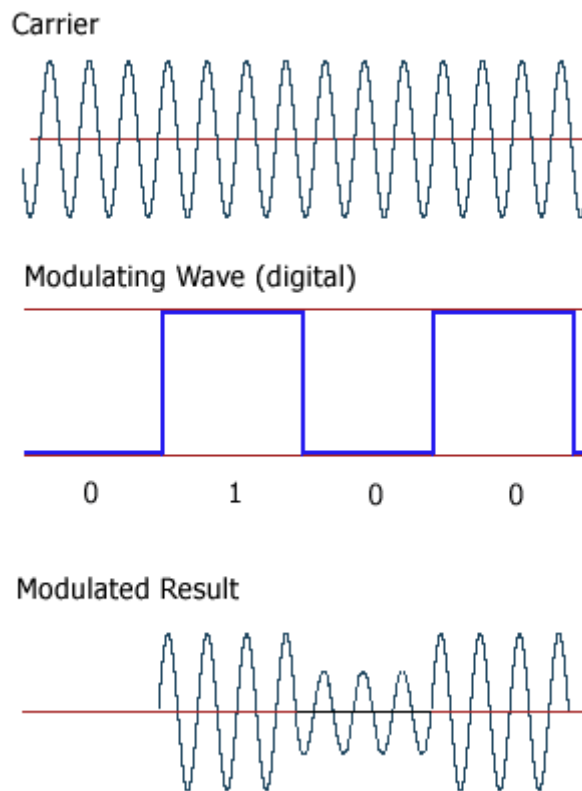


Figure 5.1 Amplitude modulation of a light depending on a transverse voltage pulse train.

The change of  $\psi$  or  $\Delta$  can be considered as a phase modulation even it is not the traditional phase of the signal – light-, but the change of ellipsometric parameter  $\psi$ ,  $\Delta$  opens the door to a new type of modulation, lets name it ellipsometric modulation.

This type of modulation can be more secured and complex modulation, because apparently the light – signal- is not changed but truly it is modulated.

The same thing can be said for fifteen-layer Bragg reflector with inverse behavior in both amplitude and ellipsometric modulation. But  $\Delta$  modulation is not suitable to be used practically because of slight change with respect to a transverse voltage.

## References

- [1] P. Markoš and C. Soukoulis, Wave Propagation, From Electrons to Photonic Crystals and Left-Handed Materials, 1st edition, Princeton University Press, New Jersey, 2008.
- [2] D. J. Griffiths, Introduction to Electrodynamics, 3rd edition, Prentice Hall, New Jersey, 1999.
- [3] J. Peatross and M. Ware, Physics of Light and Optics, Brigham Young University, 2011
- [4] M. Born and E. Wolf, Principles of optics Electromagnetic theory of propagation , interference and diffraction of light, 7<sup>th</sup> Edition, Cambridge university press, United Kingdom, 1999.
- [5] S. Khorasani and B. Rashidian, Guided light propagation in dielectric slab waveguide with conducting interfaces, J. Opt. A: Pure Appl. Opt. 3, pp. 380–386, 2001.
- [6] S. Khorasani, A. Nojeh, and B. Rashidian, Design and Analysis of the Integrated PlasmaWave Micro-Optical Modulator/Switch, Fiber and Integrated Optics, 21, pp. 173–191, 2002.
- [7] S. Khorasani and B. Rashidian, Modified transfer matrix method for conducting interfaces, J. Opt. A: Pure Appl. Opt. 4, pp 251–256, 2002.
- [8] K. Mehrany, S. Khorasani and B. Rashidian, Novel optical devices based on surface wave excitation at conducting interfaces, Semicond. Sci. Technol. 18, pp 582–588, 2003.
- [9] Elham Darabi, Sina Khorasani, and Bizhan Rashidian, Optical modulation by surface states, Semicond. Sci. Technol. 18, pp. 60-67, 2003.
- [10] E. X. Pérez, Design, fabrication and characterization of porous silicon multilayer optical devices, Ph.D. Thesis, UNIVERSITAT ROVIRA I VIRGILI, SPAIN, 2007
- [11] J. Vigoureux, Polynomial formulation of reflection and transmission by stratified structures, J. Opt. Soc. Am. A 8, pp. 1697-1701, 1991.

- [12] Ph.Grossel, J. Vigoureux, F.Baida, Nonlocal approach to scattering in a one-dimensional problem, *Phys. Rev. A* 50, pp. 3627-3637,1994.
- [13] M. Shabat., S. Taya, A new matrix formulation for one-dimensional scattering in Dirac Comb: Electromagnetic Approach, *PhysicaScripta* 67, pp. 147-152, 2003.
- [14] B. Waerden, *Modern Algebra*, Ungar, New York, 1966.
- [15] S. Lang, *Algebra*, Addison-Wesley, MA, 1965.
- [16] E. H. Newman, *Electromagnetic Field Theory I*, Unpublished EE 719 Notes, Dept. of EE, The Ohio State University, 1994.
- [17] D. Worasawate and D. Torrungrueng, "Analysis of a Multi-Section Impedance Transformer Using an Equivalent CCITL Model," *Proc. of the 2006 ECTI-CON*, UbonRatchatani, Thailand, pp. 111-114, May 10-13, 2006.
- [18] D. Torrungrueng, *Analysis of Planar Multilayer Structures at Oblique Incidence Using an Equivalent BCITL Model*, Asian University, Thailand.
- [19] D. M. Pozar, *Microwave Engineering*, 3rd Edition, NJ, Wiley, New York 2005.
- [20] T. W. BARBEE, *Atomic Engineering with Multilayers*, *Science & Technology Review*, pp 12-19, 1997.
- [21] D. K. Cheng, *Field and Wave Electromagnetics*, 2nd Edition, 1989.
- [22] J. D. Jackson , *Classical Electrodynamics* , John Wiley & Sons Ltd., 3<sup>rd</sup> Edition, 1999.
- [23] M.Wakaki, K. Kudo, and T.Shibuy, *Physical Properties and Data of Optical Materials*, CRC press, 2007.
- [24] R. Azzam, N. Bashara., *Ellipsometry and Polarized Light*, North-Holland, Amsterdam, 1977.
- [25] P. Drude, *The theory of optics*, Dover, New York 1959.
- [26] M. FOX, *Optical Properties of Solids*, 1<sup>st</sup> Edition Oxford University Press Inc., New York, 2001.

- [27] T. El-Agez, S. Taya, and A. El Tayayn, A polynomial approach for reflection, transmission, and ellipsometric parameters by isotropic stratified media , *Optica Applicata*, Vol.40, No.2, pp 501-510, 2010.
- [28] S. Taya, and T. El-Agez, "Ellipsometry of anisotropic materials: a new efficient polynomial approach", *International J. for Light and Electron Optics, Optik*, Vol. 122, pp 666–670 ,2011.
- [29] E. Palik., *Handbook of optical constants of solids*, volume 1, Academic Press, San Diego, CA 1998.
- [30] Palik E., *Handbook of optical constants of solids*, volume 2, Academic Press, San Diego, CA 1998.
- [31] Palik E., *Handbook of optical constants of solids*, volume 3, Academic Press, San Diego, CA 1998.
- [32] R. C. Weast, *CRC Handbook of Chemistry and Physics*, Edition 62 , CRC Press, Boca Raton, FL, 1981.
- [33] R. B. Ross, *Metallic Materials Specification Handbook*, Fourth Ed., Chapman & Hall, London, 1992
- [34] *Metals Handbook*, Vol.2 - Properties and Selection: Nonferrous Alloys and Special-Purpose Materials, ASM International 10th Ed, 1990.
- [35] A. F. Wells, *Structural Inorganic Chemistry*, 5th Edition, Clarendon Press, Oxford, 1990.
- [36] Alok Nayer, *The Metals Databook*, McGraw-Hill, New York, 1997.
- [37] D. R. Lide, *CRC Handbook of Chemistry and Physics*, 80th Edition, CRC Press, Boca Raton, FL, 1999.